THE ROLE OF MECHANICAL FORCES IN CARDIOMYOCYTE DIFFERENTIATION IN 3D CULTURE

by

Kelly Christina Clause

BS, University of Pittsburgh, 2005

Submitted to the Graduate Faculty of

the Swanson School of Engineering in partial fulfillment

of the requirements for the degree of

Doctor of Philosophy

University of Pittsburgh

2010

UNIVERSITY OF PITTSBURGH

SWANSON SCHOOL OF ENGINEERING

This dissertation was presented

by

Kelly Christina Clause

It was defended on

March 22, 2010

and approved by

Lance Davidson, Professor, Department of Bioengineering

Johnny Huard, Professor, Department of Orthopaedic Surgery

Bradley B. Keller, Professor, Department of Pediatrics

Sanjeev G. Shroff, Professor, Department of Bioengineering

Dissertation Director: Kimimasa Tobita, Assistant Professor, Department of Developmental Biology

THE ROLE OF MECHANICAL FORCES IN CARDIOMYOCYTE DIFFERENTIATION IN 3D CULTURE

Kelly Christina Clause, Ph.D.

University of Pittsburgh, 2010

Heart disease is the leading cause of death in many developing and industrialized countries. The loss of cardiomyocyte (CM) proliferation in the post-natal myocardium is the major barrier to myocardial regeneration, which leads to a loss of functional myocytes and thus contractile function after injury. While significant advances in cardiac tissue engineering as an alternative strategy for treatment have been made in the recent years, the application for repair of the injured myocardium remains to be realized. However, tissue engineering as an *in vitro* model system for characterizing functional properties of cardiac tissue can be used as a powerful tool now.

The overall goal of this doctoral thesis was to determine the role of mechanical strain on CM differentiation within a 3D engineered tissue to use as a system for evaluation of strategies for enhancing directed CM differentiation and tissue contractile properties. Substantial progress towards this goal was made by a combination of testing new strategies for monitoring differential CM differentiation and contractile function, such as using MDSCs in a 3D collagen gel bioreactor to induce CM differentiation and applying mechanical strain to determine the responsive cell type, and by developing new tools and methods for characterizing CM differentiation and cell morphology changes. Our *in vitro* engineered cardiac tissue from fetal/developing native cardiac cells maintained CM proliferative activity and contractile properties similar to the native myocardium which increased in response to mechanical stretch.

The implanted graft maintained CM proliferative activity *in vivo*, survived as a donor myocardial tissue, and contributed to the cardiac functional recovery of injured myocardium better than a graft with post-natal cardiac cells. Skeletal muscle derived stem cell (MDSC) aggregate formation and 3D collagen gel bioreactor (3DGB) culture (MDSC-3DGB) triggered differentiation of cells with an immature functioning CM phenotype *in vitro*. In addition, mechanical strain directed cell morphology changes were significant factors in directing CM differentiation from MDSCs within MDSC-3DGB. In conclusion, our 3D collagen gel bioreactor culture, with capabilities for spatial and temporal monitoring, represents a powerful model for elucidating the role of specific environmental factors and their underlying mechanisms on directed cell proliferation and differentiation.

TABLE OF CONTENTS

LIST OF TABLES

LIST OF FIGURES

ACKNOWLEDGEMENTS

The work presented here in this dissertation would not be possible without the guidance, encouragement, and assistance of many people I would like to acknowledge here. First, I would like to thank my advisor, Dr. Kimimasa Tobita, for his unwavering support through this process. He has provided invaluable knowledge in the field but also enabled me to look at the big questions as well as know how to ask these questions in an experimentally relevant way. He has helped me solve every problem but also encouraged me to be independent in a balance that was masterful. I could not have done this without his help.

I would also like to thank the other members of my committee, Dr. Sanjeev Shroff, Dr. Lance Davidson, Dr. Johnny Huard, and Dr. Bradley Keller who opened up their labs to me and also provided necessary guidance and suggestions during this process.

The work presented here was also done with the assistance of other members of the lab, past and present, Dr. Li Liu, Joseph Tinney, and John C. Ralphe. The surgical expertise of Dr. Kazuro Fujimoto enabled the completion of all the *in vivo* work presented here. Thanks to Burhan Gharaibeh who gave me the cells to start. Thanks to all the summer students that also contributed to this work, Mary Powell and Peter Backaris.

I would like to acknowledge the sources of funding that allowed me to pursue and complete this work, The National Institutes of Health, including the cardiovascular

bioengineering T-32 training grant and its related activities, The American Heart Association, and the University of Pittsburgh Department of Bioengineering.

Lastly I would like to thank my friends and family for all their support through this long process. Special thanks to Valentine Whittaker who not only shared in the good times but also listened to me complain when things didn't go well, which was more often than not. I am grateful for your unending love and support. Thank you for everything.

1.0 INTRODUCTION

Heart disease is the leading cause of human mortality in many developing and industrialized countries. It is estimated that one in three adults in the United States has one or more types of cardiovascular diseases, with estimated direct and indirect costs equaling 475.3 billion dollars for 2009 alone[1]. The lifetime risk of developing coronary heart disease, which accounts for nearly one in five cases of all cardiovascular diseases, is 49% for men and 32% for women after the age of forty, where approximately 38% of those afflicted will die within a year of a coronary event[1, 2]. Half of all patients with coronary heart disease will suffer a heart attack[1]. The developing fetal myocardium has a high cell proliferation rate, which rapidly declines following birth[3, 4]. The loss of cardiomyocyte (CM) proliferation in the post-natal myocardium is the major barrier to myocardial regeneration, which leads to a loss of functional myocytes and thus contractile function after injury. Thus, the high mortality rate for patients of coronary heart disease reflects the fact that the adult myocardium does not significantly regenerate after injury.

The adult population is not the only population that suffers from heart disease. In the pediatric population, 9 defects per 1000 live births are expected in the United States. Of these, several studies suggest that 2.3 per 1000 live births require invasive treatment or result in death in the first year of life[1, 5]. From 1995-2005 the death rates for congenital cardiovascular defects declined 42.1%, whereas the actual number of deaths declined 27.3%. However, there was a

suggested 192,000 life-years lost before 55 years of age because of deaths from congenital cardiovascular defects, which is about the same as the life-years lost from leukemia, prostate cancer, and Alzheimer's disease combined[1, 6].

Currently, the best treatment option available for end-stage heart failure is total heart transplantation. However, there are several disadvantages associated with this treatment: limited donor organ supply, organ mismatch, and disadvantages of immunosupression, all of which are exacerbated in the pediatric population. Despite the current pharmacological and surgical approaches, alternative strategies for treatment are necessary.

1.1 ALTERNATIVE TREATMENTS TO MYOCARDIAL INFARCTION

Much of the understanding of the structural and functional changes that occur during heart disease is derived from experiments using laboratory animal models. While these can only approximate aspects of human pathology and may not necessarily translate to human patients, they remain an invaluable tool in understanding the disease process and developing novel therapeutic approaches. Recent studies have suggested cell-based or tissue-engineered approaches as promising new therapies for repairing the damaged myocardium, including: 1) activation and stimulation of host myocardial regeneration by transplanted cells via angiogenic and/or paracrine effects[7, 8]; 2) direct transplantation of functional CMs or myogenic cells[9-11]; and 3) implantation of tissue constructs containing CMs[12, 13]. In the first case, a range of cell types have been employed in strategies to repair the damaged myocardium which include bone marrow derived stromal and stem cells, fibroblasts, skeletal myoblasts, mesenchymal stem cells, embryonic stem cells, and resident cardiac stem cells[14]. Many of these cell therapies provide

indirect beneficial effects, or paracrine effects, mostly through angiogenesis. In the latter two cases, the ideal donor CMs possess a high potential for division during cell preparation and potential for further proliferation following implantation to form a viable myocardial tissue within the surrounding injured recipient myocardium. However, cellular cardiomyoplasty also has the added disadvantages of low cell retention rate (more than 90% of injected cells are typically lost)[15], inadequate tracking mechanisms[16], as well as induced injury at the injection site. In order to resolve these issues the potential of functional cardiac tissue engineering has been investigated.

1.1.1 Functional cardiac tissue engineering approaches

Cardiac morphogenesis depends on complex cell-cell and cell-matrix interactions within a dynamic four dimensional environment (three dimensional (3D) plus time). Previous studies have shown that close cell-cell interactions and 3D culture conditions are often necessary prerequisites for CM differentiation[17-19] and that cardiac cells within 3D cultured tissues display distinct features that are more representative of native tissues[20-22] than are cells within 2D culture[23, 24]. 3D growth of cells in aggregate spheres has been shown to direct and facilitate cell-cell interactions as well as to modify the differential expression of both morphogenic and angiogenic pathways in CMs[17] and hepatocytes[25]. Cell aggregate culture has been shown to enhance CM gene expression patterns[17], increase the synthesis and release of ECM components[26], and accelerate CM differentiation efficiency of embryonic stem cells[27] and liver stem cells[18]. Similarly, Albrecht et al. found that chondrocyte matrix biosynthesis was dependent on cell cluster size, rather than overall cell density[28]. Aggregate culture has also been used to enhance survival and differentiation of various stem cell types[27, 29, 30], versus static

culture. These studies suggest that aggregation imparts many of the necessary structural cues required for maintaining differentiated phenotype, including proper dimensionality, shape, cell–ECM, and cell–cell interactions. Bursac et al. investigated the effect of 3D vs. 2D culture on CM properties and found that the 3D microenvironment plays critical role in maintenance of CM metabolism, sarcomere formation, cell-to-cell connections, and electrophysiological properties[31]. 3D growth of fibroblasts[14, 32], endothelial cells[33], and mammary gland cells[34] also exhibits cell morphology and function similar to native tissue over 2D culture[35]. Eschenhagen et al. described physiologic contractile force and action potentials in 3D neonatal engineered heart tissue[13, 22, 36-39]**.** These studies show that a 3D environment is required for the proper cell-cell and cell-matrix interactions that drive proper CM differentiation and maturation with contractile function. Tissue engineering offers these advantages as well as flexibility of size and shape, high cell retention, and the ability to monitor three-dimensional tissue formation and function *in vitro.* Studies using various cell types and scaffolds, both natural and synthetic, have been successful in creating engineered cardiac tissue that resembles the native heart muscle in morphological, biochemical, and functional properties[13, 20, 38, 40-45].

1.1.1.1 Cell sources and composition

Various types of cells have been used in cardiac tissue engineering, including primary cardiac myocytes[20, 37, 40-42, 46-50]. Freshly isolated primary cardiac myocytes are used because of their structural and physiologic attributes as well as their intrinsic contractile properties. Engineered cardiac constructs from cardiac myocytes have been created in a number of forms: free floating monolayers, chambers, ring-like structures, rectangular patches, and cylinders[13, 20, 40, 41, 51, 52]. These have been constructed with many different natural and synthetic scaffolds, such as gelatin, fibrin glue, collagen, porous alginate, polyglycolic acid, and polyurethane[46-48, 51,

[53-57]. They can generate an active stress between 1 and 2 mN/mm^2 [20] which, although it is less than 5% of the average isometric maximum twitch stress generated by a papillary muscle from the rat heart, 44.4 ± 3.37 kPa[58], is 10 times better than engineered tissue from non-primary cardiac myocytes[209].

It is also important to understand the role of non-myocyte cells in the heart, of which tissue engineering can provide the controlled experimental system to elucidate. During early embryonic development, CMs require direct cell-to-cell contact or paracrine signaling from non-cardiac endoderm cells to differentiate into working CMs[59, 60]. A similar observation was reported in CM induction from stem cells[61, 62]. Other studies showed that non-cardiac cells, such as fibroblast and/or endothelial cells, are required for CMs to maintain contractile function and cell survival[63-65]. CM function, morphology, and survival are also influenced by extracellular matrices[66]. Therefore, cell-cell interactions, both homo- and hetero-typic, and proper cell-ECM contact under 3D environment are also important in maintaining functioning CM differentiation, maturation, and survival.

While engineered cardiac tissue generated from freshly isolated primary cardiac myocytes are beneficial because of their intrinsic contractile properties, structural, and physiologic attributes, they are contraindicated for clinical use. Stem cells provide an alternative cell source. The original assumption in the stem cell field was that transplanted cells would directly participate in tissue formation and recovery; however, it is now clear that paracrine effects are important. A number of stem cell cardiomyoplasty studies in adult heart infarct models have shown improvement in the recipient heart function through paracrine effects, mostly through angiogenesis[7, 8]. However, in the pediatric population, congenital heart defects, or structural problems arising from abnormal formation of the heart or major blood vessels, are

the major problem and in many cases the underlying heart structure is not always present. A number of stem cell populations have been used in cardiac tissue engineering, including embryonic stem cells or embryonic stem cell-derived cells, endothelial progenitor cells, bone marrow stromal and stem cells, skeletal muscle cells, and others[56, 65, 67-73]. Being stem cell populations, they also have the property of multipotency, allowing the possibility of myocyte and non-myocyte populations within the engineered tissue. However, despite some promising results[74], the rate of CM differentiation from transplanted stem cells remains insufficient to fully recover the recipient myocardial function[14, 33, 34, 75, 76]. Current findings suggest that cellular cardiomyoplasty remains to be improved toward the ultimate (or long-term) goal of completely healing the injured myocardium. Thus, while stem cell cardiomyoplasty plays an important role in protection of myocardial tissue loss, mainly through a paracrine mechanism and/or angiogenic effects within insufficient levels of cardiomyocyte differentiation, it is not enough to regenerate healthy myocardium. Therefore, a preferred strategy for cellular cardiomyoplasty might be the delivery of progenitor/stem cell-derived CMs, rather than undifferentiated cells, into injured myocardial tissue[77]. Though tissue engineered strategies provide evidence as promising therapeutic options to treat the damaged myocardium, practical benefits remain inconclusive due to inconsistent results, weak function, small size, and a limited understanding of the underlying mechanisms. To begin to address these issues, it is necessary to understand the basic structural and functional properties of the native myocardium.

1.2 THE NATIVE MYOCARDIUM

1.2.1 Cellular components in the myocardium

Cardiomyocytes comprise approximately only 30% of the ventricular cell population[78]. Transmission and scanning electron microscopy have identified five types of non-muscle cells within the adult myocardium: endothelial cells, fibroblasts, pericytes, smooth muscle cells, and macrophages, which comprise approximately 65-70% of ventricular cells[79]. In addition to these cell types, the 3D extracellular matrix (ECM) of the myocardium plays an important role in its function. The myocardium ECM consists of collagen, fibronectin, elastin, and laminin, as well as various growth factors, proteoglycans, and glycosaminoglycans[80, 81]. Collagen is the most abundant ECM component in the heart and contributes to structural stability and integration of cardiomyocytes and myofibrillar bundles[82]. The various components of the myocardium, cells and matrix, play important roles in both the healthy and diseased heart. However, as stated previously, cardiac morphogenesis is a complex process within a 4D environment. Thus we must also examine the myocardium over time.

1.2.2 Fetal vs. post-natal cardiomyocytes

There are marked phenotypic differences between fetal and post-natal CMs, including age-dependent changes in protein kinase expression, β-adrenergic signaling[83], contractile apparatus maturity, and the hyperplastic[84] versus hypertrophic[85] responses to mechanical stress. The accumulation of maturation specific isoforms of sarcomeric proteins including cardiac myosin heavy chain, sarcomeric actin and actinin, titin, cardiac troponin-T and -I, and the

maturation of sarcolemmal and SR ion channels[86-88] allow the functional characterization of CM identity and maturation. These characteristics determine the overall phenotypic appearance of CMs, which can differ depending on their location.

Stem cell derived-CMs have been suggested as a promising option for use in tissue engineered constructs, however, there is currently no standard as to what a stem cell derived-CM is. Many groups use the expression of early cardiac genes: Nkx2.5 or GATA4 and the presence of rhythmic beating. This is not necessarily sufficient because skeletal and smooth muscle also contracts. Also, it has been widely accepted that terminally differentiated mature cardiac muscle does not express proteins that are specific to skeletal muscle. However, studies have shown that several skeletal muscle specific proteins, such as skeletal muscle specific troponins or ion channels, are transiently present in the developing heart[89, 90]. Similarly, "cardiac" and "skeletal" excitation-contraction coupling mechanisms co-exist in the developing skeletal muscle with the "cardiac" type dominant in the early phases of myogenesis and the "skeletal" dominating in more mature muscle[91]. These studies suggest the co-existence of many cardiac and skeletal muscle specific proteins (MHCs, troponins, etc.) as well as excitation-contraction coupling mechanisms within the developing tissue, but also within cultured cells, especially those that are considered to be immature. Thus, the functional characterization of CMs for extrapolation to composite tissue engineered specimens is another fundamental step in optimizing approaches for cellular repair.

1.3 THE EFFECTS OF THE MECHANICAL ENVIRONMENT ON NATIVE AND ENGINEERED TISSUES

The effects of mechanical factors on myocardial mechanical properties, CM differentiation, proliferation, death, and molecular mechanisms in the developing myocardium have been well documented[4, 92-105]. A detailed understanding of the cellular responses to exogenous stimuli is critical in order to elucidate and therefore control tissue development and remodeling for the generation of optimal tissue engineered grafts for myocardial repair. Time-varying changes in stresses and strains significantly influence the fundamental cellular response in terms of cell morphology, phenotype, and function of growing cardiac tissue[92-95]. Sedmera et al.[4] showed that altered mechanical loads on developing embryonic myocardium influenced cell proliferation; however, cellular apoptosis was not changed. These studies indicate that mechanical stimulation is one of the key factors that regulate developing fetal CM proliferation, tissue formation, contractile function, and cell survival.

Mechanical strain has been shown to elicit cell responses in engineered cardiac tissue, including activation of MAPKs[106-109], reprogramming of gene expressions[106, 107], increasing protein synthesis[106, 107], and triggering adaptive responses in muscle phenotype via the expression of contractile proteins[108, 110]. Embryonic rat CMs subjected to cyclical mechanical stretch resulted in parallel orientation of CM and their intracellular myofibrils[111, 112]. With neonatal CMs, passive mechanical stretch has been reported to upregulate myosin heavy chain expression and induce parallel CM orientation[113]. Adult CMs were however weakly stimulated by passive mechanical load[114]. Mechanical stretching of neonatal CMs induced secretion of growth promoting factors[115], as well as upregulation of connexin-43[116] and myosin heavy chain[117], which are markers of CM maturity. Fink et al. reported that six days of phasic,

unidirectional stretch led to cardiac myocyte hypertrophy with marked improvement in contractility and cellular morphology in 3D engineered heart tissue[118]. Akhyari et al. observed similar behavior in cultured gelatin extracts seeded with cardiac myocytes in which tensile strength and stiffness were increased and cell proliferation, collagen matrix formation, and sarcomere organization were improved[119]. We have shown previously in engineered early embryonic cardiac tissue that developing fetal CM within 3D engineered tissue subjected to cyclic mechanical stretch by increasing cellular proliferation and contractile function[20]; specifically, that mechanical stretch positively regulates CM proliferation, but not non-CM proliferation[120]. The *in vitro* tissue culture conditions necessary for controllable and highly proliferative donor CM preparation remains to be determined. Similarly, few studies have looked at the role of mechanical forces in regulating structural and mechanical properties within *in vitro* engineered tissue constructs[121-123].

The chemical and physical microenvironment has been shown to modulate stem cell proliferation, migration, differentiation, and survival[124-126]. However, few studies have been devoted to understanding the role of the mechanical environment in CM induction from progenitor/stem cells, CM maturation, and contractile function[121-123]. Various methods have been used to manipulate endogenous and exogenous progenitor cells to differentiate into CMs[127] with the focus being on chemical or growth factors and co-culture. However, previous studies have shown that soluble induction factors tend to be less selective than mechanical factors in driving cell specification and cannot reprogram mesenchymal stem cells that are precommitted[128]. Aggregate culture has been used to enhance survival and differentiation of various stem cell types[27, 29, 30], but the emergence of CM in spheroid cultures remains stochastic[129, 130]. The ability of mechanical forces to stimulate stem cell differentiation into

cardiovascular lineages has only recently been shown[131] and the mechanisms controlling CM differentiation remain unknown. Therefore, strategies for directing differentiation of pluripotent stem cells into CMs are needed.

1.3.1 Cell shape regulation of fate switching

The regulation of stem cell differentiation has been a challenge in regenerative medicine. Stem cell commitment toward a particular program is highly context dependent and requires both the activation and suppression of interdependent signaling pathways in order to shift molecular cascades between migration, growth, differentiation, and apoptosis[132, 133]. Changes in cell shape, via mechanical cues, and binding of specific growth factors and ECM proteins to their respective cell surface receptors all switch cells between these same discrete cell fates[132, 134, 135]. Engler et al. has shown that hMSCs could be induced to differentiate into multiple tissue lineages by simply altering substrate compliance[128]. However, Chicurel et al. has shown that when cells are forced to become round, they undergo apoptosis even though they receive growth factor stimulation and remain attached to the ECM, which would normally induce proliferation[136]. Thus, one physical parameter, cell distortion, can control the switch between multiple cell fates. Recent studies have also revealed that mesenchymal stem cells can be reliably switched between different lineages (e.g., bone versus fat) through changes of cell shape[137] and that cells are tuned mechanically so that they preferentially differentiate on ECM with a mechanical stiffness similar to that of their natural tissue[138]. Yang et al. has shown that embryonic mesenchymal cells attached to microsurfaces with a diameter less than the cell diameter conserved their original round shape, whereas cells attached to surfaces with diameters larger than the cell diameters became elongated with a shape similar to their *in vivo* counterparts. Within 24hrs the elongated

cells differentiated into smooth muscle while the round cells remained undifferentiated as long as they conserved their shape[139]. Thus, generalized cell deformation can produce discrete changes in cellular phenotype.

Despite numerous proof-of-principle studies showing that mechanical conditioning can improve the structural and functional properties of engineered tissues, little is known about the specific mechanical forces or regimes that are stimulatory for a particular tissue or for inducing a particular stem cell down a selected lineage. Similarly, despite studies indicating cell deformation can produce cell phenotype changes, whether mechanical forces are the only factor responsible for these cell shape changes is unclear. In addition, engineered tissues at different stages of development might require different regimes of mechanical conditioning owing to the increasing accumulation of extracellular matrix and developing structural organization. In this context, bioreactors can have an important role, providing controlled environments for reproducible and accurate application of specific regimes of mechanical forces to 3D constructs. Thus, an adequate model to analyze mechanically driven stem cell derived CM induction, differentiation, and contractile maturation within the context of a developing engineered tissue is necessary.

1.4 AIMS OF THE STUDY

With this in mind we hypothesize that there are unique aspects of the 3D culture microenvironment and associated biophysical factors that are essential for CM phenotype induction. Thus, the objective of the present study is to 1) determine the underlying mechanisms that regulate native cardiomyocyte proliferation within an engineered tissue both *in vitro* and *in*

vivo, and 2) analyze mechanically driven stem cell derived CM differentiation and contractile maturation within the context of a developing engineered tissue, specifically by investigating the relationship between regional mechanical strain variations and CM induction efficiency. Achieving these aims will have an impact in tissue engineering, developmental biology, and regenerative medicine research while lending to the overall goal of developing a functional cardiac graft to repair congenital as well as acquired heart disease.

2.0 EFFECT OF MECHANICAL STRETCH ON ENGINEERED CARDIAC TISSUE FROM NATIVE CARDIAC CELLS

2.1 INTRODUCTION

The developing fetal myocardium has a high cell proliferation rate, which rapidly declines following birth[3, 4]. The loss of cardiomyocyte (CM) proliferation in the post-natal myocardium is the major barrier to myocardial regeneration following injury in higher vertebrates. With heart-related diseases being the leading cause of death in America and an inadequate supply of donor organs, there is an increasing demand for alternative therapeutic options. The long-term goal of cardiac tissue engineering is to create heart tissue constructs for clinical use that have morphologic and functional properties similar to native heart muscle. In the short term, engineered tissues can also provide powerful model systems for *in vitro* investigations.

As discussed in section 1.0, there are several approaches to increase the number of CM within injured myocardium including implantation of functional CMs or myogenic cells or tissue constructs containing CMs, with the ideal donor CMs possessing a high potential for division and potential for further proliferation following implantation. In this vein, studies suggest that fetal, finitely proliferating CMs display the best cell survival, functional integration, and sustained cardiac recovery and that 3D *in vitro* culture conditions may be optimal for donor CM

preparation[11, 12, 16, 75]. Tissue engineered cardiac tissue constructs provide the necessary 3D environment for efficient cell survival, functional integration, and sustained cardiac recovery[12, 13].

Researchers have reported findings that mechanically stimulating engineered cardiac tissues during culture resulted in more highly differentiated cardiac tissues that resembled the adult native myocardium[47], induced cardiac myocyte hypertrophy[118], improved contractile function[20, 118], and increased collagen content[140]. A study where cyclic mechanical stretch was applied to a gelatin scaffold seeded with human heart cells also reported improved cell proliferation and cell distribution, enhanced matrix organization, and increased tensile strength of the construct[119]. We have recently developed a 3D engineered cardiac tissue from chick early embryonic ventricular cells (EEECT) that maintains high cellular proliferation activity and contractile properties that mimic the native developing fetal myocardium[20]. In a study using our EEECT we found that tissues that were cyclically stretched during culture displayed significant improvements in active contractile function such that active contractile stress nearly doubled in fetal cardiac tissues that were under cyclical mechanical stretching[20]. Also, mechanical stretch stimulation of EEECT induces increased cellular proliferation, not cellular hypertrophy, a response noted in adult and neonatal CMs[20]. However, it remained unclear which cellular subpopulation, CMs or non-CMs, responds to the cyclic mechanical stretch within this *in vitro* engineered cardiac construct.

Numerous signaling pathways alone, or in combination with growth factors and/or environmental factors, have been investigated to identify the regulation of CM proliferation[141]. p38-mitogen-activated protein kinase (p38MAPK) is a highly conserved signal transduction molecule which mediates extracellular signals to a variety of intracellular responses. p38MAPK

has been extensively studied in post-natal CM growth (hypertrophy) and survival[10, 142-144]. Recent studies have also shown that p38MAPK plays a key role in CM proliferation in both developing fetal and post-natal myocardium[87, 143, 145, 146]. Therefore, the purpose of the present study was to elucidate the factors that regulate the proliferation activity of immature CMs within an *in vitro* engineered cardiac tissue construct independent of the non-CM population proliferation activity. We tested the hypotheses that cyclic mechanical stretch increases specifically CM proliferation within EEECT, mediated by p38MAPK activity and the inhibition of p38MAPK activity decreases CM proliferation.

2.2 METHODS

2.2.1 Chick engineered early embryonic cardiac tissue (EEECT) construction

Fertile White Leghorn chicken eggs (Utah State University, Logan, Utah) were incubated in a forced-draft, constant-humidity incubator until Hamburger-Hamilton (HH) stage 31[147]. Cells isolated from 10-15 embryonic ventricles were used to construct each individual EEECT[102]. Our research protocols conform to the Guide for the Care and Use of Laboratory Animals published by the National Institutes of Health (NIH Publication No. 85-23, Revised 1985). Embryonic ventricles were then enzymatically digested by 2mg/ml of collagenase type II followed by 0.05% trypsin-EDTA solution (Invitrogen). Isolated cells were preplated for 1 hour and then cultured on a gyratory shaker (60 or 50 rotations/min for chick and rat respectively) for 24 hours to reaggregate viable CMs[20]. Approximately 5.0×10^5 cells were mixed with acid-soluble rat-tail collagen type I (Sigma, St. Louis, MO) and matrix factors (Matrigel, BD Science,

Franklin Lakes, NJ) to generate a single construct[20]. Briefly, isolated cells were suspended within a culture medium (Modified Dulbecco's Essential Medium. Invitrogen) containing 20% FBS (Invitrogen). Acid-soluble collagen type I solution (pH 3) was neutralized with alkali buffer (0.2 M NaHCO3, 0.2 M HEPES, 0.1 M NaOH) on ice. Matrigel (17% of total volume, BD Sciences) was then added and the cell suspension and matrix solution mixed to reach a final collagen type I concentration of 0.67 mg/ml. Cylindrical-shaped EEECT were constructed using collagen type I-coated silicone membrane culture plates (Tissue Train, Flexcell International, Hillsborough, NC) and FX-4000TT system (Flexcell International) as follows: 1) the center of the silicone membrane of a Tissue Train culture plate was deformed by vacuum pressure to form a 20-mm-length x 2-mm-width trough using a cylindrical loading post (Tissue Train and FX-4000TT). 2) Approximately 200 μl of cell/matrix mixture was poured into the trough and then incubated for 120 min in a standard CO_2 incubator (37°C, 5% CO_2) to form a cylindrical-shaped construct. Both ends of the construct were held by anchors attached to the Tissue Train culture plate. When the tissue was formed, the culture plate was filled with a growth medium containing 10% FBS and 1% chick embryo extract (SLI, Horsted Keynes, UK). The vacuum pressure was then gradually released, allowing the construct to float within the culture plate. Growth medium was exchanged every 48 hours.

2.2.2 Mechanical Stretch Stimulation and p38MAPK inhibition

To determine the effect of cyclic mechanical stretch and/or p38MAPK inhibition on EEECT cell proliferation, contractile force, and p38MAPK and Akt phosphorylation, we exposed culture day 10 EEECT to either uniaxial cyclic mechanical stretch (0.5Hz, 5% elongation), inhibition of p38MAPK with a selective inhibitor, SB202190 (10μM), or concurrent

p38MAPK inhibition (SB202190) with cyclic mechanical stretch. In the preliminary study, we found that 0.5Hz, 5% strain of cyclic stretch increased both EEECT contractile force generation and cellular proliferation activity with minimal technical EEECT loss due to detachment of the tissue from anchors of the culture plate. We performed cyclic mechanical stretch stimulation or p38MAPK inhibition for 2 hours or 48 hours beginning on culture day 10. For 48 hours p38MAPK inhibition, we treated EEECTs with SB202190 containing culture medium and the culture medium was changed with fresh SB containing culture medium at 24 hours after initial treatment. For cyclic mechanical stretch stimulation, we also changed culture medium at 24 hours after the beginning of cyclic mechanical stretch stimulation.

2.2.3 CM and non-CM proliferation assays

Each EEECT was fixed with 4% paraformaldehyde/PBS for 15 minutes. For BrdU staining each tissue was incubated with 60μg/ml bromodeoxyuridine (BrdU, Sigma, St. Louis, MO) for 16 hours prior to fixation[20]. Samples were then embedded in a 13% polyacrylamide gel oriented in the longitudinal direction, and 150μm thickness serial sections were made using a standard vibrating microtome (Vibratome-1000, Vibratome.com, St Louis, MO)[20]. Sections were permeabilized with 0.1% Triton X-100 for 30 minutes and stained for BrdU using an Alexa Fluor 594 conjugated mouse-monoclonal anti-BrdU antibody (Invitrogen, Carlsbad, CA) and DAPI (Vector Laboratories, Burlingame, CA). To differentiate between proliferating CM and non-CM within EEECT we used phospho-Histone H3 (ser10, Upstate cell signaling solutions, Temecula, CA) and Alexa Fluor 594 secondary antibody (Invitrogen) staining to detect cells undergoing mitosis while also counterstaining for CM phenotype with α-sarcomeric actinin (EA53, Sigma, St. Louis, MO) and Alexa Flour 488 secondary antibody (Invitrogen).

We reconstructed 3D projection images from stacks of z-axis optical scans (1μm scanning interval, up to 50μm thickness) using a standard laser confocal microscope system (FV1000, Olympus, Tokyo, Japan) and Scion Image software (Scion Corp, MD)[20]. The reconstructed composite 3D projection images were visualized at different rotation angles to identify proliferating CMs by co-localization of phospho-histone H3 positive nuclei staining and α-sarcomeric actinin staining. Overlapping positive histone-H3 and sarcomeric α-actinin staining in all views confirmed CM phenotype (Figure 2-1). To quantify total cellular and CM proliferation activities, 10-20 regions from 3D composite images from each EEECT were randomly chosen for analysis. Cellular proliferation and CM proliferation rates were calculated as: [BrdU (+) nuclei] / [DAPI (+) nuclei] (%) and [Histone H3 (+) nuclei within α-sarcomeric actinin (+) cells] / [DAPI (+) nuclei] (%), respectively. We also calculated CM cell ratio (%) by [DAPI (+) nuclei with α-sarcomeric actinin (+) cells] / [DAPI (+) nuclei] (%).

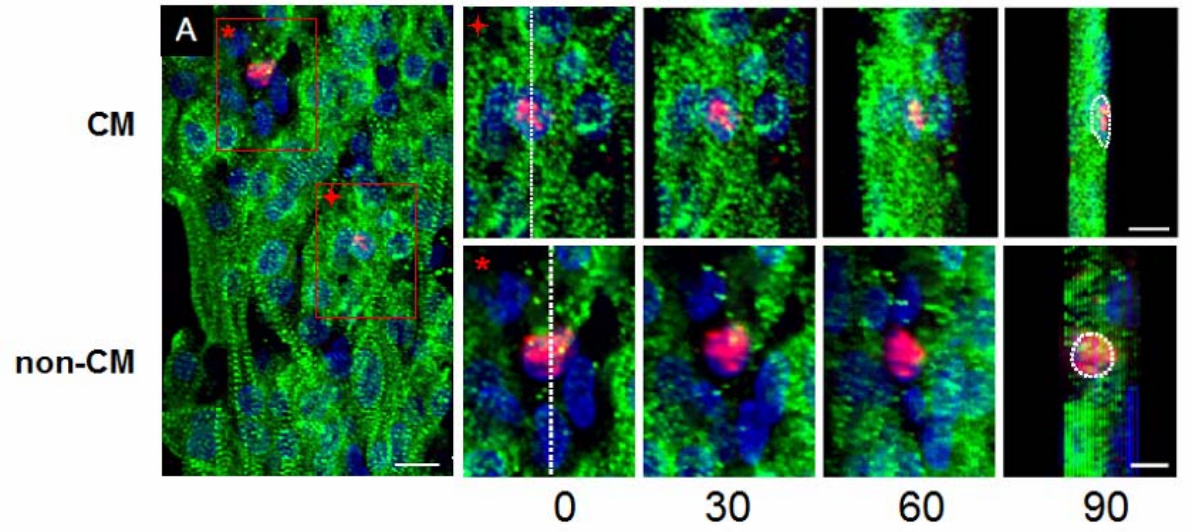

Figure 2-1. Identification of phospho-histone positive CMs and non-CMs within EEECT. **(A)** EEECT were stained for α-sarcomeric actinin **(green)**, phospho-histone H3 **(pink)**, and DAPI **(blue)**. 3D projection images were reconstructed using a laser confocal microscopy. Scale bar indicates 10 μm in A. Red boxed areas in A are shown at a higher magnification and Histone positive nuclei (✛; CM and *; non-CM) were visualized at

several different rotation angles. At 0^{o} rotation, the nuclei were sliced in half **(white dotted line)** and were visualized at 90^{o} rotation angle. A proliferating CM was identified as a histone positive nucleus surrounded by sarcomere **(upper panel)**. Non-CMs were not surrounded by sarcomere staining in all views **(lower panel)**. Scale bar indicates 5 μm in higher magnification views.

2.2.4 SDS-PAGE Western Blot and ELISA assays

Whole cell lysates were prepared from EEECT and separated by SDS-PAGE (7.5% separating gel, Bio-Rad Laboratories). Immunoblotting was carried out using routine protocols. Each lane contained 20μg of total protein. Mouse monoclonal β-actin antibody (Abcam), mouse monoclonal anti-p38MAPK activated (diphosphorylated p38) antibody (Sigma, St. Louis, MO), and mouse monoclonal anti-p38MAPK non-activated antibody (Sigma) and mouse-monoclonal α-sarcomeric actinin primary antibody (EA53, Sigma) were visualized with IR-Dye 800 donkey anti-mouse secondary antibody (Rockland Immunochemicals, Gilbertsville, PA). Rabbit monoclonal phospho-Akt antibody (Cell Signaling) was visualized with IR-680 donkey anti-rabbit secondary antibody (Rockland Immunochemicals). All proteins were visualized using an infrared western blot imaging system (Odyssey, LI-COR Biosciences Lincoln, NE). Immunoblots were quantified using densitometry and an expression ratio was calculated (Scion Image, Scion Corp.). Standard ELISA protocols from phospho-p38α-MAPK sandwich ELISA kit (Cell Signaling) and Akt [pS473] ELISA kit (Biosource) were used to assay p38MAPK and Akt phosphorylation. We pooled 3 to 4 EEECTs for a single western blot or ELISA assay, and all western blot and ELISA assays were completed in triplicate (total 9 to 12 EEECTs were used per experimental group).

2.2.5 Contractile force measurement

EEECT passive and active forces were recorded as previously described[20]. In brief, each construct was excised and transferred to a cold (25°C) calcium free Ringer solution containing (in mM): 135.0 NaCl, 4.0 KCl, 10.0 Trizma-HCl, 8.3 Trizma-base, 11.0 glucose, and gassed with 95% O_2 /5% CO_2 (pH 7.4). One end of the construct was attached using 10-0 mono-filament nylon sutures to a force transducer (model 403A, Aurora Scientific, Ontario, Canada) and the other end to a rigid stainless bar mounted on a micromanipulator. The perfusion chamber containing the construct was then filled with warmed buffer (37°C, 2 cc total volume) and perfused at 1ml/min with 2mM Ca^{2+} Ringer solution. The construct was field-stimulated (1Hz, 4ms, 70 to 100v) using a stimulator (Harvard Apparatus, Holliston, MA). Construct length was increased stepwise in 5% increments up to a 15% elongation from original length or until total force reached maximum (L_{max}). Construct external diameters were recorded at each stretch increment using a video microscopy system (Model KPD-50, Hitachi, Japan and PowerMac 8600 system, Apple, CA) and cross-sectional area (mm^2) was calculated assuming cylindrical geometry. Force (mg) was normalized by each specimen's adjusted cross-sectional area to yield active stress (mN/mm^2).

2.2.6 Statistical analysis

Data are expressed as mean ± SE. One factor analysis of variance (ANOVA) with Tukey post-hoc test was performed to compare the p38MAPK and Akt activities after 2 and 48 hours stimulation. Two-factor ANOVA with a Tukey test was performed to compare the BrdU positive ratio, the phospho-histone H3 positive ratio, the p38-MAPK or Akt kinase

phosphorylation ratios, and α-actinin/β-actin expression ratios. Two-factor repeated ANOVA with a Tukey test was performed to compare the active contractile force. Statistical significance was defined by a value of $P<0.05$. All calculations were performed using SigmaStat (Systat Software Inc, Point Richmond, CA).

2.3 RESULTS

2.3.1 Effect of cyclical mechanical stretch and p38MAPK inhibition on EEECT CM and non-CM proliferation activity

Culture day 12 EEECT, which developmentally corresponds to late fetal chick myocardium with the cumulative age of 19 incubation days of 21 incubation days (hatching), displayed a high BrdU positive ratio comparable to native embryonic myocardium and cyclic mechanical stretch further increased the BrdU positive ratio (Table 2-1). EEECT CM cell ratio also increased in response to cyclic mechanical stretch [75.3 ± 3.4% (stretch, n=3), vs. 63.9 ± 7.0% (control, n=3), $P<0.05$]. These results are consistent with our previous study[20]. Both p38MAPK inhibition, SB202190 treatment, and concurrent p38MAPK inhibition and mechanical stretch stimulation decreased the EEECT BrdU positive ratio (Table 2-1). Phospho-histone positive ratios followed similar trends to the BrdU positive ratios (Table 2-1, Figure 2-2). Notably, the increase in histone positive cell ratio following cyclic mechanical stretch occurred only in the CM fraction not the non-CM fraction. In contrast, p38MAPK inhibition, SB202190 treatment, decreased both the CM and non-CM phospho-histone positive ratios. Concurrent p38MAPK inhibition and mechanical stretch stimulation also decreased the CM and non-CM

phospho-histone positive ratios, similar to p38MAPK inhibition alone. Thus, the negative CM proliferation effect of SB202190 treatment was not reversed by concurrent cyclic mechanical stretch stimulation.

Table 2-1. Effects of cyclic mechanical stretch and p38MAPK inhibition on EEECT CM and non-CM proliferation. Data are mean ± SE. n; number of samples. *; $P<0.05$ vs. Control EEECT within group. †; $P<0.05$ vs. Stretch EEECT. §; $P<0.05$ vs. Control EEECT CM fraction. ¥; $P<0.05$ vs. Control EEECT non-CM fraction. ‡; $P<0.05$ vs. Stretch non-CM fraction. SB: p38MAPK inhibition, SB202190 treatment. Stretch+SB: concurrent cyclic mechanical stretch and p38MAPK inhibition (SB202190). Stretch: uniaxial cyclic mechanical stretch (0.5Hz, 5% elongation).

		Control	Stretch	SB	Stretch+SB
BrdU Positive Ratio (%)		22.2 ± 2.4% (n=4)	40.7 ± 1.9% (n=4)*	14.8 ± 2.1% (n=4)*†	16.2 ± 2.1% (n=4)*†
Histone Positive Ratio (%)	**CM**	8.9 ± 0.9% (n=4)	16.5 ± 2.4% (n=4) ‡§¥	1.1 ± 0.4% (n=3) §¥	2.0 ± 0.5% (n=3) §¥
	non-CM	7.7 ± 4.2% (n=4)	9.0 ± 4.4% (n=4)	1.0 ± 0.6% (n=3) ¥§	3.8 ± 1.2% (n=3) ¥§

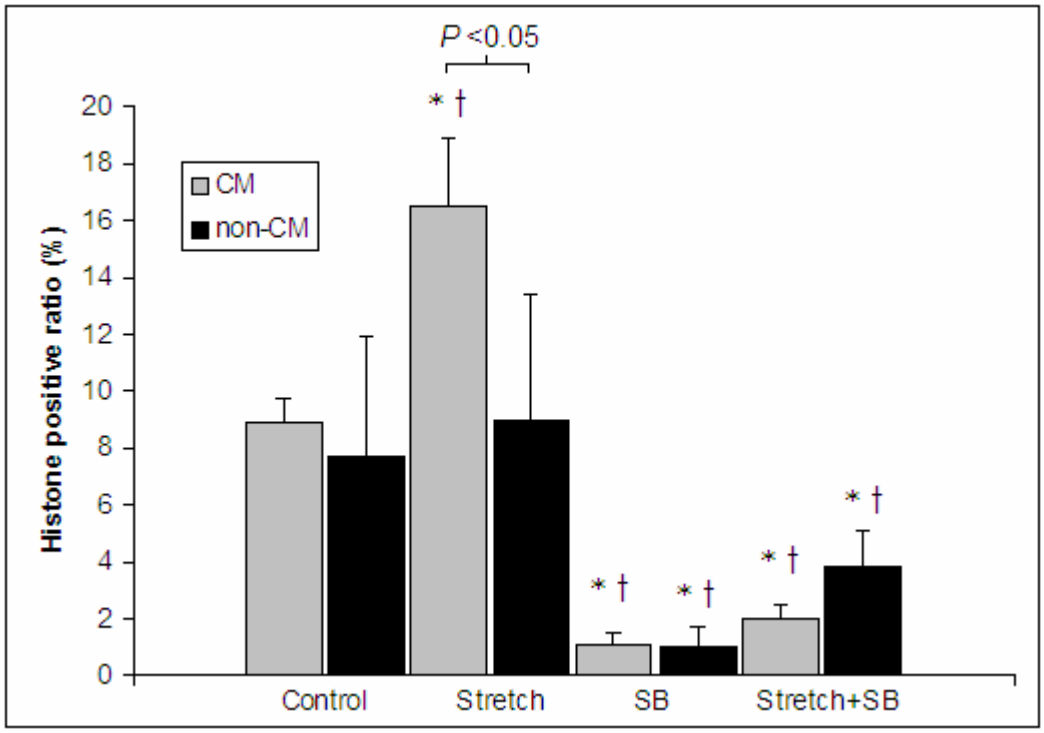

Figure 2-2. Quantification of CM and non-CM Histone H3 positive fractions in each group**.** *P<0.05 vs. control EEECT CM fraction. †P<0.05 vs. control EEECT non-CM fraction.

2.3.2 Effect of cyclical mechanical stretch and SB202190 treatment on p38MAPK and Akt activities

Western blots indicated that total p38MAPK and α-actinin (normalized by β-actin) expression did not change in response to 48 hours cyclic mechanical stretch stimulation suggesting CM proliferation (Figure 2-3A). ELISA analysis showed that both p38MAPK and Akt phosphorylation levels increased following 2 hours cyclic mechanical stretch and decreased following 2 hours SB202190 treatment or concomitant SB202190 treatment with cyclic mechanical stretch (Figure 1-3B and 1-3C) at which EEECT contractile force and CM proliferation rate did not change from control EEECT (data not shown). Phosphorylated p38MAPK and Akt consistently increased following 48 hours cyclic mechanical stretch and

decreased following 48 hours SB202190 treatment or concomitant SB202190 treatment with cyclic mechanical stretch (Figure 2-3B and 2-3C).

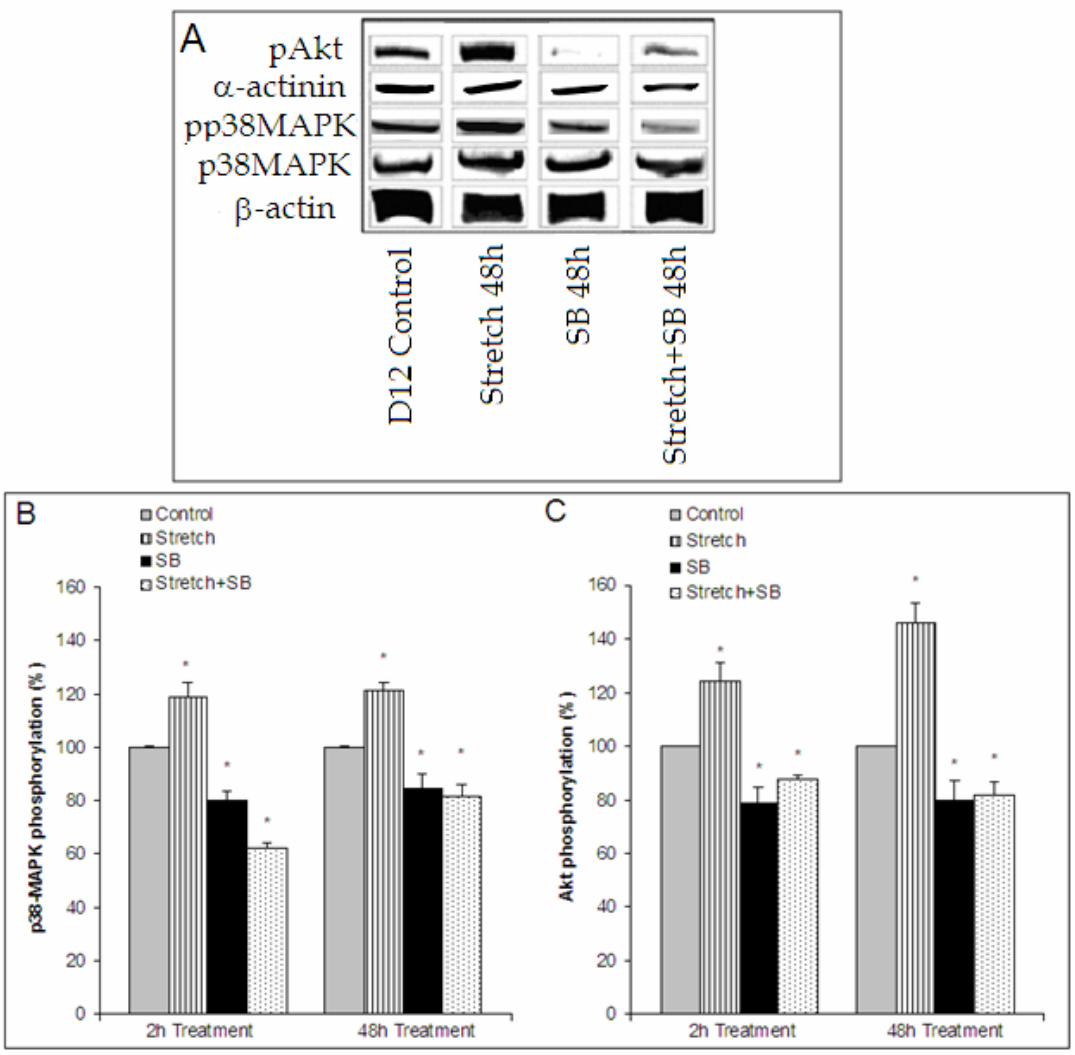

Figure 2-3. Representative western blots and ELISA analysis of EEECT p38MAPK and Akt expression following mechanical stretch stimulation and/or p38MAPK inhibition**. (A)** Stimulation or inhibition did not change β-actin, α-actinin, or p38MAPK non-phosphorylated expression. Stretch stimulation increased EEECT phosphorylated p38MAPK and phosphorylated Akt expression while inhibition and concurrent stretch and inhibition decreased phosphorylated p38MAPK and phosphorylated Akt expression. **(B and C)** phosphorylated p38MAPK and Akt expression increased following 2 and 48 hours of cyclic stretch, decreased following 2 and

48 hours of p38MAPK inhibition, and decreased following 2 and 48 hours of concurrent stretch and p38MAPK inhibition**.** **P*<0.05 vs. normalized control EEECT expression. †*P*<0.05 2h vs. 48h stimulation.

2.3.3 EEECT contractile force

All EEECT specimens displayed a positive Frank-Starling response to increased construct length (*P*<0.05). Cyclic mechanical stretch stimulation for 48 hours increased EEECT active stress at L_{max} [1.64 ± 0.09 mN/mm^2 (n=10), *P*=0.017] while p38MAPK inhibition reduced active stress [0.53 ±0.07 mN/mm^2 (n=8), *P*=0.04], as did the combination of p38MAPK inhibition and mechanical stretch [0.46 ±0.05 mN/mm^2 (n=8), *P*=0.025] compared to control EEECTs [1.00 ±0.06 mN/mm^2 (n=10)] (Figure 2-4).

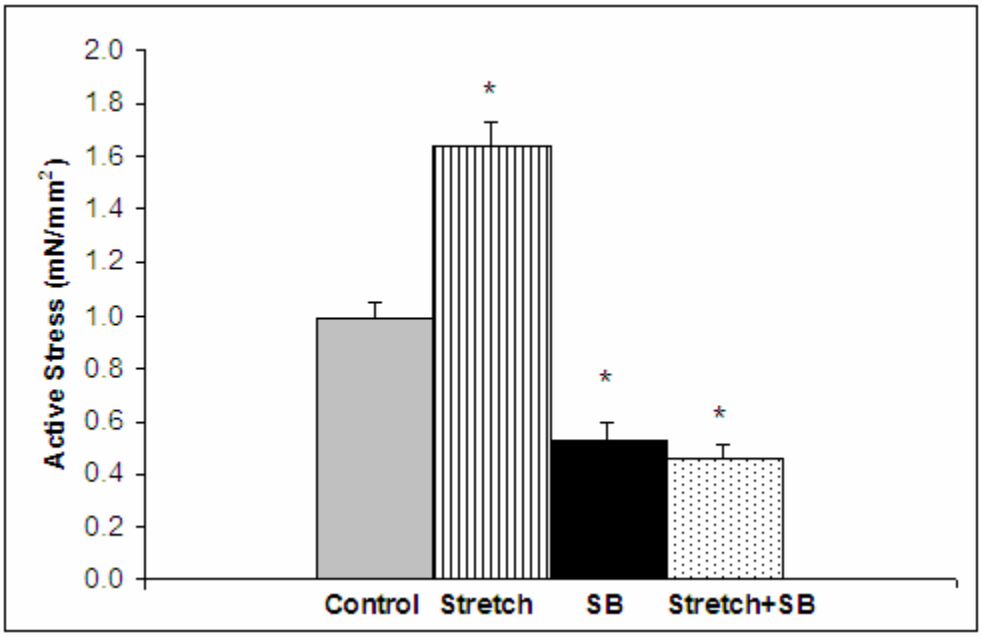

Figure 2-4. Active contractile force at L_{max} of culture day 12 EEECT**.** Active force of culture day 12 EEECT increased in response to cyclic stretch stimulation for 48 hours and decreased following either p38MAPK inhibition or concomitant stretch and p38MAPK inhibition. **P*<0.05 vs. control EEECT.

2.4 DISCUSSION

Increased mechanical loads trigger various molecular signaling pathways that can result in cardiac growth or pathologic hypertrophy in post-natal myocardium[106, 107, 148]. In contrast, the immature embryonic/fetal myocardium responds to increased mechanical loads via cellular proliferation (myocardial hyperplasia)[4, 149, 150]. In our previous study, we showed that engineered cardiac tissue from chick early embryonic ventricular cells, termed EEECT, maintains a relatively high cellular proliferation activity and cyclic mechanical stretch stimulation further increases cellular proliferation similar to the developing fetal myocardium[20]. However, it was unclear which cellular subpopulation, CMs or non-CMs, responds to the mechanical stretch within this *in vitro* engineered cardiac construct. In the present study, we found that both CMs and non-CMs proliferate within EEECT and that CMs, but not non-CMs, increase proliferation in response to cyclic mechanical stretch stimulation. In addition, mechanical stretch increased p38MAPK phosphorylation, which preceded increases in EEECT contractile force and CM proliferation. In contrast, the inhibition of p38MAPK significantly decreased CM proliferation activity and the negative effects of p38MAPK inhibition overrode the positive cyclic mechanical stretch stimulation effects on EEECT contractile function and CM proliferation.

There are currently conflicting results regarding the role of p38MAPK in the regulation of CM growth (hypertrophy) and survival[106, 142]. Many of these studies investigate post-natal (neonatal or adult) CMs. Extrapolation of the results from post-natal CMs to fetal CMs is difficult because of the marked phenotypic differences between fetal and post-natal CMs, including age-dependent changes in protein kinase expression, β-adrenergic signaling[83], contractile apparatus maturity, and most importantly, by the hyperplastic[84] versus

hypertrophic[85] responses to mechanical stress. Zimmermann et al. reported that culture day 14 engineered heart tissue (EHTs) generated using neonatal rat CMs morphologically resembled adult myocardium and the addition of mechanical stretch to the EHTs induced cardiac hypertrophy[47]. In our EEECT made from embryonic cardiac cells, we found that EEECT resembled the developing immature fetal myocardium and that mechanical stretch induced CM proliferation, not hypertrophy[20, 120]. The disparate culture time and CM type is likely responsible for these differing results, underlining the phenotypic differences between post-natal and fetal CMs. Olson et al. recently reported that p38MAPK activity increased in response to increase in hemodynamic loads in a fetal ovine myocardium suggesting a role for p38MAPK in regulating fetal CM proliferation[145, 151]. The stretch-induced increase in CM over non-CM phospho-histone H3 expression shown here may be dependent upon the activation of p38MAPK since it was abolished by the selective inhibitor SB202190. These results suggest that p38MAPK is a mediator of stretch induced fetal type CM proliferation within *in vitro* engineered cardiac tissue.

The observation that an increase in p38MAPK phosphorylation by cyclic mechanical stretch occurred coincident with increased Akt phosphorylation suggests that p38MAPK may regulate EEECT cell proliferation via Akt. Akt is a serine–threonine kinase and has been implicated in numerous intracellular processes including cell growth and survival[152, 153]. Akt has also been shown to be a downstream target of p38MAPK that can be directly regulated via gene transcription as well as by protein activation during myogenesis[154]. Previous work has indicated that both Akt[155] and p38MAPK[156] are important for myogenesis. Gude et al. has recently shown that Akt acts as a facilitator of cellular proliferation for cardiac progenitor cells and young committed CMs in the heart and that an increase in Akt correlated not only with

replicating cells, but also with increased GATA-4 expression[157]. Some myogenic specific transcription factor downstream targets of p38MAPK including GATA-4 and MEF2 have been shown to be activated directly by p38MAPK[158-160] and recent work has shown that the PI3 kinase pathway is involved in activating MEF2[154, 155]. Aouadi et al. reported that inhibition of p38MAPK activity reduced MEF2C expression and blocked CM lineage induction in embryonic stem cells suggesting that the p38MAPK effect could be due to MEF2C regulation[161]. We have shown that cyclic mechanical stretch stimulates p38MAPK and results in Akt activation and that inhibition of p38MAPK reduces Akt activation. These changes in p38MAPK and Akt content and activity within EEECT parallel changes in the CM proliferation. Therefore, it is likely that even though p38MAPK and Akt function via distinct, though parallel, signaling pathways, p38MAPK functions upstream of Akt in the response to mechanical stretch, suggesting that Akt function may be another important link in the regulation of CM proliferation.

Our data also suggests that p38MAPK activity within EEECT impacts contractile function in addition to cell proliferation. EEECT responded to mechanical stretch with increased active force and CM proliferation, which is similar to the developing fetal myocardium[92, 102, 162]. Cyclic mechanical stretch has previously been shown to induce a variety of cellular processes including activation of MAPKs[106-109], reprogramming of gene expressions[106, 107], and an increase in protein synthesis[106, 107] as well as trigger adaptive responses in muscle phenotype via the expression of contractile proteins[108, 110]. Recent studies in adult CMs have shown that p38MAPK activation upregulates Na^{+}-Ca^{2+} exchanger expression similar to cardiac hypertrophy and failure in adult myocardium[163]. In contrast, immature proliferative (not hypertrophic) embryonic/fetal CMs have different Na^{+}-Ca^{2+} exchanger properties from adult CMs and the changes in its properties depend on developmental stages[164, 165]. Some regulatory factors, PKA,

PKC, and cyclic nucleotides, of the Na^+-Ca^{2+} exchanger could also change expression, location, or compartmentalization with respect to developmental stages[165] which would also lead to altered Na^+-Ca^{2+} exchanger function in embryonic/fetal CMs compared to adult CMs. There are no previous reports that investigated the relationship between p38MAPK (and other MAPKs) and Na^+-Ca^{2+} exchanger function within developing immature CMs. We speculate that cyclic mechanical stretch mediated p38MAPK activity within EEECT may not upregulate Na^+-Ca^{2+} exchanger expression like what is seen in adult, mature CMs. Further investigation into the Na^+-Ca^{2+} exchanger functions within EEECT and its role in regulating the active contractile force along with CM proliferation following stretch induced p38MAPK activation is necessary.

2.4.1 Limitations

Several limitations should be noted in the present study. First, cyclic mechanical stretch selectively increased CM proliferation and both p38MAPK and Akt phosphorylation whereas p38MAPK inhibition reduced both CM and non-CM proliferation activities as well as reduced Akt activity. These results suggest that the positive cyclic mechanical stretch effects on CM proliferation may not be directly mediated by p38MAPK activity of CMs. The noted increase in p38MAPK activity and Akt activity induced by mechanical stretch may be independent events. It is also important to note that EEECT contains both CM population [65 to 75% in cell number, more than 90% in cellular volume ratio[20]] and non-CM population, such as fibroblasts, endothelial cells, vascular smooth muscle cells, etc. CM-to-non-CM and CM-to-extracellular matrix interactions may greatly influence CM proliferation and p38MAPK/Akt activities. Second, the p38MAPK inhibition dose used in the current study (10μM, SB202190) may also have toxic effects on both CM and non-CM populations other than its noted effects on cellular

proliferation. In our preliminary study, we found that 1 and 5μM SB202190 treatment for 48 hours tended to decrease p38MAPK phosphorylation levels and CM proliferation rate (by histone H3 positive cell counting) while there was no change in the EEECT contractile force. Only 10μM SB202109 treatment showed statistically significant decreases in p38MAPK phosphorylation, CM proliferation, and EEECT contractile force production. We note that EEECT tissue architecture stained by α-sarcomeric actinin did not vary between treatment doses. Therefore, we chose the 10μM SB202190 treatment dose for p38MAPK inhibition for the current study. However, other factors remain to be investigated, such as CM apoptosis, or altered CM metabolism, which could be triggered by p38MAPK inhibition[166]. Third, we have not yet determined the roles of other MAP-kinases, such as JNK, or ERK that have also been closely associated with the regulation of CM growth, survival, and proliferation. These alternate kinases may directly or indirectly participate in the regulation of both CM and non-CM responses to cyclic mechanical stretch. Forth, while our current cyclic mechanical stretch protocol significantly increased EEECT force generation and CM proliferation, alternate stretch protocols may be optimal for immature CMs at different developmental stages. Finally, our finding of positive mechanical stretch effects on immature CM derived from avian and rat embryo (unpublished data) myocardium need to be confirmed for immature CM derived from large mammals or in stem / progenitor cell-derived CMs. Nevertheless, our results suggest that immature CM proliferation can be positively regulated by cyclic mechanical stretch and unwanted, excessive CM and non-CM proliferation can be negatively regulated by p38MAPK inhibition within this *in vitro* tissue culture environment which is one of the key factors for the development of an optimal tissue culture method of functioning CM preparation for cardiac repair.

2.4.2 Conclusion

In summary, immature (fetal) CMs within a 3D engineered cardiac construct increased CM proliferation in response to cyclic mechanical stretch and this proliferative response is blocked by p38MAPK inhibition. Our findings confirm a role for cyclic mechanical stretch and p38MAPK in the regulation of CM proliferation within tissue engineered cardiac constructs that may be relevant in designing optimized donor CM preparation and culture approaches for cardiac repair paradigms. Further research is required to define the underlying mechanisms by which p38MAPK activation regulates the fetal CM proliferation, growth, and mechanical properties.

3.0 ENGINEEDED FETAL CARDIAC GRAFT PRESERVES CM PROLIFERATION AND SUSTAINS CARDIAC FUNCTION WITHIN POST-INFARCTED MYOCARDIUM

3.1 INTRODUCTION

Recent studies suggest that a three-dimensional (3D) tissue culture environment is necessary for efficient CM survival, functioning myocardial tissue formation *in vitro*, functional integration, and sustained cardiac recovery[12, 13, 37, 42, 45, 53, 118]. Primary neonatal rat cardiac myocytes have an intrinsic ability to contract synchronously in culture and attach to 3D matrix scaffolds, and therefore have been used extensively for generating spontaneously beating engineered cardiac tissues[37, 40-42, 46-49, 50]. Using neonate CMs, pioneering studies from Eschenhagen and Zimmermann validated an engineered heart tissue paradigm for cardiac graft implantation onto post-infarct left ventricular (LV) myocardium[12, 13]. Their results were reported for 4 weeks following graft implantation, and graft survival required the use of immunosuppression[13].

In contrast to neonatal CMs, studies suggest that fetal CMs display a high level of cell survival and sustained cardiac function when transplanted into injured myocardium[11, 13, 75, 167-1172]. Embryonic/fetal CMs possess high proliferative activity during development which declines shortly after birth and terminally differentiated mature CMs have limited proliferative activity[173, 174].

As shown previously and in 2.0, EEECT, 3D engineered cardiac tissue from embryonic chick cardiac cells, maintains high cellular proliferation activity and contractile properties that mimic the native developing fetal myocardium[20]. In response to cyclic mechanical stretch stimulation, chick EEECT increases CM proliferation, rather than the cellular hypertrophy response noted in adult and neonate CMs[20, 120]. Therefore, in the current study, we tested the hypothesis that the proliferating fetal CMs within engineered cardiac tissue graft maintain CM proliferative activity *in vivo*, survive as a donor myocardial tissue, and contribute to the cardiac functional recovery of injured recipient myocardium in a syngeneic rat model.

3.2 METHODS

3.2.1 Experimental animals

Gestational day 14 time-pregnant, neonatal day 3, and 12 week-old adult female Lewis rats weighing 200g to 250g were used (Harlan Sprague Dawley Inc., Indianapolis, IN). In order to track the fate of implanted GFP(+)-CMs within EFCT, we used gestation day 14 EGFP(+)-transgenic rat fetal hearts identified by using a fluorescent light (Dark Reader Stop Lamp, Clare Chemical Research, Dolores, CO) during heart excision from the fetuses and female adult nude rats as recipients (200 to 250g body weight). The EGFP-transgenic rats were originally generated by Dr. Masaru Okabe (University of Osaka, Osaka, Japan)[175] and EGFP transgenic rat colonies were maintained within the animal facility of the Children's Hospital of Pittsburgh of UPMC. All experimental protocols followed the National Institutes of Health guidelines for

animal care and were approved by the University of Pittsburgh's Institutional Animal Care and Use Committee and Children's Hospital of Pittsburgh Animal Research Care Committee.

3.2.2 Rat engineered fetal cardiac tissue (EFCT) and engineered neonatal cardiac tissue (ENCT) construction

For EFCT construction, pregnant mothers were anesthetized using 3% isoflurane inhalation with 100% oxygen and hysterectomy was performed. Immediately after hysterectomy, the mother was euthanized by induced asystole under 5% isoflurane anesthesia. The excised uteri were transferred to a sterilized Petri-dish filled with cold PBS buffer and 1% antibiotic-antimycotic solution, which contains 100units/mL of penicillin, 100units/mL of streptomycin, and 0.25μg/mL of amphotericin-B (Invitrogen, Carlsbad, CA), and the fetuses were excised by hysterotomy, and then fetal hearts were harvested. Great vessels and atrium were removed from each fetal heart and ventricular tissue was collected and pooled. For ENCT construction, neonatal day 3 rat pups were euthanized by cervical truncation under 5% inhaled isoflourane with 100% oxygen and the ventricular tissue was excised and pooled. Pooled fetal or neonatal ventricles were then enzymatically digested by 2mg/ml of collagenase type II followed by 0.05% trypsin-EDTA solution (Invitrogen). Isolated cells were preplated for 1 hour and then cultured on a gyratory shaker (50 to 55 rotations/min) for 24 hours to reaggregate viable CMs[20]. Approximately 5.0 x 10^5 of cardiac cells / construct (350cells/cell aggregate, 3.0 x 10^6/ml) were mixed with acid-soluble rat-tail collagen type I (Sigma, St. Louis, MO) and matrix factors (Matrigel, BD Science, Franklin Lakes, NJ)[20]. Cell/matrix mixture was performed as follows. 1) Cells were suspended within a culture medium (Modified Dulbecco's Essential Medium, Invitrogen) containing 20% FBS (Invitrogen). 2) Acid-soluble collagen type I solution (pH 3)

was neutralized with alkali buffer (0.2 M NaHCO3, 0.2 M HEPES, 0.1 M NaOH) on ice. 3) Matrigel (15% of total volume, BD Sciences) was added to the neutralized collagen solution. 4) Cell suspension and matrix solution were mixed. The final concentration of collagen type I was 0.67 mg/ml.

Cylindrical-shaped EFCT or ENCT were constructed by using a collagen type I-coated silicone membrane culture plate (Tissue Train, Flexcell International, Hillsborough, NC) and FX-4000TT system (Flexcell International). Briefly, the center of the silicone membrane of a Tissue Train culture plate was deformed by vacuum pressure to form a 20-mm-length x 2-mm-width trough using a cylindrical loading post (FX-4000TT). Approximately 200µl of cell/matrix mixture was poured into the trough and incubated for 120min in a standard CO_2 incubator (37°C, 5% CO_2) to form a cylindrical-shaped construct. Both ends of the construct were held by anchors attached to the Tissue Train culture plate. When the tissue was formed, the culture plate was filled with a growth medium containing 10% FBS (Invitrogen) and 1% antibiotics/antimycotics solution (Invitrogen). The vacuum pressure was then gradually released, and the construct was floated within the growth medium. Constructed engineered tissue was cultured for 7 days and the culture medium was changed every other day.

3.2.3 Contractile force measurement

Contractile force was measured on culture day 7 EFCT (n=6) and ENCT (n=7) as previously described[20]. In brief, each engineered cardiac construct was excised from anchors of Bioflex culture plate and transferred to a cold (25^{o}C) calcium free Ringer solution containing (in mM): 135.0 NaCl, 4.0 KCl, 10.0 Trizma-HCl, 8.3 Trizma-base, 11.0 glucose and gassed with 95% O_2 /5% CO_2 (pH 7.4). One end of the EFCT or ENCT was attached using 10-0 mono-

filament nylon sutures to a rigid stainless steel bar connected to force transducer (model 403A, Aurora Scientific, Ontario, Canada) and the other end to a rigid stainless steel bar mounted on a micromanipulator (Figure 3-1A). The perfusion chamber containing the construct was then filled with warmed buffer (37^{o}C, 2ml chamber volume) perfused at 1ml/min with 2mM [Ca^{2+}] Ringer solution. We performed measurement of force-length relations followed by 1μM isoproterenol (ISP) treatment from the same construct. After 10 minutes pre-conditioning of the construct at a slack length (by adjusting construct length as the same length as that in a Bioflex culture plate) under perfusion of oxygenized, 2mM [Ca^{2+}] ion containing warmed ringer solution (baseline ringer solution), the tissue was electrically stimulated at 1Hz, 4msec, 50 to 70V using a field stimulator for 5 minutes. We then measured active force-length relations. The active contractile force was measured at given strain (0, 5, 10, and 15% elongation from the original length). We repeated force measurement at given length 3 times and averaged in each construct. We note that the weakening of force was not found throughout the test at all given tissue length. Measured force at given length were averaged in each construct. The construct was then maintained at $L_{0.15}$ (15% elongation from the original length) and was perfused for 5 to 10 minutes with baseline ringer solution and then treated with 1μM ISP. The contractile force was monitored for 5 minutes during ISP treatment and the largest contractile force was measured as the contractile response of ISP treatment at 5 minutes after ISP treatment. After the force measurement, ISP was washed out by baseline ringer solution to confirm force level was returned to the baseline. We repeated ISP treatment for 3 times and averaged in each construct.

3.2.4 Chronic left ventricular infarction model

EFCT or ENCT recipient adult (Lewis or nude) rats were anesthetized using 3.0% isoflurane inhalation with 100% oxygen gas followed by endotracheal intubation and connection to a rodent volume controlled mechanical ventilator (Model 683, Harvard Apparatus, Holliston, MA). The heart was exposed through a left thoracotomy, monitoring electrocardiogram (THM 1000, VisualSonics, Toronto, Canada). The proximal left anterior descending coronary artery was ligated with 7-0 polypropylene. Myocardial ischemia was confirmed by regional cyanosis and changes in electrocardiogram (ST-segment elevation). The incision was closed in layers with 4-0 silk continuous sutures[176]. A total of 45 rats underwent left coronary artery ligation. 7 animals died within 24 hours of coronary artery ligation and 38 animals survived. These survived rats were considered as cardiac graft recipients. Therefore, survival rate at 2 weeks after permanent left coronary artery ligation was 83.3%[176].

3.2.5 EFCT or ENCT implantation

Two weeks following coronary artery ligation (pre-implantation), animals were anesthetized with isoflurane and the infarction size and cardiac function were assessed by transthoracic echocardiography. LV infarction size was estimated in a standard LV short-axis view by the percentage of scar area (akinetic or dyskinetic regions) to LV free wall area[176]. We excluded 4 Lewis rats due to insufficient LV infarction and 34 rats with infarcts greater than 25% of the LV free wall were included in the present study. We performed CM proliferation (histone H3) and apoptosis (caspase-3) assays at 3 days after EFCT graft implantation (n=6). Eight EFCT implanted, 6 ENCT implanted, and 8 sham operated animals were studied for longitudinal

echocardiography and histological assessment at 8 weeks after graft implantation. We also used 3 additional nude rats with infarcts to allow EFCT cell tracking and to evaluate EFCT derived cell fate. The LV anterior wall was exposed through left thoracotomy again. Using 7-0 polypropylene with peripheral sutures, the anterior infarcted myocardium was covered with 4 engineered tissue constructs into the LV circumferential direction (Figure 3-1B). For the sham operated group, a thoracotomy was performed 2 weeks after coronary ligation, but no EFCT implantation was performed. EGFP positive transgenic rat EFCTs (EGFP-EFCTs) were implanted onto post-infarcted LV myocardium in nude rats.

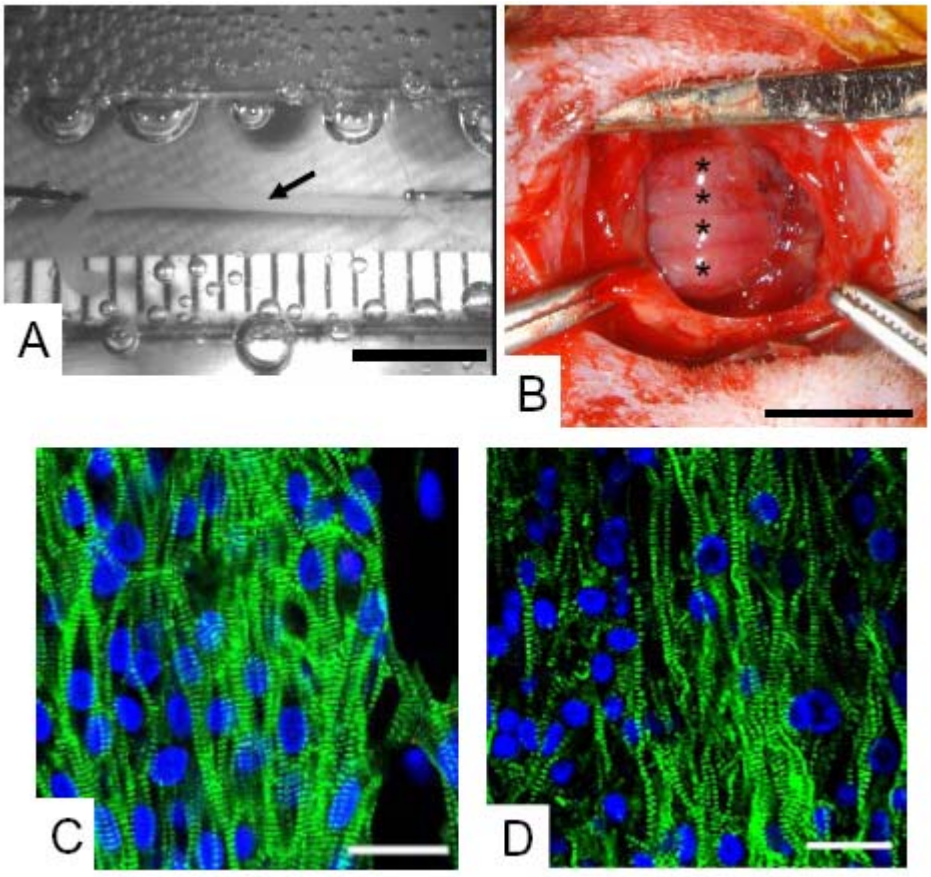

Figure 3-1. External shape of constructed EFCT, EFCT implantation onto post-infarcted LV surface and tissue structure of EFCT. **(A)** Culture day 7 cylindrical shape EFCT is suspended within a mechanical testing chamber and is field stimulated to measure contractile force. Minor scale indicates 1mm**.** Photograph of EFCT graft implantation onto the post-infarcted myocardium. **(B)** Four EFCTs (indicated by *) were implanted to

cover the infarct myocardium. Scale bar indicates 5mm**. (C)** Confocal microscope image of α-sarcomeric actinin and DAPI staining of culture day 7 EFCT tissue. CMs oriented into the longitudinal axis **(white arrows)** of the EFCT forming myocardial tissue like structure**. (D)** Confocal microscope image of culture day 7 chick EEECT tissue**.** Rat EFCT myocardial tissue architecture **(C)** is similar to chick EEECT **(D)**. Scale bars indicate 20μm in C and D.

3.2.6 Histological assessment

Culture day 7 EFCTs or ENCTs were fixed with 4% paraformaldehyde/PBS for 15 minutes. For BrdU staining each tissue was incubated with 60μg/ml bromodeoxyuridine (BrdU, Sigma, St. Louis, MO) for 16 hours prior to fixation, then embedded in a 13% polyacrylamide gel oriented in the longitudinal direction of the construct, and 150μm thickness serial sections were made using a standard vibrating microtome (Vibratome-1000, Vibratome.com, St Louis, MO)[20]. For post-implant EFCT or ENCT tissue and LV myocardium, the hearts were exposed under 3.0% isoflurane inhalation with 100% oxygen gas and arrested by apical injection of 2 ml of a hypothermic arresting solution (28mmol/l NaCl, 100mmol/l KCl, 36mmol/l $NaHCO_3$, 2.0mmol/l $MgCl_2$, 1.4mmol/l Na_2SO_4, 11mmol/l dextrose, 30mmol/l butanedione monoxime, 10,000U/l of heparin). The embedded frozen LV tissues were serially sectioned at 8μm in the LV transverse direction using a standard cryo-microtome (MICROM HM505E, Pacific Southwest Lab Equipment Inc. Vista, CA). Sections were permeabilized with 0.1% Triton X-100 and stained for BrdU using a mouse-monoclonal anti-BrdU antibody (Molecular Probes, Eugene, OR) and DAPI (Vector Laboratories, Burlingame, CA). Mitotic phase CMs were identified by triple staining with anti-α-sarcomeric actinin (EA53, Sigma), anti-phospho-S10 Histone H3 (Upstate cell signaling solutions, Temecula, CA) with Alexa Flour secondary antibodies, and DAPI (Vecta-Shield, Vector Labs, Burlingame, CA)[120]. To identify cellular

apoptosis, sections were triple-stained with anti-α-sarcomeric actinin (EA53, Sigma), anti-active caspase-3 (Abcam, Cambridge, MA), and DAPI. Capillary vessels formation was identified using a triple staining of sections with anti-α-sarcomeric actin (Abcam), anti-CD31 (Abcam), and DAPI (Vecta-Shield).

3.2.7 Identification of CM proliferation or CM apoptosis

We reconstructed 3D composite images from stacks of z-axis optical scans of each stained sample using a standard laser confocal microscope system (FV1000, Olympus, Tokyo, Japan) and Scion Image software (Scion Corp, MD)[120]. The images were visualized at different rotation angles to identify proliferating/apoptotic CMs by co-localization of phospho-histone H3/active Caspase-3 positive nuclei staining and α-sarcomeric actinin staining. To quantify total cellular and CM proliferation activities, 10-20 regions from multiple representative sections from each EFCT or ENCT tissue, or non-infarct areas of EFCT implanted myocardium (>200μm apart from graft tissue implantation site or infarction border in each section), which expressed α-sarcomeric actinin similar to the normal, non-infarcted myocardium, were randomly chosen for analysis at 400x or 600x magnification. Total cellular proliferation (both CM and non-CM fractions), and CM proliferation or apoptosis ratios were calculated as: [Total cellular proliferation] = [BrdU (+) nuclei] / [DAPI (+) nuclei] (%) and [CM proliferation or CM apoptosis] = [Histone H3 or Caspase-3 (+) nuclei within α-sarcomeric actinin (+) cells] / [DAPI (+) nuclei] (%), respectively. To measure CM ratio of EFCT and ENCT at pre- and 8 weeks after graft implantation, we randomly captured at least 20 fields at 400x magnification of α-sarcomeric actinin/DAPI sections in each tissue sample and the CM ratio was calculated as, [α-sarcomeric actinin positive nuclei number]/[total nuclei number] x 100 (%).

3.2.8 Capillary density measurement of EFCT and ENCT implanted myocardium

We measured capillary density of EFCT (n=8), ENCT (n=6) and sham (n=8) post-infarct myocardium at 8 weeks after graft implantation by counting von Willebrand factor (vWF) positive cells. Using a confocal microscope, 20 non-overlapped image fields at 400x magnification were randomly selected in each section and vWF positive cells were counted. Data were normalized as vWF(+) counts/mm^2.

3.2.9 Assessment of *in vivo* recipient cardiac function

LV function was measured by non-invasive echocardiography (Acuson Sequoia and 13-MHz 15L8 probe) at pre-implantation (2 weeks after coronary artery ligation), 4 weeks, and 8 weeks (10 weeks after coronary ligation) after graft implantation. End-diastolic area (EDA) and end-systolic area (ESA) of the LV cavity were measured by endocardial planimetry, and %LV fractional area change (%FAC) was measured as [(LVEDA – LVESA)/LVEDA] x 100%. Echocardiography was performed using isoflurane anesthesia (1.5% with 100% oxygen) via nose cone. LV pressure was measured at 8 weeks after EFCT implantation prior to euthanasia for histological assessment. Rats underwent anesthesia with isoflurane and intubation followed by introduction of a pressure-transducer tip Millar catheter (model SPR-1000, Millar Instruments, Austin, TX) retrograde from the right carotid artery into the LV. LV pressure was acquired to calculate EDP, P_{max}, $+dP/dt_{max}$, and $-dP/dt_{min}$ for an analysis with a custom LabVIEW virtual instrument.

3.2.10 Statistical analysis

Data are expressed as mean ± SE. Student *t*-test was performed to compare the data of LV pressure measurement. Paired Student *t*-test was performed to compare the data of *in vitro* active contractile force and contractile response to the ISP stimulation. One-factor analysis of variance (ANOVA) with Turley post-hoc test was performed to compare capillary density. Two-factor ANOVA with a Tukey post-hoc test was performed to compare the BrdU, phospho-histone H3, or active caspase-3 positive cells. Two-factor repeated ANOVA with a Tukey test was performed to compare the echocardiogram data. Statistical significance was defined by a value of $P<0.05$. All calculations were performed using SigmaStat (Systat Software Inc, Point Richmond, CA).

3.3 RESULTS

3.3.1 *In vitro* EFCT morphology and contractile force

Both EFCT and ENCT displayed spontaneous tissue contraction from culture day 4 and EFCT CM orientation within engineered construct assessed by α-sarcomeric actinin staining was similar to culture day 7 chick EEECT using embryonic day 7 chick cardiac cells (Figure 3-1C and 3-1D)[20]. Culture day 7 EFCT and ENCT generated active contractile force in response to cyclic field electric stimulation and displayed a positive Frank-Starling response to increased tissue longitudinal length ($P<0.05$, Figure 3-2A). While active contractile force of ENCT at $L_{0.15}$ was much higher than EFCT (P=0.001), physiologically maximum isoproterenol (ISP)

stimulation (1μM) did not increase contractile force in both tissues suggesting that both fetal and neonatal CM phenotypes within the cardiac construct remain immature (Figure 3-2B, Table 3-1).

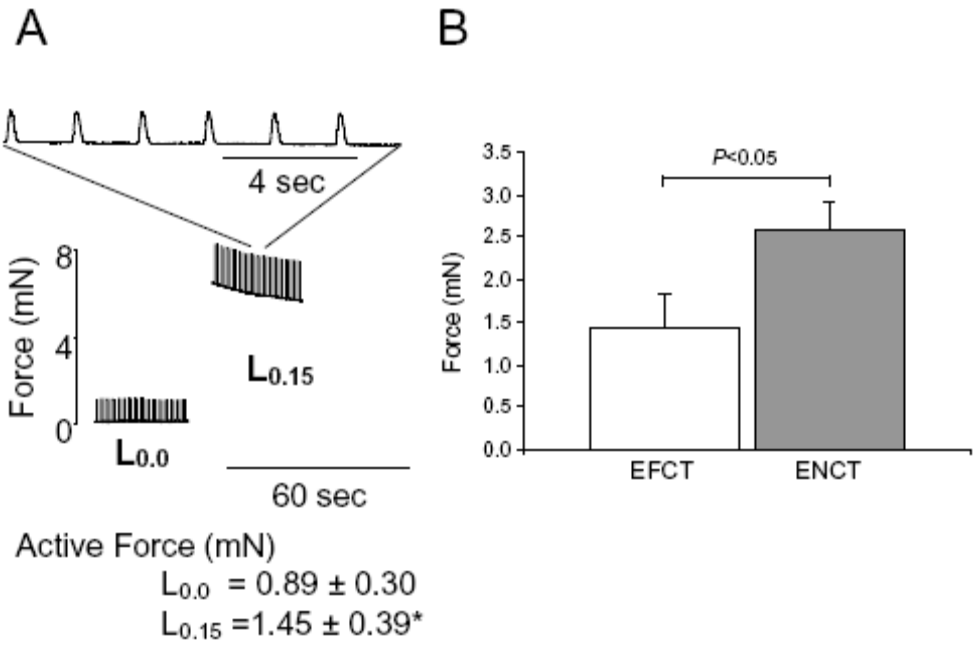

Figure 3-2. Culture day 7 EFCT and ENCT contractile force. **(A)** Representative contractile force waveform tracing at slack length (L_0) and 15% stretched length ($L_{0.15}$). EFCTs were field stimulated by an electric pacing stimulator at 1Hz. EFCT increased contractile force at L_{max}. **(B)** Comparison of maximum active force at $L_{0.15}$ between EFCT and ENCT. ENCT active force was significantly higher than EFCT at culture day 7.

Table 3-1. *In vitro* contractile response of EFCT and ENCT to β-adrenergic stimulation. Data are mean ± SE. Baseline active force at $L_{0.15}$, *; P<0.05 vs. ENCT. Five minutes after 1μM isoproterenol (ISP) stimulation did not increase active contractile force in both EFCT and ENCT. Contractile force was measured under presence of 2mM [Ca^{2+}] containing Ringer solution.

	Baseline (Pre)	1μM-ISP	% of Change vs. Pre	*P*
EFCT (n=7)	1.45 ± 0.39	1.67 ± 0.43	13.8 ± 8.5	0.37
ENCT (n=8)	2.6 ± 0.31*	2.99 ± 0.59*	15.2 ± 10.1	0.31

3.3.2 *In vitro* culture day 7 EFCT and ENCT total cellular and CM proliferation

Total cellular proliferation ratio of culture day 7 EFCT assessed by BrdU (DNA synthetic phase) assay was significantly higher than that of culture day 7 ENCT [23.3 ± 3.0% (n=7) vs. 1.69 ± 0.4% (n=8), P=0.001]. CM proliferation ratio of EFCT assessed by triple staining of phospho-histone H3 (mitotic phase), α-sarcomeric actinin, and DAPI, was also significantly higher than that of ENCT (16.0 ± 3.7‰ vs. 6.8 ± 0.7‰, P=0.018).

3.3.3 EFCT graft survival after EFCT implantation onto post-infarcted syngeneic adult LV myocardium

There were no early or late postoperative deaths related to graft implantation in any experimental group. Two weeks after EGFP-EFCT implantation onto post-infarcted nude rat myocardial surface, GFP positive cells within EFCT did not migrate out from the implanted EFCT and maintained EFCT myocardial tissue integrity (Figures 3-3A to 3-3C). At 8 weeks after Lewis rat graft implantation, the implanted grafts were still recognized without dislocation from the original implanted area and the grafts were merged with host LV surface by visual inspection (Figure 3-3D). The implanted grafts were covered with thin connective tissue and no strong adhesions with the chest wall were found. Hematoxylin-eosin (HE) staining of microtome sections revealed that implanted EFCTs and ENCTs were recognized as an eosin positive muscle like tissue at the implanted sites (epicardial surface) of infarcted myocardium in all hearts, which was not observed in the sham operated LVs (Figure 3-3E, upper panel). Capillary vessel formation was also recognized within implanted EFCT. Implanted grafts were positive to α-sarcomeric actinin and the high magnification images showed that CMs within implanted EFCTs

preserved a typical striated sarcomere structure (Figure 3-3E, middle and lower panels). CM ratio identified by α-sarcomeric actinin positive nuclei of EFCT or ENCT at pre-implantation was similar to each other (60.9±3.8% in EFCT vs. 60.4±6.6% in ENCT, P=1.0, ANOVA), whereas CM / non-CM ratio of EFCT at 8 weeks after implantation was higher than that of ENCT (33.8±7.2% in EFCT vs. 13.4±2.7 in ENCT, P=0.039) suggesting that EFCT retains higher CM fraction than ENCT 8 weeks after graft implantation. We note that typical tumor-like tissue formations assessed by HE staining were not found in all graft implanted LVs.

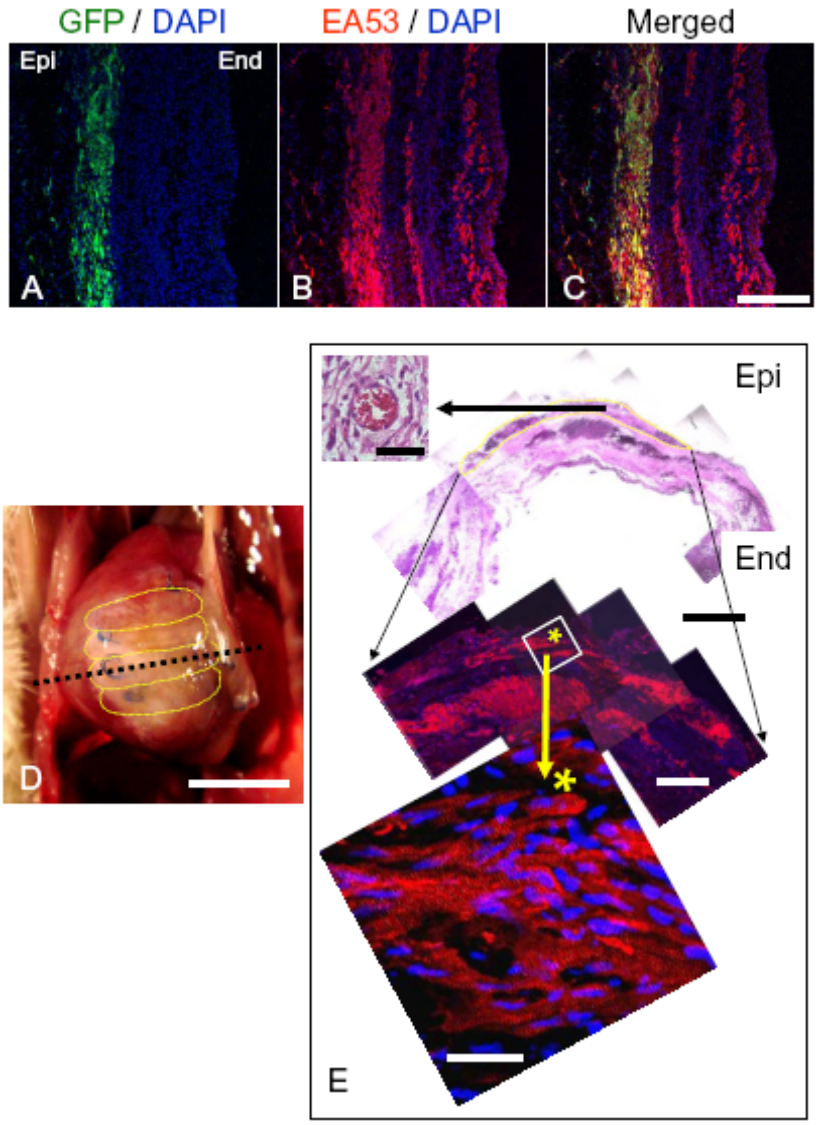

Figure 3-3. Histological assessments of implanted EFCT fate within post-infarcted LV myocardium. ***(A-C)*** Representative fluorescent histological sections of 2 weeks after EGFP transgenic EFCT implantation onto post-infarcted nude rat LV myocardium. Cells within EFCT stayed within the implanted site and preserved the graft myocardial tissue structure *in vivo*. Green color indicates GFP signal, red color indicates α-sarcomeric actinin, and blue color indicates nuclei (DAPI). Scale indicates 50μm. ***(D)*** Implanted EFCTs were well merged onto host infarcted myocardial surface and thin connective tissue covered EFCT implantation site. ***(E)*** Yellow dot curves indicate implanted EFCTs and black dotted line indicates histological section of. Scale indicates 10mm. ***(E)*** Implanted EFCT were recognized at epicardial implantation sites in all samples at 8 weeks after graft implantation. Capillary vessel formation was found within implanted EFCT **(insert)**.

Immunohistochemistry revealed that implanted EFCT preserved myocardial tissue and the α-sarcomeric actinin staining showed typical striated muscle patterns indicating that EFCT maintained its myocardial tissue structure. Scale bars indicate 50μm **(E insert)**, 500μm **(HE staining, upper panel)**, 250μm **(middle panel)**, and 20μm **(lower panel)**, respectively.

3.3.4 Capillary vessel formation within EFCT and ENCT implanted myocardium

The vWF positive cells were recognized well within EFCT or ENCT implanted post-infarcted myocardium (Figure 3-4A to C). The capillary density of EFCT (133 ± 5 counts/mm^2) or ENCT (115 ± 10 counts/mm^2) implanted LV myocardium was significantly higher than infarction controls (68 ± 5 counts/mm^2, P<0.05, ANOVA, Figure 3-4D and Table 3-2). However, the capillary densities within donor EFCT or ENCT grafts were the same (EFCT: 183 ± 16 counts/mm^2, ENCT: 176± 10, respectively). These results suggest that both EFCT and ENCT implantation promotes capillary vessel formation within post-infarcted myocardium and the capillary density within donor graft does not influence donor graft CM proliferation and apoptosis activities.

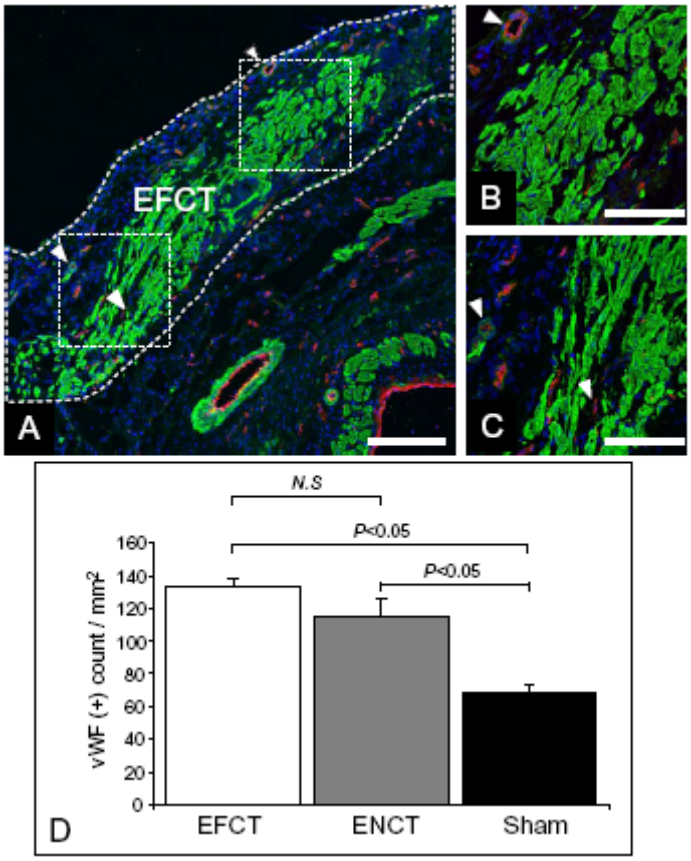

Figure 3-4. Capillary vessel formation of EFCT graft implanted post-infarct myocardium at 8 weeks after graft implantation and capillary density count in EFCT, ENCT implanted myocardium. **(A)** Triple staining of α-sarcomeric actinin (green), von-Willebrand factor (vWF, red), and DAPI in EFCT graft implanted myocardium at low magnification, scale indicates 200μm. **(B and C)** Higher magnification images, scale indicates 100μm. Capillary formation (vWF positive nuclei) was detected though the post-infarcted myocardium and vessels also penetrated into EFCT graft. **(D)** Capillary density assessed by vWF positive cell counting within post-infarcted myocardium indicates that both EFCT and ENCT increased capillary density significantly higher than sham-operated myocardium (P<0.05), whereas these between EFCT and ENCT was not statistically different.

3.3.5 *In vivo* EFCT graft CM proliferation and apoptosis activities

We assessed phospho-histone H3 and active caspase-3 positive CM ratios within implanted EFCT and non-infarcted host myocardium at 3 days and these within EFCT, ENCT,

and non-infarcted host myocardium at 8 weeks after graft implantation (Figure 3-5, Table 3-2). Phospho-histone H3 positive CM ratios of EFCT at 3 days and 8 weeks after implantation remained at the same level as pre-implantation [12.8 ± 4.0‰ (pre-implantation), 16.7 ± 9.0‰ (3 days), and 21.9 ± 4.1‰ (8 weeks), respectively, P=0.39] and were higher than the host non-infarcted myocardium 8 weeks after graft implantation (0.8 ± 0.1‰, P=0.01 vs. EFCT at 8 weeks, Figure 3-5C). Phospho-histone H3 positive CM ratio of ENCT at 8 weeks after implantation was lower than that of EFCT (1.1 ± 1.2‰, P<0.001 vs. EFCT, Table 3-2). Active caspase-3 positive CM ratio of EFCT at culture day 7 was 0.4‰ ± 0.1‰, which was lower than histone positive CM ratio (P<0.001 vs. CM Histone positive ratio). While CM caspase-3 ratio increased at 3 days after graft implantation in comparison to pre-implantation (culture day7), the caspase-3 positive ratios remained the same at 3 days and 8 weeks after implantation [2.3 ± 1.5‰ (3 days), and 3.0 ± 1.0‰ (8 weeks), respectively, P=0.29]. The CM caspase-3 positive ratio of EFCT was at a similar level as the host non-infracted myocardium, whereas that of ENCT was not detected at 8 weeks after graft implantation (Figure 3-5D, Table 3-2).

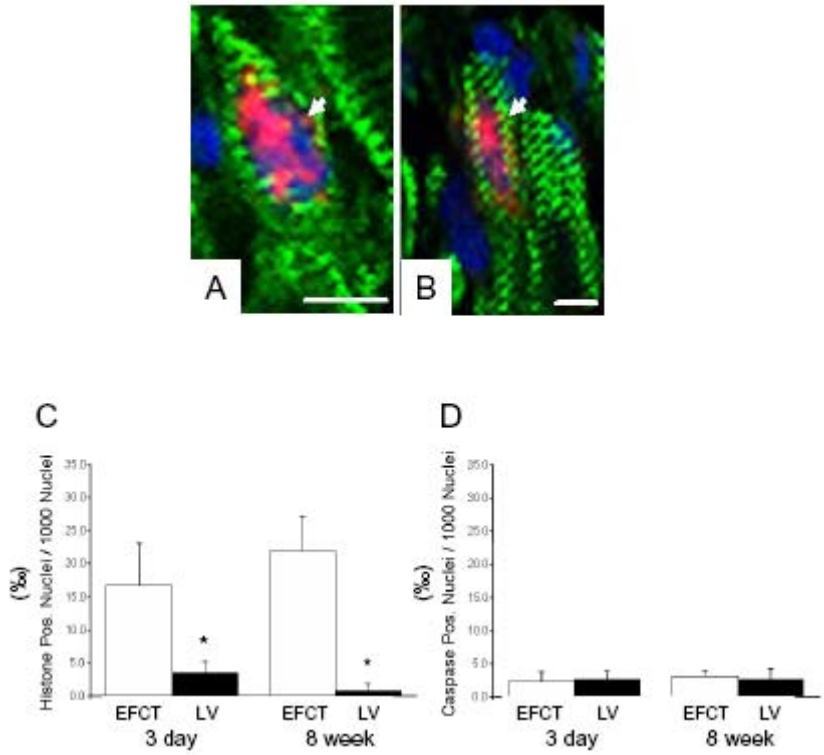

Figure 3-5. Cardiomyocyte proliferation and apoptosis of implanted EFCT and remote recipient myocardium. **(A and B)** Identification of phospho-histone H3 positive CM nuclei and caspase-3 positive CM nuclei, respectively. **(C)** Phospho-histone H3 positive CM ratios at 3 days and 8 weeks after the implantation were maintained at the same levels as pre-implantation. The CM proliferation rate was higher than recipient myocardium at both 3 days and 8 weeks. **(D)** Active caspase-3 positive CM ratios of implanted EFCT remained low and were at the same levels as recipient myocardium. *; $P<0.05$ vs. EFCT (Tukey post-hoc test, ANOVA).

Table 3-2. Phospho-histone H3 and Caspase-3 positive CM ratios of EFCT and ENCT at 8 weeks after implantation. Data are mean ± SE. *; $P<0.05$ vs. ENCT. Remote LV; non-infarct LV myocardium which was at least 200μm apart from EFCT implant border. EFCT showed higher CM proliferation and apoptosis ratios in comparison to ENCT and Remote LV at 8 weeks after graft implantation.

	EFCT (n=8)	ENCT (n=6)	EFCT Remote LV (n=8)
Phospho Histone-H3 (‰)	21.9 ± 4.1 *	1.1 ± 1.2	0.8 ± 1.0
Caspase-3 (‰)	3.0 ± 1.0 *	0.0 ± 0.0	2.6 ± 1.6

3.3.6 Cardiac function of EFCT and ENCT implanted LV

At 2 weeks after permanent coronary artery ligation (pre-implantation state, 0 week) LV EDA was increased approximately twice larger than pre-coronary artery ligation state (n=34, pre-coronary ligation EDA; 0.34 ± 0.02cm^2, 2 weeks after ligation EDA: 0.68 ± 0.03cm^2, %EDA change after coronary ligation; 199 ± 10% from pre-coronary artery ligation, P<0.001, paired t-test) and LV FAC was decreased less than half of pre-coronary artery ligation state (pre-coronary ligation FAC; 61 ± 1.4%, 2 weeks after ligation FAC: 26 ± 2.6%, %FAC change after coronary ligation; 42 ± 4.0% of pre-coronary artery ligation state, P<0.001) indicating that the permanent coronary artery induced post-myocardial infarcted heart failure (LV dilatation and impaired LV contraction). Longitudinal echocardiography after graft implantation showed that the sham operated LVs further increased EDA at 8 weeks (P<0.001, 8 weeks vs. 0 week), whereas EFCT or ENCT implanted LVs did not increase EDA indicating that implanted EFCTs or ENCT prevented further LV dilatation (Figure 3-6A). LV FAC decreased in the sham operated LV by 8 weeks (P=0.030, 8 weeks vs. 0 week) whereas ENCT implanted LV sustained contractile function and that of EFCT significantly increased at 8 weeks (P=0.04, 8 weeks vs. 0 week, Figure 3-6B). At 8 weeks after graft implantation, LV FAC in EFCT was significantly higher than sham operated LVs (P=0.009) while the LV FAC of ENCT tended to higher than sham operated LV (P=0.07 vs. Sham). LV pressure measurement revealed that EFCT implanted hearts showed higher heart rates, peak systolic pressures, and maximum dP/dt versus infarction controls and a lower minimum dP/dt. End-diastolic pressure of EFCT implanted LV was the same level as sham operated LVs (Table 3-3).

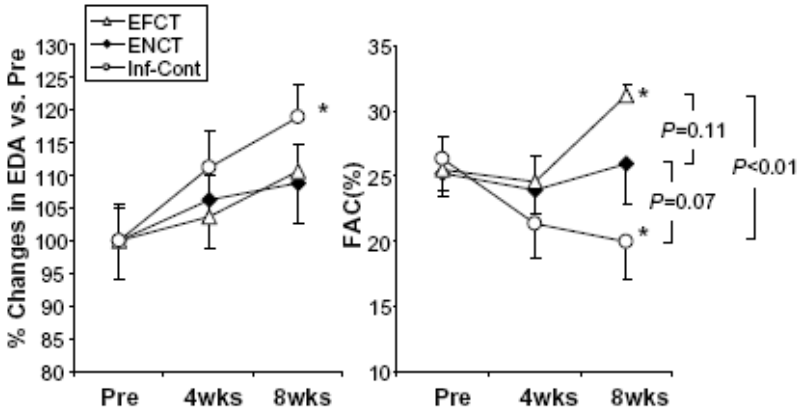

Figure 3-6. Echocardiographic assessment of EFCT and ENCT implanted post-infarcted myocardium. Data are expressed as % change in both LV EDA and FAC ± SE. The value of 100% EDA indicates EDA at cardiac graft implantation. **(Left panel)** Sham operated LV cavity area increased and contractile function decreased by 8 weeks after graft implantation (*, $P<0.05$) while EFCT and ENCT implanted LV did not increase LV cavity area. **(Right panel)** LV contraction of sham operated LV decreased by 8 weeks (*, $P<0.05$) whereas EFCT implanted LV increased LV contraction (*, $P<0.05$). ENCT implanted LV retained LV contraction by 8 weeks. EFCT implanted LVs at 8 weeks after graft implantation significantly increased LV FAC in comparison to sham operated LVs ($P=0.009$ vs. sham-operated LV) while ENCT implanted LV FAC tended to increase ($P=0.07$). Data support that implanted EFCTs attenuate LV remodeling of post-infarcted LV. *; P<0.05 within group (ANOVA). 0wk; pre-implantation, 4wks and 8wks; 4 weeks and 8 weeks after implantation.

Table 3-3. Left Ventricular Pressure in 8 weeks after EFCT implantation. Data are mean ± SE. Heart rate, left ventricular peak systolic pressure, and maximum and minimum dP/dt in EFCT implanted hearts were significantly different from the sham operated LVs (*; $P<0.05$ vs. sham operated LV). Left ventricular end-diastolic pressure of EFCT implanted hearts was not different from the infarction control ($P=0.30$).

	Sham Operation (n=8)	EFCT Implantation (n=8)
Heart Rate (bpm)	335 ± 21	384 ± 8 *
Peak Systolic Pressure (mmHg)	98 ± 5.1	121 ± 3.6 *
End-Diastolic Pressure (mmHg)	5.3 ± 1.3	4.1 ± 0.7
Maximum dP/dt (mmHg/sec)	4676 ± 418	6301 ± 415 *
Minimum dP/dt (mmHg/sec)	-4517 ± 444	-6034 ± 300 *

3.4 DISCUSSION

In the current study we found that EFCT maintained active CM proliferation within *in vitro* culture conditions (pre-implantation) and this proliferation activity was maintained for 8 weeks after EFCT implantation onto post-infarcted adult myocardium without formation of tumor-like abnormal tissue (evaluated by HE staining in all sample sections). The implanted EFCT graft also survived, preserved cardiac tissue structure, and improved the contractile function of the post-infarct LV.

Our previous study of chick EEECT showed that EEECT maintains high cellular proliferation activity[20]. In this study, we constructed EFCT from gestational day 14 fetal rat cardiac cells in order to investigate the efficacy of an EFCT post-infarction cardiac repair paradigm. Culture day 7 rat EFCT, which developmentally corresponds to gestational day 21 rat fetal hearts, displayed active cellular proliferation activity whereas culture day 7 ENCT, which developmentally corresponds to post-natal day 10, displayed a low CM proliferation rate similar to post-natal myocardium[173] . We used the same method of tissue construction for these 2 types of cardiac tissue. Therefore, our data indicate that the differences in *in vitro* CM proliferation activity between EFCT and ENCT parallel intrinsic differences in fetal and neonatal CM properties.

Eschenhagen et al. first reported engineered heart tissue (EHT) from post-organogenesis chick embryonic or neonatal rat cardiac cells using a 3D liquid collagen-extracellular matrix / cell mixture culture method, which we adapted for EFCT construction in the current study[37]. Their pioneering work and successful generation of ring-shaped EHT reported by Zimmerman et al. showed that EHT exhibits native mature myocardial-like tissue architecture and contractile properties[12, 177]. Cyclic mechanical stretch stimulation of EHT induced CM hypertrophy

(cellular growth) and increased the EHT contractile properties similar to mature adult myocardium[12, 118, 177]. The implanted EHTs maintained myocardial tissue for 4 weeks after the EHT implantation and electrically coupled with the recipient myocardium and attenuated further LV dilatation and preserved contractile function[13]. In the present study, active contractile force of culture day 7 ENCT was significantly higher than EFCTs, whereas contractile response to the physiologically maximum β-adrenergic stimulation (1μM, ISP) was the same in both construct. Zimmermann et al. have shown that culture 12 ring-shaped engineered heart tissues from neonate rat cardiac cells responds to β-adrenergic stimulation similar to mature myocardium under presence of 0.2mM [Ca^{2+}][13, 118, 177]. In our study we did not see dramatic inotropic response of EFCT and ENCT to the ISP. However, we measured the active contractile force and contractile response to ISP under presence of 2mM [Ca^{2+}] ion. In our pilot study, both EFCT and ENCT did not generate contractile without presence of [Ca^{2+}] ion and we believed that 2mM [Ca^{2+}] concentration represents physiological extracellular [Ca^{2+}] concentration. Although we could not conclude that ENCT contractile properties represent more matured myocardium than EFCT, CM proliferation activity and peak active force of EFCT may indicate that CMs within EFCT remain more immature fetal CM phenotype[20, 120, 173, 178].

Zimmermann et al. described that immunosuppression treatment was necessary to promote donor graft survival even in the syngeneic rat animal model[13, 177]. In the current study we did not treat animals with any immuno-suppressive drugs before or after the graft implantation. Leor et al. reported that implanted fetal ventricular tissue fragments into post-infracted rat myocardium survive and sustain cardiac function of recipient rat heart[172]. Roell et al. showed that embryonic CMs engraft well within post-infarcted myocardium sustaining recipient cardiac function[91, 167]. Although underlying mechanisms of EFCT survival without

immuno-suppression and its functional contribution to the recipient myocardium remain to be elucidated, our results support that immature fetal type CMs have active CM proliferation, engraftment without immunosuppression drug treatment, and functional contribution to the recipient injured myocardium. Further studies are necessary to investigate whether the active CM proliferation is associated with immuno-tolerance for graft survival.

Li et al. showed that fetal cardiac cells maintain proliferative activity and form a myocardium-like tissue within a 3D gelatin-mesh scaffold *in vitro*. The implanted gelatin-mesh maintains the myocardial-like tissue architecture within post-infarcted myocardium and contributes to preservation of post-infarcted LV contraction[53]. In their study, however, whether the high cellular proliferation activity reflects CM proliferation was not investigated. In the present study, we specifically analyzed CM proliferation and apoptosis activities. EFCT displayed higher CM proliferation activity before graft implantation compared to ENCT and the higher CM proliferation activity at 8 weeks after EFCT implantation was maintained at the same level as pre-implantation, whereas CM proliferation activity at 8 weeks after ENCT implantation remained low. Our previous study of EEECT showed that cyclic mechanical stretch stimulation increases both EEECT cellular proliferation and contractile function, which mimics the adaptive capacity of the developing fetal myocardium to altered mechanical loads[4, 96, 150]. We speculate that the implanted EFCTs were exposed to active mechanical deformation by recipient myocardial contraction, which might increase CM proliferation and the contractile properties resulting in EFCT tissue survival and prevention of further LV remodeling[4].

In the present study we did not observe ENCT CM apoptosis activity at 8 weeks after implantation. Although it remains to be elucidated whether ENCT CM death occurred in shortly after graft implantation (we did not investigate CM apoptosis in 3 days post-ENCT implant

myocardium), which was not observed in EFCT, we speculate that EFCT may maintain higher myocardial tissue survival (higher CM ratio of implanted graft at 8 weeks) by active CM proliferation with low CM apoptosis, whereas ENCT maintains myocardial tissue survival by protecting CM apoptosis, rather than CM proliferation at 8 weeks after graft implantation. Capillary density counting within post-infarct myocardium showed that both EFCT and ENCT promoted capillary formation, whereas the capillary density counting within graft did not show difference between EFCT and ENCT suggesting that capillary vessel formation was not related to CM proliferation and CM apoptosis activities. These results suggest that the active CM proliferation of EFCT might be one of the critical factors for donor graft survival and functional contribution to the damaged recipient myocardium.

3.4.1 Limitations

Several limitations of the current study should be mentioned. First, we used Matrigel as supplemental extracellular matrices (ECMs) for EFCT construction. In our preliminary study we found that matrigel plays an important role in cell aggregate expansion within EFCT. However, Matrigel is derived from mouse tumor cells, which is contraindicated for clinical use[179]. In addition, it remains unknown which ECM proteins and/or growth factors within Matrigel play a role in cell expansion and EFCT tissue formation. Further studies are necessary to replace the Matrigel by clinically approved ECM/growth factor mixture. Second, ECM and/or growth factor treatment itself may have beneficial effects on myocardial regeneration and recipient cardiac function[180, 181]. In the preliminary study, we attempted acellular collagen/Matrigel construct (same concentrations as EFCT) implantation onto infarcted myocardium. However, acellular construct was too fragile to maintain tissue structure after the implantation and myocardial tissue

formation was not observed at the implantation site, which was seen in EFCT implanted LV. Therefore, we speculated that beneficial effects of EFCT implantation on recipient LV function is associated with survived EFCT, not ECM proteins and/or growth factor effects. Further studies are required. Third, constructed engineered cardiac tissue samples were of adequate size for the rat animal LV infarction model. However, simple nutrients/oxygen diffusion through EFCT may limit the size of constructs generated to repair larger injured hearts. CM proliferation activity and contractile function are greatly influenced by the oxygen and nutrient distribution of the tissue[45, 182]. It remains unknown whether the high CM proliferation activity would be preserved in a larger-scaled engineered cardiac graft. Further studies are necessary to determine whether the high CM proliferation and low CM apoptosis activities within EFCT are purely intrinsic properties of fetal type CMs. Forth, it remains to be elucidated whether our results of donor tissue survival and functional contribution to the recipient myocardium will be maintained over extended time periods at which finite CM proliferation activity within EFCT may be lost. In the present study we found that GFP(+) EFCT cells did not migrate out from the graft tissue 2 weeks after implantation and the implanted Lewis rat EFCT survived at 8 weeks after implantation maintaining myocardial tissue structure. We speculate that cells within EFCT may stay within the graft maintaining tissue structure. However, we could not track fate of GFP(+)EFCT cells in prolonged period due to risk of allogeneic EFCT graft rejection between GFP(+)EFCT and nude rats. Therefore, further study is necessary to track GFP(+)EFCT cells using near GFP(+) graft implantation onto GFP(-) host implantation using in-bred GFP transgenic rat implantation model[175]. Finally, the underlying mechanisms that regulate CM proliferation within EFCT following graft implantation are currently unknown and require further investigation. Various potential cell sources of cellular cardiomyoplasty, including

stem/progenitor cell-derived CMs, are under investigation and each cell source may have unique mechanisms that regulate cell survival, proliferation, and functional integration[9, 32, 183, 184]. It also remains unknown the tumorogenic potential of active donor CM proliferation. Therefore, elucidation of regulatory factors of CM proliferation will play a key role for optimal CM preparation for cardiac repair.

3.4.2 Conclusion

In conclusion, implanted EFCTs onto post-infarcted LV myocardium maintained active CM proliferation with minimal CM apoptosis, preserved myocardial tissue structure, and attenuated functional deterioration of post-infarcted LV. Our findings suggest that active CM proliferation of donor cardiac tissue graft may play an important role for graft survival and functional contribution to the recipient injured myocardium which may be relevant in designing optimized donor CM preparation and culture approaches for cardiac repair paradigms.

4.0 ENGINEERED CARDIAC TISSUE FROM SKELETAL MUSCLE DERIVED STEM CELLS (MDSC-3DGB)

4.1 INTRODUCTION

Studies suggest that fetal, finitely proliferating CMs display the best cell survival, functional integration, and sustained cardiac recovery, and thus could be an optimal cell type for cardiac repair[75, 167]. However, the use of fetal heart cells is contraindicated for clinical use. Stem cells provide an alternative solution, and a range of cell types have been employed in cellular cardiomyoplasty strategies including bone marrow derived stromal and stem cells, fibroblasts, skeletal myoblasts, mesenchymal stem cells, embryonic stem cells, and resident cardiac stem cells[14]. However, despite some promising results[74], the rate of CM differentiation from transplanted stem cells remains insufficient to fully recover the recipient myocardial function[14, 33, 34, 75, 76]. Therefore, a preferred strategy for cellular cardiomyoplasty might be the delivery of progenitor/stem cell-derived CMs, rather than undifferentiated cells, into injured myocardial tissue[77].

Skeletal muscle derived stem cells (MDSCs) are a somatic stem cell population obtained from skeletal muscle specimens in animals and humans that can be readily expanded *in vitro* and then transplanted as an autologous graft[76, 185, 186]. MDSCs are multipotent and have been shown to differentiate along skeletal and smooth muscle, bone, tendon, nerve, endothelial, and

hematopoietic lineages[185, 187, 188]. Previous studies, including our own work, have shown that MDSCs, isolated using variations of a modified preplate technique, can differentiate into CMs or cells with cardiac phenotypes and can facilitate cardiac repair[8, 76, 189-194]. However, none of the previous studies investigated whether differentiated MDSC-derived CMs generate contractile force similar to the native CMs. In addition, undifferentiated MDSCs or MDSCs preconditioned with chemical reagents were used to evaluate *in vivo* CM differentiation from MDSCs, not transplanted MDSC-derived CMs in animal models of injured myocardium[32, 74]. Our recent studies have also shown that the rate of CM differentiation of transplanted MDSCs within acute myocardial infarction model is not sufficient to replace injured CMs and improvement of recipient cardiac function by MDSC transplantation is due to combined effects of myogenic differentiation of transplanted MDSC, angiogenesis, stimulation of recipient CM proliferation, and reduction of recipient CM apoptosis[8, 76]. Therefore, it remains unclear whether differentiated CM phenotypic cells replace recipient dead CMs and have contractile function that improves recipient cardiac function.

The effects of various biomechanical stimuli on multipotent stem cells have been investigated to elucidate their roles in CM induction and differentiation. Previous studies have shown that cell-cell interactions and specific culture conditions are often necessary prerequisites for efficient CM differentiation[17, 18, 195]. The culture of multipotent stem cells in aggregate spheres has been shown to facilitate cell-cell coupling, increase differentiation capacity, modify cellular metabolism, modulate the response to therapeutic agents[18, 27, 196], and stimulate the synthesis and release of extracellular matrix constituents[26]. Studies also suggest that 3D *in vitro* culture conditions may be optimal for donor CM preparation[12, 75, 167] and that tissue engineered

cardiac tissue constructs provide the requisite 3D environment for efficient cell survival, functional integration, and sustained cardiac recovery[12, 13].

Thus, the objective of the present study was to develop a culture method which induces CM differentiation from MDSCs and facilitates myocardial tissue formation that enables us to directly evaluate the contractile properties of MDSC-derived CMs *in vitro*. We tested the hypothesis that the combined MDSC-aggregate formation and 3D collagen gel bioreactor can induce MDSCs to differentiate into cells with a CM phenotype and that the differentiated CMs form a working 3D cardiac like tissue *in vitro*. We determined that MDSC-aggregate formation followed by 3D gel bioreactor (3DGB) culture succeeded in generating cells with an immature CM phenotype mimicking the native fetal myocardium. Thus, our results suggest that MDSC-3DGB is a useful 3D culture system to directly assess the contractile properties of differentiated CMs from MDSCs *in vitro*. We then tested the hypothesis that MDSC-derived CMs within MDSC-aggregate 3DGB would respond similarly to EEECT when subjected to cyclic mechanical stretch stimulation and EFCT when implanted on an injured myocardium.

4.2 METHODS

4.2.1 MDSC isolation

MDSCs were isolated from neonatal Lewis rat hind-leg muscles using an established preplate technique[185-187, 197-199]. Briefly, 5 post-natal day 3 rat pups were euthanized with 5% isoflurane anesthesia followed by cervical truncation. Gastrocnemius muscles were excised, minced in HBSS, and enzymatically digested. Briefly, tissue slurry underwent sequential

incubation of collagenase XI (0.2% collagenase XI), dispase (2.4 U/mL), and 2x trypsin. Isolated cells then underwent sequential preplating (24 hours interval between each preplate) until the 6th preplate phase[199] in standard MDSC growth medium containing high glucose DMEM w/ l-glutamine (Invitrogen, Carlsbad, CA), 10% horse serum (Invitrogen), 10% fetal bovine serum (FBS, Invitrogen), 0.5% chick embryo extract (US Biological, Swampscott, MA), and 1% anti-biotic/anti-mycotic solution (AAS, Invitrogen)[20, 26, 199]. Our research protocol followed the National Institutes of Health (NIH) guidelines for animal care and was approved by the University of Pittsburgh's Institutional Animal Care and Use Committee and the Children's Hospital of Pittsburgh Animal Research Care Committee.

Isolated rat MDSCs were passaged 15 times and expanded to obtain enough cell number (at least 20 million cells per mL)[187, 197]. Fluorescent-activated cell sorting (FACS, FACS Aria, BD biosciences, San Jose, CA) revealed that cultured rat MDSCs were approximately 60% positive to Sca-1 antigen (BD biosciences), and negative to CD34 (BD biosciences), CD45 (BD biosciences), and c-kit (BD biosciences) antigens (Figure 4-1, Table 4-1). Zuba-Surma et al. have shown that Sca-1 (-) skeletal muscle stem cells are "inherently predisposed to undergo cardiac differentiation[190]". Thus, we sorted Sca-1 (-) MDSCs which were expanded in standard two-dimensional (2D) flasks for 48 hours to reach a cell number of 3 million. These Sca-1 (-) MDSCs maintained no Sca-1 expression throughout culture (Figure 4-2).

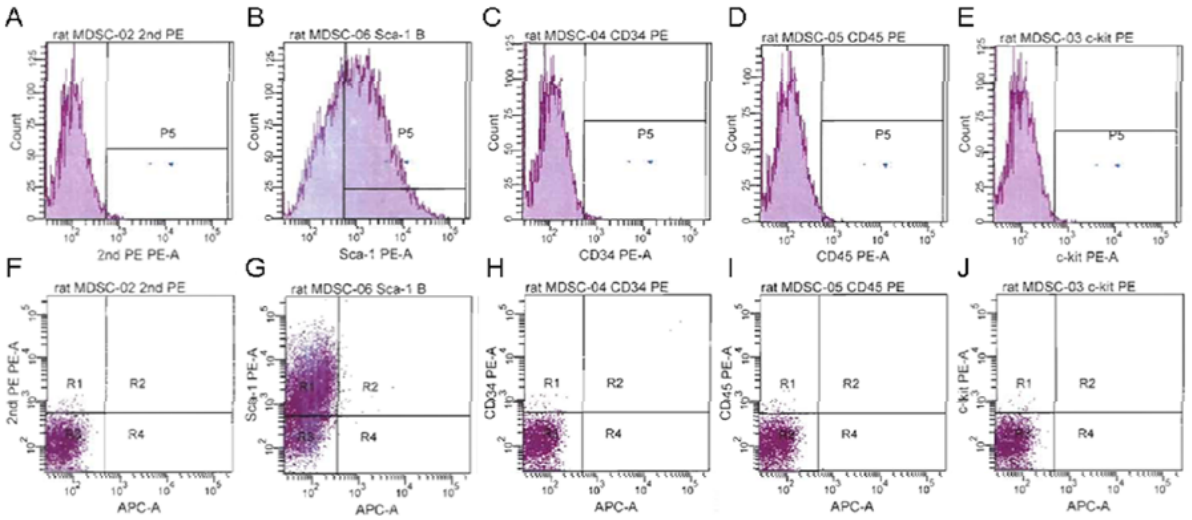

Figure 4-1. FACS analysis of MDSCs. MDSCs were approximately 57.3 ± 2.8% positive to Sca-1 antigen, and negative to CD34, CD45, and c-kit antigens. **(A and F)** isotype control. **(B and G)** Sca-1. **(C and H)** CD34. **(D and I)** CD45. **(E and J)** c-kit.

Table 4-1. FACS analysis of unsorted MDSCs and MDSC-3DGB. Data are mean ± SE. n; number of FACS sets; for MDSCs: 10 million cells/set, for MDSC-3DGB: 6 MDSC-3DGBs /set.

MDSCs	% Positive
Sca-1	57.3 ± 2.8 (n=4)
CD34	0.1 ± 0.0 (n=4)
CD45	0.0 ± 0.0 (n=2)
c-kit	0.1 ± 0.1 (n=2)

MDSC-3DGB	% Positive
cTn-T	18.6 ± 2.5 (n=3)

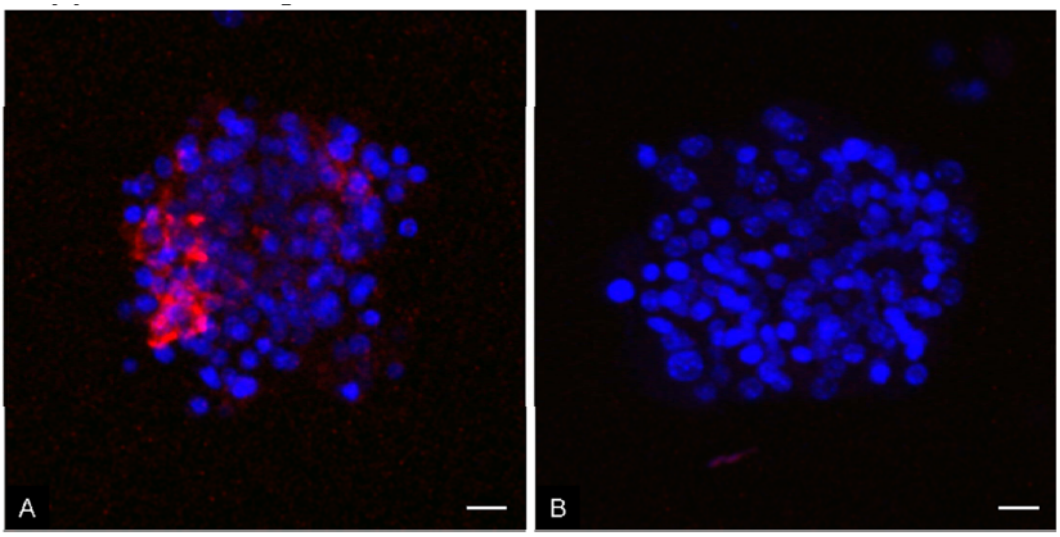

Figure 4-2. Sca-1 staining of MDSC-aggregates. **(A)** Unsorted MDSC-aggregates. **(B)** Sca-1(-) sorted MDSC-aggregates. Sac-1 expressed in unsorted MDSC-aggregates whereas the sorted Sca-1(-) MDSC-aggregates had no Sca-1 expression. Blue staining (DAPI) indicates nuclei. Scale bars indicate 20μm.

4.2.2 MDSC-3-dimensional collagen gel bioreactor (MDSC-3DGB) construction

Expanded MDSCs on the 2D flask were trypsinized using a 0.05% trypsin/EDTA solution (Invitrogen) and the cell suspension was cultured on a 100mm-dimeter suspension culture dish (Corning, Lowell, MA) for 24 hours at 37°C using a gyrating shaker (50 rotations/min) to form 50 to 70μm diameter MDSC aggregates (MDSC-aggregate, 330-350 cells/aggregate) under standard MDSC growth medium. Acid-soluble rat tail collagen type-I solution (pH 3, Sigma, St. Louis, MO, USA) was neutralized with alkali buffer (0.2 M NaHCO3, 0.2 M HEPES, 0.1 M NaOH) on ice. Matrigel (13% of total volume, BD biosciences) was then added and the cell suspension and matrix solution mixed to reach a final collagen type-I concentration of 0.67 mg/mL. Approximately 200μL of the cell/matrix mixture was poured into the 20mm long x 2mm wide cylindrical cast of a Flexcell Tissue Train collagen type-I coated silicone membrane culture plate (FX4000TT, Flexcell International, Hillsborough, NC) and

incubated for 120 minutes (37°C, 5% CO_2)[20] to form a cylindrical MDSC-3DGB. Each MDSC-3DGB was cultured in a 5% FBS containing growth medium. We compared the efficiency of CM induction from culture day 7 MDSC-3DGBs to; 1). Freshly formed MDSC-aggregates after 24 hours rotation culture in standard culture medium; 2). 2-dimensional MDSC culture at culture day 7 (2D-MDSC) on rat tail collagen type-I (Sigma) coated tissue culture plates (Corning) with 5% FBS and Matrigel (17% of total volume, a concentration equivalent to 3D culture, dissolved in cell suspension at the beginning of culture, BD biosciences); or 3). 3-dimensional MDSC culture (3D-MDSC) at culture day 7 in which the MDSCs were embedded into collagen gel without MDSC-aggregate formation. We also constructed engineered cardiac tissue from gestational day 14 fetal cardiac cells (EFCT) or neonatal day 1 cardiac tissue (ENCT) to investigate whether MDSC-3DGB contractile properties mimic engineered cardiac tissue from native immature cardiac cells. For EFCT construction, pregnant mothers were anesthetized using 3% isoflurane inhalation with 100% oxygen and hysterectomy was performed. Immediately after hysterectomy, the mother was euthanized by induced asystole under 5% isoflurane anesthesia. The excised uteri were transferred to a sterilized Petri-dish filled with cold PBS buffer and 1% antibiotic-antimycotic solution (Invitrogen), the fetuses were excised by hysterotomy, and the fetal hearts were harvested. Isolated cells were preplated for 1 hour and then cultured on a gyratory shaker (50 rotations/min) for 24 hours to reaggregate viable CMs for the cell suspension for 3D construction. For ENCT construction, neonatal day 1 rat pups were euthanized by cervical truncation under 5% inhaled isoflurane with 100% oxygen and the ventricular tissue was excised and pooled. Great vessels and atrium were removed from each heart and ventricular tissue was collected and pooled. Pooled ventricles were then enzymatically digested by 2mg/ml of collagenase type II followed by 0.05% trypsin-EDTA solution

(Invitrogen). Isolated cells were preplated for 1 hour and then cultured on a gyratory shaker (50 rotations/min) for 24 hours to reaggregate viable CMs for the cell suspension for each construct. Engineered cardiac tissue construction was the same as MDSC-3DGB and the constructed EFCT or ENCT was culture with 10% FBS containing growth medium for 7 days.

4.2.3 RT-PCR

Total RNA was prepared using Trizol solution (Invitrogen) and treated with TURBO DNA-free kit (Ambion, Austin, TX, USA). A *cardiac α-actin* primer was designed using Primer-3 (For5'-3' GCCCTGGATTTTGAGAATGA; Rev5'-3' CCTTTTGCATACGATCAGCA, product size of 289bp). Other primers, whose target genes were *Nkx2.5, GATA4, α-and β-cardiac myosin heavy chains (MHCs), and connexin-43 (Cx-43),* were obtained from Qiagen Quanti-Tect Primer Assay with the target fragment sizes approximately 100 base pairs. One step RT was performed with a total volume of 1μg RNA in a total volume of 25μL that used MuLy (Roches, Pleasanton, CA, USA) with the program: 42^{o}C 15 min, 99^{o}C 5min, 5^{o}C 5min, 1 cycle. cDNA (1μL) was used for PCR which used the program: 94^{o}C 2min, 95^{o}C 50second, 58^{o}C 30 second, 72^{o}C 1 min, 35 cycles 72°C 7 min extension. For normalization of RT-PCR results, *β-actin* was used as an internal control. All PCR products were confirmed by University of Pittsburgh DNA Sequence Core Facilities, performed by Eppendorf Mastercycles. All RT-PCR assays were completed in triplicate (total n=18 MDSC-3DGBs).

4.2.4 SDS-PAGE and Immunoblotting

Whole cell lysates were prepared from native adult and gestational day 20 fetal hearts (n=6) and gastrocnemius muscle tissue (n=6), MDSC-3DGB tissue (n=18), 3D-MDSC (n=18), Stretch MDSC-3DGB (MDSC-3DGB subjected to cyclic mechanical stretch (0.5Hz, 5%) for 48 hours) (n=6), and MDSC-aggregate (n=6 culture plates) pooled populations, and separated by SDS-PAGE (7.5% separating gel, Bio-Rad Laboratories). Immunoblotting was carried out using routine protocols. Each lane contained 20μg of total protein. Mouse monoclonal β-actin antibody (Abcam, Cambridge, MA, USA), mouse monoclonal cardiac troponin-T (cTn-T, Abcam), mouse monoclonal anti-connexin-43 (Cx-43, Abcam), and mouse monoclonal cardiac troponin-I (cTn-I, Abcam) were visualized with IR-Dye 800 donkey anti-mouse secondary antibody (Rockland Immunochemicals, Gilbertsville, PA, USA). Anti-phospho-S10 Histone H3 (Upstate cell signaling solutions, Temecula, CA) was visualized with IR-Dye 680 donkey anti-rabbit secondary antibody (Rockland Immunochemicals). All proteins were visualized using an infrared western blot imaging system (Odyssey, LI-COR Biosciences Lincoln, NE, USA). Immunoblots were performed in triplicate and quantified using densitometry and an expression ratio was calculated (Odyssey, LI-COR Biosciences Lincoln, NE, USA).

4.2.5 Confocal microscopy

3D tissue constructs and fetal ventricular samples were fixed with 4% paraformaldehyde/PBS for 15 minutes and embedded in the 13% polyacrylamide gel. 150μm thick sections were made using a vibratory microtome (Vibratome-1000, Vibrotome.com)[20]. 2D-MDSC samples were fixed with 4% paraformaldehyde/PBS for 5 minutes. Sections or 2D-

MDSC samples were permeabilized with 0.1% Triton X-100 for 30 or 5 min, respectively, and stained for mouse monoclonal anti-cTn-T (Abcam), cTn-I (Abcam), α-sarcomeric actinin (Sigma), or Cx-43 (Abcam) primary antibodies and Alexa Fluor 488, Alexa Fluor 647, or Alexa Fluor 594 secondary antibodies (Invitrogen). We reconstructed 3D projection images from stacks of z-axis optical scans using a standard laser confocal microscopy system (FV1000, Olympus, Tokyo, Japan) and Scion Image software (Scion Corp, MD, USA)[20]. The composite 3D projection images were further processed using Adobe Photoshop software (Adobe, San Jose, CA, USA).

4.2.6 Spontaneous beating activity

Culture day 7 MDSC-3DGBs (n=8) were imaged at two different regions / construct using a digital video microscopy system and Scion Image Software with a CG-7 frame-grabber board (Scion Corp.) to determine baseline spontaneous beat frequency. MDSC-3DGBs were then treated with 2μM of the non-selective β-adrenergic receptor agonist, isoproterenol (ISP) or 1mM of the non-selective sodium and calcium ion channel inhibitor, cadmium chloride. Five minutes after treatment, MDSC-3DGBs were imaged again, and were then incubated with fresh growth media for 15 min and re-imaged to determine a post-treatment baseline.

4.2.7 Mechanical testing

The passive and active force of MDSC-3DGB (n=7), 3D-MDSC (n=6), and EFCT (n=7) constructs was measured as previously described[20]. In brief, each construct was transferred from the Flexcell culture dish to the perfusion chamber of the muscle testing station containing a

cold (25°C) calcium free Ringer solution composed of (in mM): 135 NaCl, 4.0 KCl, 10 Trizma-HCl, 8.3 Trizma-base, 11.0 glucose and gassed with 95% O_2 /5% CO_2 (pH 7.4). One end of the construct was attached to a force transducer (model 403A, Aurora Scientific, Ontario, Canada) and the other end to a length controller mounted on a micromanipulator using 10-0 mono-filament nylon sutures. The buffer within the perfusion chamber (1.5mL total chamber volume) was then replaced with a warmed Ringer solution buffer (37°C, containing 2mM Ca^{2+}) and perfused at a rate of 1 mL/min. The construct was field-stimulated (1Hz, 4ms, 50-100V, rectangular pulses) using a stimulator (Harvard Apparatus, Holliston, MA, USA). The longitudinal length of the construct was increased in 5% increments up to a 15% elongation from original length ($L_{0.15}$). The external diameters of the construct were recorded at each stretch increment using a digital video microscopy system (Model KPD-50, Hitachi, Japan, and Scion Image Software with a CG-7 frame-grabber board, Scion Corp.).

4.2.8 Intracellular free calcium ion transient recording

MDSC-3DGBs (n=3) or ENCTs (n=5) were loaded for 30 min at 25°C with Fura 2-AM (Invitrogen) at a final concentration of 5μM within a custom-built muscle chamber equipped for the simultaneous measurement of force (force transducer 403A, high speed length controller model 22C and 322C, digital control system Series 600A, Aurora Scientific) and intracellular free calcium ($[Ca^{2+}]_i$) recording using fluorescent probes and IonOptix hardware and software (IonOptix Corporation, Milton, MA, USA). The muscle chamber was perfused with 37°C Ringer solution at a rate of 1 mL/min. MDSC-3DGBs were field-stimulated (1 Hz, 5msec, 50V, Harvard Apparatus) and Fura-2 fluorescence was recorded at a sampling rate of 100 Hz by alternately illuminating the preparation with light of 340- and 380-nm wavelength while

measuring fluorescence at 510nm. Acquired data was stored for offline analysis. To characterize $[Ca^{2+}]_i$ transients, the maximal ratio (F_{340}/F_{380}) and minimal ratio (F_{340}/F_{380}) for 10 successive transients were calculated and averaged. We also determined $[Ca^{2+}]_i$ transients at $L_{0.15}$, and pacing frequencies of 1 to 6 Hz.

4.2.9 Mechanical stretch stimulation

To determine the effect of cyclic mechanical stretch on MDSC-3DGB cell proliferation and contractile force we exposed culture day 5 MDSC-3DGB to uniaxial cyclic mechanical stretch (0.5Hz, 5% elongation). In the preliminary study, we found that 0.5Hz, 5% strain of cyclic stretch increased both MDSC-3DGB contractile force generation and cellular proliferation activity with minimal technical loss due to detachment of the tissue from anchors of the culture plate. We performed cyclic mechanical stretch stimulation for 48 hours beginning on culture day 5. For cyclic mechanical stretch stimulation, we also changed culture medium at 24 hours after the beginning of cyclic mechanical stretch stimulation.

4.2.10 Chronic left ventricular infarction model

MDSC-3DGB recipient adult rats were anesthetized using 3.0% isoflurane inhalation with 100% oxygen gas followed by endotracheal intubation and connection to a rodent volume controlled mechanical ventilator (Model 683, Harvard Apparatus, Holliston, MA). The heart was exposed through a left thoracotomy, monitoring electrocardiogram (THM 1000, VisualSonics, Toronto, Canada). The proximal left anterior descending coronary artery was ligated with 7-0 polypropylene. Myocardial ischemia was confirmed by regional cyanosis and

changes in electrocardiogram (ST-segment elevation). The incision was closed in layers with 4-0 silk continuous sutures[176].

4.2.11 MDSC-3DGB implantation

12 week-old adult female Lewis rats weighing 200g to 250g were used (Harlan Sprague Dawley Inc., Indianapolis, IN) as recipients. Two weeks following coronary artery ligation (pre-implantation), animals were anesthetized with isoflurane and the infarction size and cardiac function were assessed by transthoracic echocardiography. LV infarction size was estimated in a standard LV short-axis view by the percentage of scar area (akinetic or dyskinetic regions) to LV free wall area[176]. LV infarctions greater than 25% of the LV free wall were included in the present study. MDSC-3DGB implanted and sham operated animals were studied for longitudinal echocardiography and histological assessment at 8 weeks after graft implantation. Using 7-0 polypropylene with peripheral sutures, the anterior infarcted myocardium was covered with 4 engineered tissue constructs into the LV circumferential direction. For the sham operated group, a thoracotomy was performed 2 weeks after coronary ligation, but no MDSC-3DGB implantation was performed.

4.2.12 Assessment of *in vivo* recipient cardiac function

LV function was measured by non-invasive echocardiography (Acuson Sequoia and 13-MHz 15L8 probe) at pre-implantation (2 weeks after coronary artery ligation), 4 weeks, and 8 weeks (10 weeks after coronary ligation) after graft implantation. End-diastolic area (EDA) and end-systolic area (ESA) of the LV cavity were measured by endocardial planimetry, and %LV

fractional area change (%FAC) was measured as [(LVEDA – LVESA)/LVEDA] x 100%. Echocardiography was performed using isoflurane anesthesia (1.5% with 100% oxygen) via nose cone. LV pressure was measured at 8 weeks after MDSC-3DGB implantation prior to euthanasia for histological assessment. Rats underwent anesthesia with isoflurane and intubation followed by introduction of a pressure-transducer tip Millar catheter (model SPR-1000, Millar Instruments, Austin, TX) retrograde from the right carotid artery into the LV. LV pressure was acquired to calculate EDP, P_{max}, $+dP/dt_{max}$, and $-dP/dt_{min}$ for an analysis with a custom LabVIEW virtual instrument.

4.2.13 Statistical analysis

Data are expressed as mean ± SE. Student *t*-test was performed to compare the data of LV pressure measurement. One-factor analysis of variance (ANOVA) was used to compare the protein analysis and spontaneous beat frequency among experimental groups. Two-factor repeated ANOVA was performed to compare the active stress-length relations and the echocardiogram data among experimental groups. We performed a Tukey post-hoc test to determine individual differences between experimental groups. Statistical significance was defined by a value of $P<0.05$. All calculations were performed using SigmaStat (Systat Software Inc, Point Richmond, CA, USA).

4.3 RESULTS

4.3.1 CM phenotype cell differentiation within MDSC-3DGB

Prior to embedding MDSC-aggregates or MDSCs in 3D culture, we assessed the cellular proliferation activity of MDSC-aggregates. MDSC-aggregate formation significantly decreased MDSC cellular proliferation [16.6 ± 4.5% (n=3 experimental sets, $P<0.05$)] versus standard 2D culture [36.1 ± 2.8% (n=3)] (Figure 4-3).

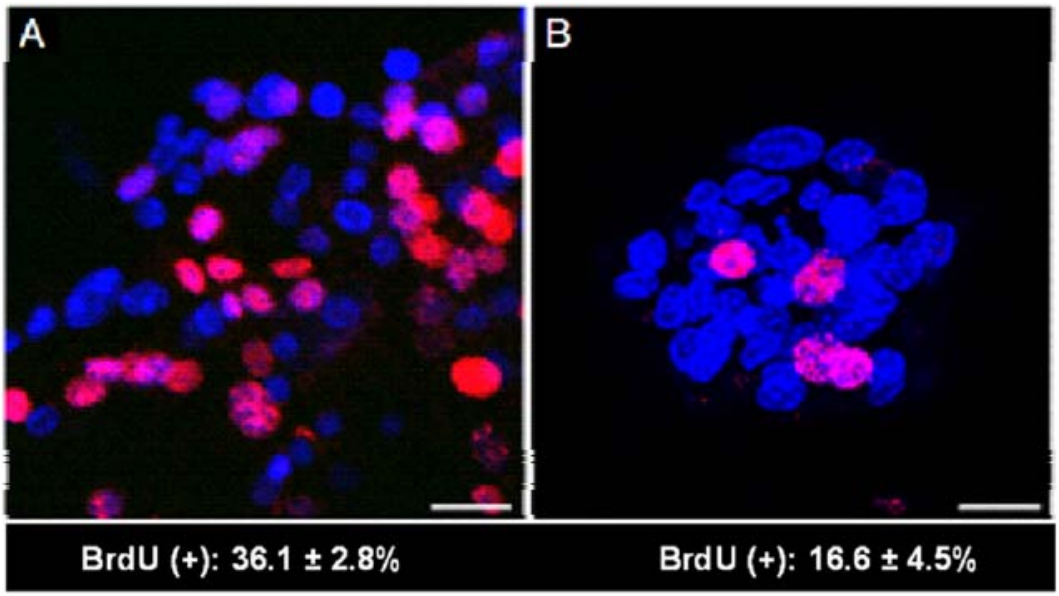

Figure 4-3. BrdU assay of 2D-MDSC and MDSC-aggregates. **(A)** BrdU positive ratio of 2D-MDSC. **(B)** BrdU positive ratio of MDSC-aggregate. BrdU positive ratio of MDSCs decreased with MDSC-aggregate formation compared with 2D-MDSCs at culture day 1. MDSC-aggregates and 2D-MDSC were fixed with 4% paraformaldehyde/PBS for 5 minutes. Each sample was incubated with 60μg/ml bromodeoxyuridine (BrdU, Sigma, St. Louis, MO) for 1 hour prior to fixation[20]. MDSC-aggregate samples were then embedded in a 13% polyacrylamide gel, and 150μm thickness serial sections were made using a standard vibrating microtome (Vibratome-1000, Vibratome.com, St Louis, MO)[20]. Sections or 2D-MDSC were permeabilized with 0.1%

Triton X-100 for 30 or 5 minutes, respectively and stained for BrdU using an Alexa Fluor 594 conjugated mouse-monoclonal anti-BrdU antibody (Invitrogen) and DAPI (Vector Laboratories, Burlingame, CA).

When MDSC-aggregates were cultured under standard 2D conditions, MDSC-aggregates attached to the culture dish bottom within an hour and MDSC-aggregates had completely disappeared and MDSCs were randomly oriented similar to standard 2D-MDSC culture at 24 hours. MDSC-aggregates expanded within each 3DGB and the majority of cells aligned along the construct longitudinal axis forming a muscle-like tissue (Figure 4-4A) and the cells were noted to spontaneously beat by culture day 5, which was observed in all MDSC-3DGBs. The cells within 3D-MDSC (without MDSC-aggregate formation) expanded along the construct longitudinal axis by culture day 3, which was faster than MDSC-aggregates placed in 3DGB. However, we noted a lower incidence of spontaneous beating cells at culture day 7 within the 3D-MDSC constructs (6 of 36 constructs or 17%), which was substantially lower than the spontaneous beating rate of MDSC-3DGB constructs (48 of 48 constructs or 100%, $P<0.05$ by Fisher exact test). Synchronous tissue contraction of MDSC-3DGB was observed by culture day 7. Histological assessment revealed that MDSC-3DGB contained cells with cardiac specific protein cTn-T organized in a striated pattern (Figure 4-4C), whereas the cTn-T positive cells in 2D-MDSC were not organized in a clear striated pattern (Figure 4-4D). MDSC-3DGB also expressed the cardiac specific protein cTn-I organized in a striated pattern similar to cTn-T (Figures 4-4E and 4-4F), whereas cTn-I was negative in 2D-MDSC. FACS analysis based on cTn-T expression revealed that the fraction of cTn-T positive cells from culture day 7 MDSC-3DGB was 18.6 ± 2.5% (from 6 MDSC-3DGBs in each FACS analysis, 3 independent sets of pooled MDSC-3DGBs) (Figure 4-5, Table 4-1). Cx-43 was expressed in cTn-T positive cells within MDSC-3DGB and the Cx-43 expression pattern of cTn-T positive cells was not typical to

mature adult CMs, but was similar to CMs of gestational day 20 native fetal left ventricular papillary muscle (Figure 4-6).

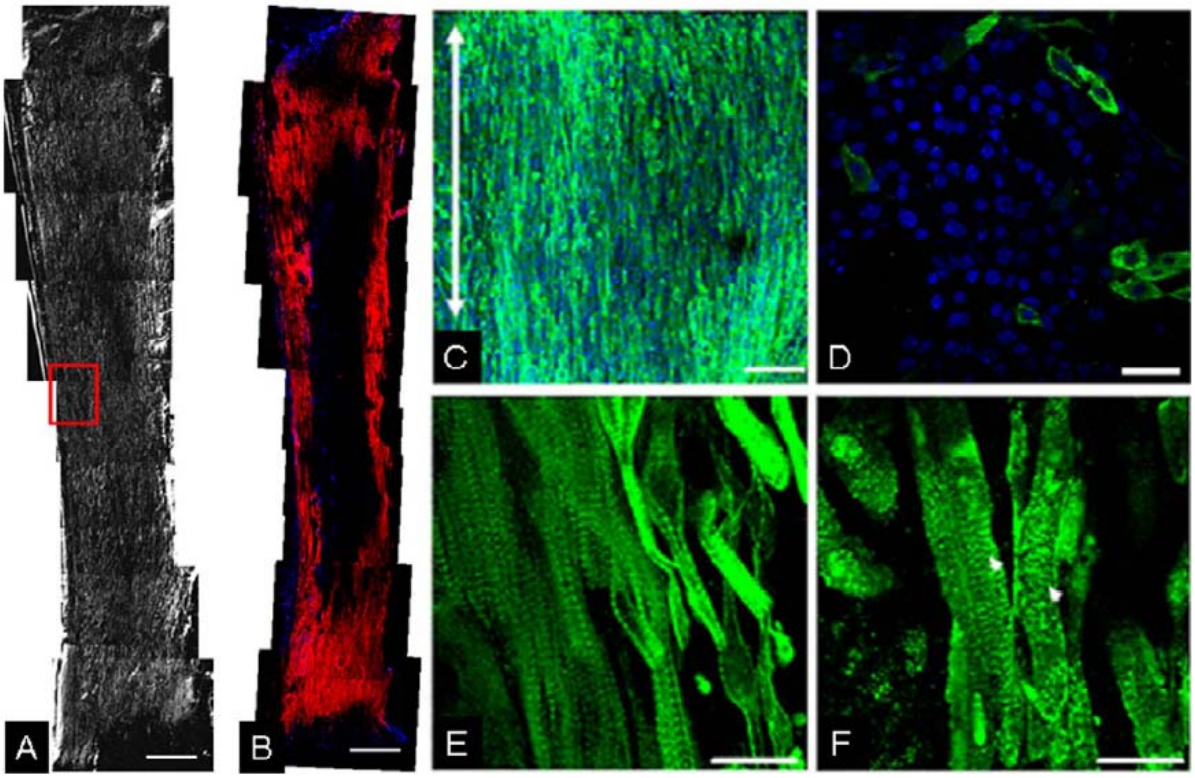

Figure 4-4. Histologic analysis of MDSC-3DGB. **(A)** Phase contract image of culture day 7 MDSC-3DGB. Scale bar indicates 500μm. Red box indicates the area of the tissue where high magnification images are taken. **(B)** α-sarcomeric actinin expression in MDSC-3DGB. Scale bar indicates 500μm. **(C)** Cardiac specific troponin-T (cTn-T) expressed in oriented cells of MDSC-3DGB. Blue staining (DAPI) indicates nuclei. Scale bar indicates 50μm. White double arrow indicates MDSC-3DGB longitudinal axis. **(D)** cTn-T expression of MDSC-2D. Scale bar indicates 20μm. **(E)** cTn-T expression of MDSC-3DGB was a typical striated muscle pattern at a higher magnification. Scale bar indicates 20μm. **(F)** Cardiac specific troponin-I (cTn-I) also expressed in a typical striated pattern **(white arrowheads).** Scale bar indicates 20μm.

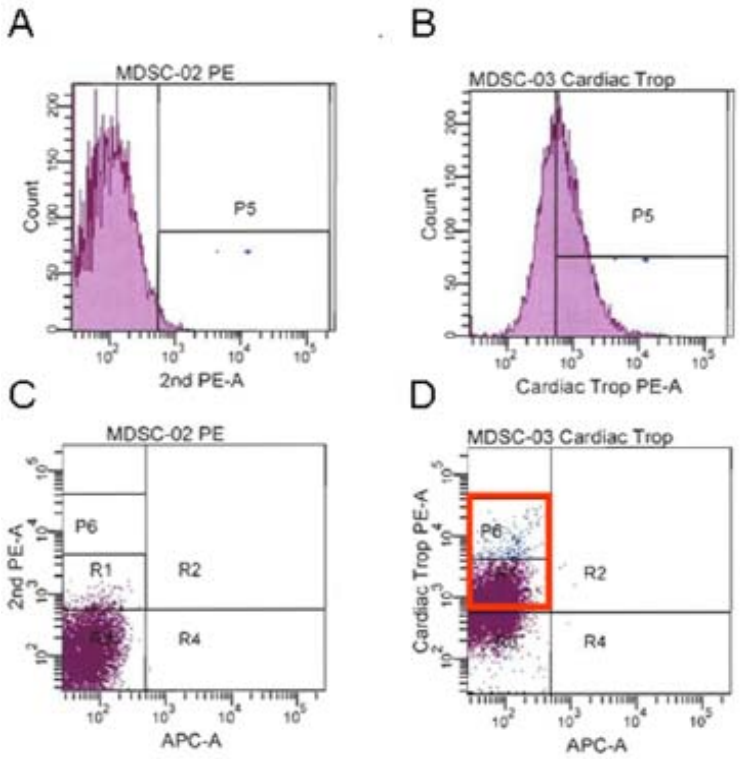

Figure 4-5. FACS analysis of culture day 7 MDSC-3DGB. Cardiac specific troponin-T was expressed in 18.6 ±2.5% of cells within MDSC-3DGB at culture day 7.

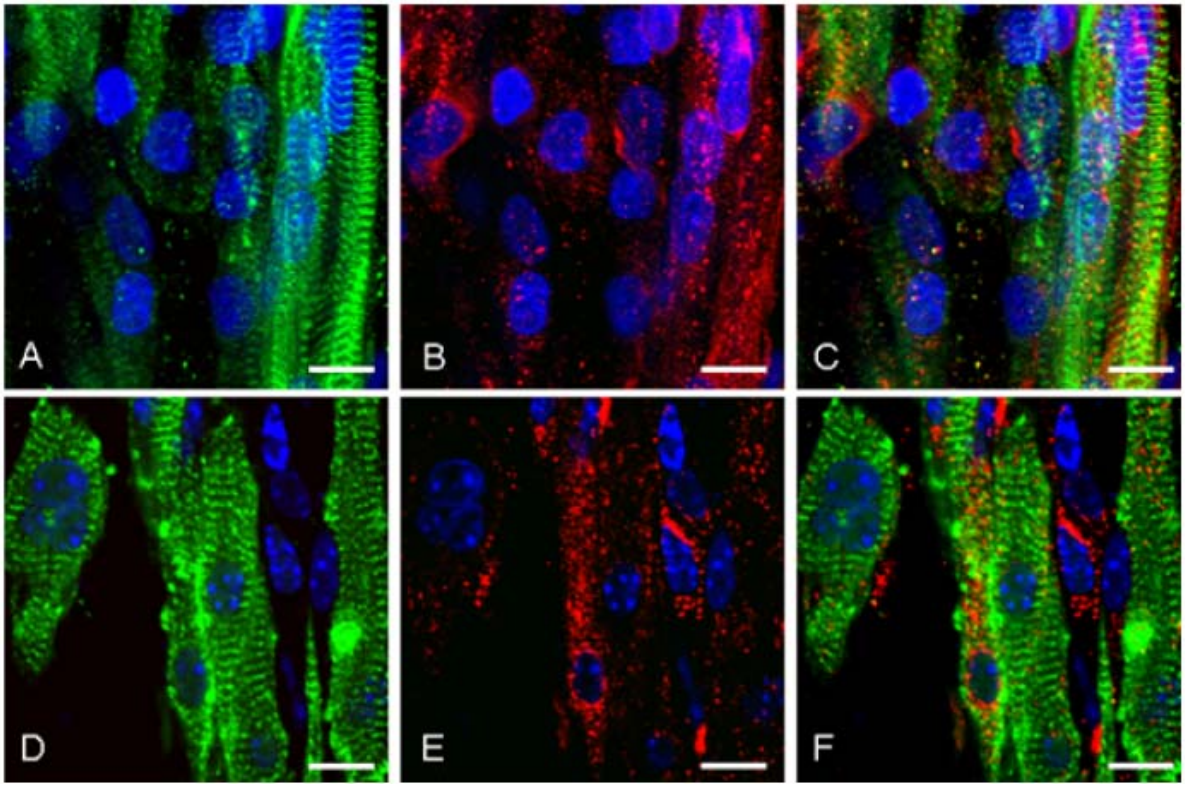

Figure 4-6. Connexin 43 expression pattern of native fetal left ventricular (LV) papillary muscle at gestational day 20 and MDSC-3DGB at culture day 7. **(A)** Native fetal left ventricular (LV) papillary muscle at gestational day 20 stained for α-sarcomeric actinin **(green)**, **(B)** gap junction protein connexin-43 **(red)**, and **(C)** merged. **(D)** Culture day 7 MDSC-3DGB stained for α-sarcomeric actinin **(green), (E)** gap junction protein connexin-43 **(red)**, and **(F)** merged. Cx-43 expression of MDSC-3DGB was similar to gestational day 20 fetal LV papillary muscle Cx-43 expression. Blue staining (DAPI) indicates nuclei. Scale bars indicate 10μm.

4.3.2 Cardiac specific gene and protein expression

Cardiac specific genes were expressed in culture day 7 MDSCs, regardless of the culture condition (Figure 4-7); suggesting that 7 days culture can trigger cardiac gene expression of rat MDSCs. Western blots showed that both MDSC-aggregates and 3D-MDSC and MDSC-3DGB groups expressed cTn-T and Cx-43 proteins (Figure 4-8A). Native tissue protein expression shows that developmental stage alters cardiac specific protein expression in both heart and

skeletal muscle. Maturation causes cardiac specific protein expression to increase in heart muscle and remain unchanged in skeletal muscle. MDSC-3DGB had similar protein expression to gestational day 20 fetal heart (Figure 4-8A). Densitometry analysis of each protein normalized to β-actin expression demonstrated that 3D culture (MDSC-3DGB and 3D-MDSC groups) was associated with higher cTn-T, Cx-43, and cTn-I expression versus MDSC-aggregate culture ($P<0.05$). Within 3D culture groups, we noted that both cTn-I and Cx-43 expression levels were higher in the MDSC-3DGB group than in the 3D-MDSC group ($P<0.05$) (Figure 4-8B). Notably, MDSC-3DGB had similar cTn-I and Cx-43 expression levels as well as a cTn-T/cTn-I ratio [9.1 ± 0.4 (n=3)] to gestational day 20 fetal heart [9.3 ± 1.7 (n=3)] which was significantly different compared to adult ventricular tissue [0.8 ± 0.1 (n=4), ($P<0.05$) cTn-T/cTn-I ratio as well as cTn-I and Cx-43 expression levels ($P<0.05$) (Figure 4-8B). These data indicate that while MDSCs express cardiac specific genes at 7 days in culture, regardless of culture method, the cardiac specific protein expression profiles differed with culture method; specifically that MDSC-aggregate formation followed by 3DGB culture synergistically increased induction of cells with an immature CM phenotype.

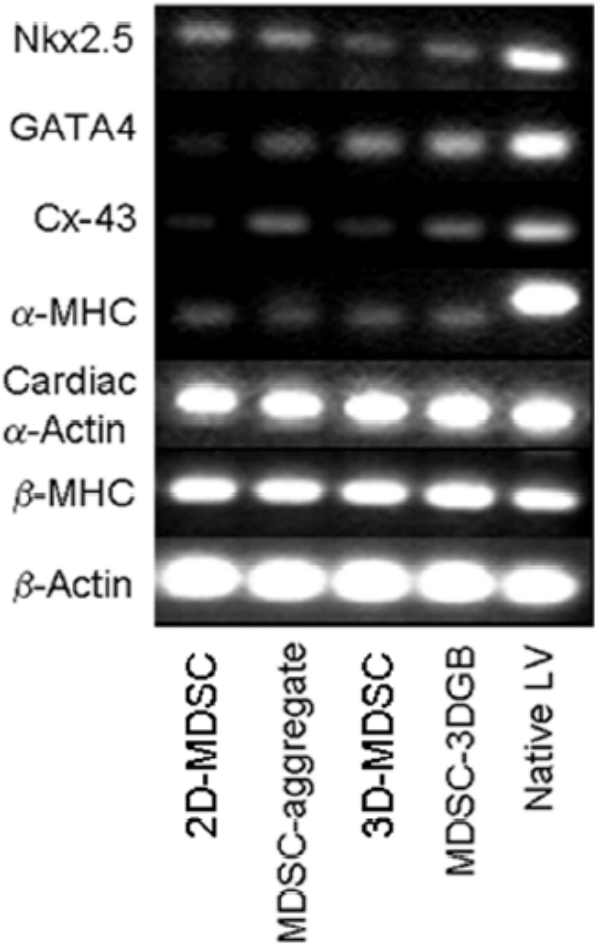

Figure 4-7. Cardiac specific mRNA expression. **Lane 1:** 2D-MDSC evaluated after 7 days in culture; **Lane 2:** MDSC-aggregate evaluated after 24 hours rotation culture; **Lane 3**: 3D-MDSC (without MDSC-aggregate formation) evaluated 7 days after tissue construction; **Lane 4**: MDSC-3DGB evaluated 7 days after tissue construction; **Lane 5**: adult rat ventricular tissue.

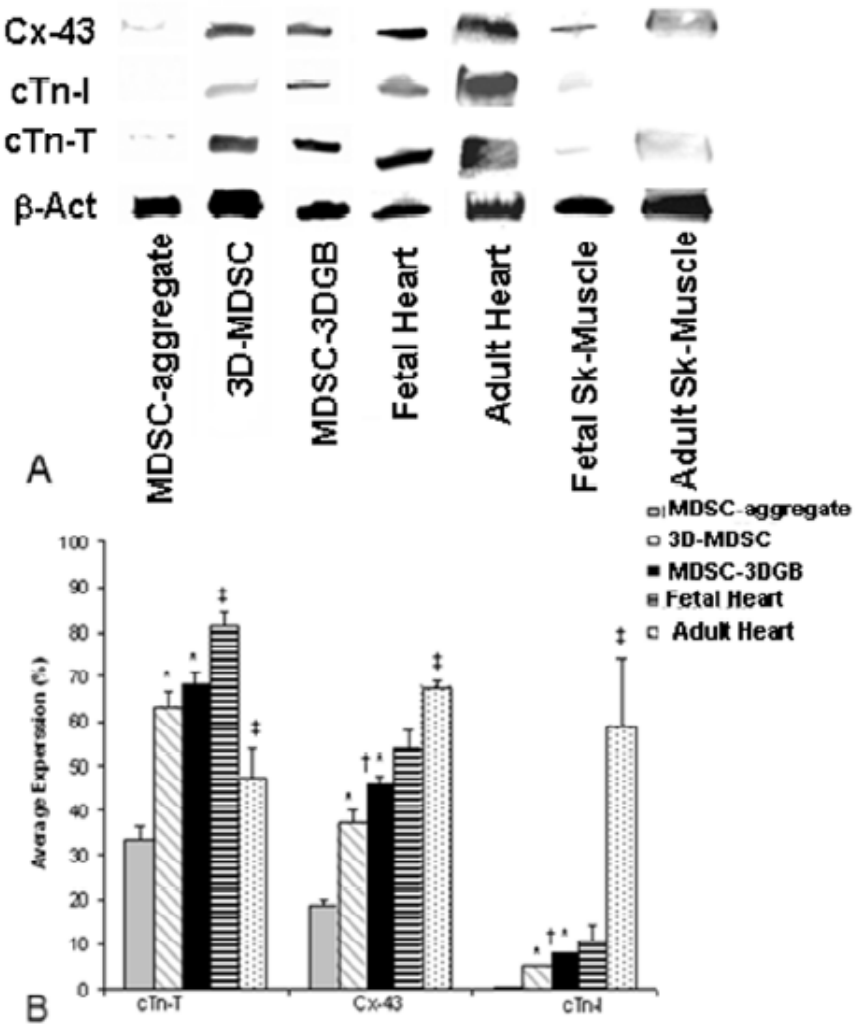

Figure 4-8. Cardiac specific protein expression and quantification. **(A)** Representative western blot analysis of **Lane 1**: MDSC-aggregate evaluated after 24 hr rotation culture; **Lane 2**: 3D-MDSC (without MDSC-aggregate formation) evaluated 7 days after tissue formation; **Lane 3**: MDSC-3DGB evaluated 7 days after tissue formation; **Lane 4**: Gestational day 20 fetal rat ventricular tissue; **Lane 5**: Twelve week-old adult rat ventricular tissue; **Lane 6**: Gestational day 20 fetal rat lower leg skeletal muscle; **Lane 7:** Twelve week-old adult rat gastrocnemius muscle. **(B)** Densitometric data normalized to β-actin expression (Average Expression vs. β-actin, %). *; $P<0.05$ vs. MDSC-aggregate culture normalized expression. †; $P<0.05$ vs. MDSC-3D culture normalized expression. ‡; $P<0.05$ vs. MDSC-3DGB culture normalized expression. Each lane contains 20 μg of protein per sample and experiments were repeated in triplicate.

4.3.3 Chronotropic effects of ISP and $CdCl_2$ on MDSC-3DGB

Culture day 7 MDSC-3DGBs were treated with ISP or cadmium chloride. Five minutes after treatment, ISP increased MDSC-3DGB spontaneous beat frequency [5.62 ± 0.54 Hz (n=8, P<0.05)] vs. pre-treatment [4.05 ± 0.20 Hz (n=8)] while cadmium chloride suppressed spontaneous beating activity [0.44 ± 0.16 Hz (n=8, P<0.05)] compared to pre-treatment [4.27 ± 0.44 Hz (n=8)] (Figure 4-9). No changes in pre-treatment baseline spontaneous beat frequency and post-treatment baseline spontaneous beat frequency were noted indicating reversible effects. These chronotropic responses do not occur in twitching mature skeletal muscle or skeletal myotubes[191].

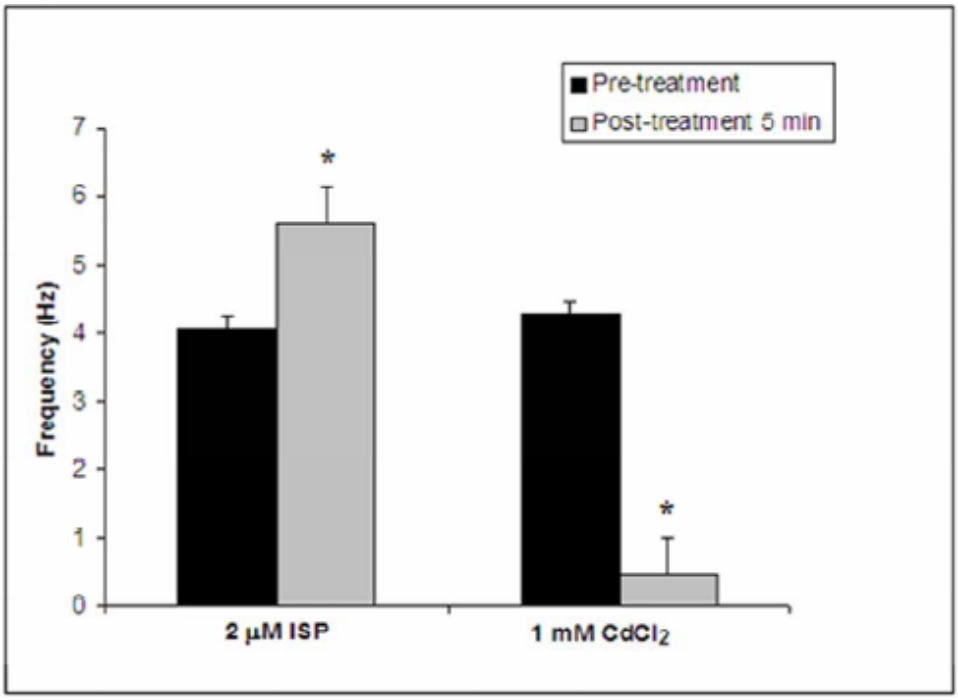

Figure 4-9. Effects of ISP and $CdCl_2$ treatment on spontaneous beating activity of MDSC-3DGB. Culture day 7 MDSC-3DGBs treated with 2µM ISP for 5 min. increased spontaneous beat frequency. MDSC-3DGBs treated with 1mM $CdCl_2$ for 5 min. decreased spontaneous beating. *; $P<0.05$ vs. pre-treatment.

4.3.4 Contractile properties of 3D MDSC culture

Upon field stimulation, both 3D-MDSC and MDSC-3DGB generated contractile force (Figure 4-10). MDSC-3DGB generated contractile force similar to engineered cardiac tissue from native fetal cardiac cells (EFCT). MDSC-3DGB as well as culture day 7 EFCT displayed a positive Frank-Starling response to increased construct length, whereas 3D-MDSC did not (P<0.05, Figure 4-10B and 4-10C). MDSC-3DGB generated a greater maximum active force [0.41 ± 0.06 mN (n=7, P<0.05)] compared with 3D-MDSC [0.22 ± 0.04 mN (n=5)] which was approximately one third of EFCT [1.45 ± 0.39 mN (n=7), P<0.05] (Figure 4-10C).

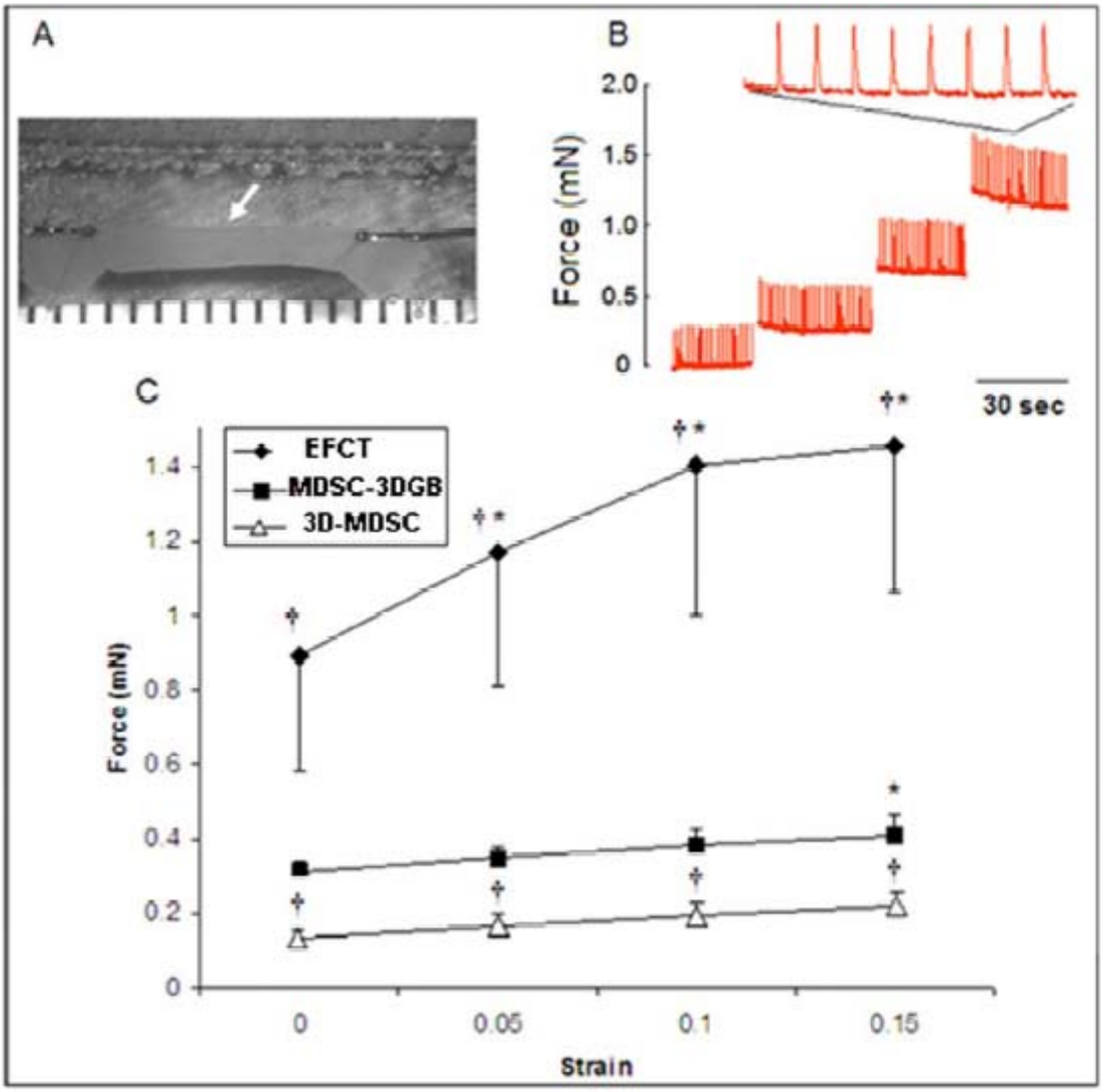

Figure 4-10. Biomechanical testing of MDSC-3DGB. **(A)** MDSC-3DGB mounted on a mechanical testing station (white arrow). Scribed x-axis minor scale divisions represent 1 mm. **(B)** Representative contractile force tracing of MDSC-3DGB at increasing resting lengths. **(C)** Active force-strain relations of culture day 7 MDSC-3DGB, culture day 7 MDSC-3D, and EFCT at strain deviations of 0 to 0.15. †; $P<0.05$ vs. MDSC-3DGB. Active force increased in response to increased strain (positive Frank-Starling response, *; $P<0.05$, ANOVA).

4.3.5 Intracellular free calcium ion $[Ca^{2+}]_i$ transients in MDSC-3DGB

We further investigated calcium handling by simultaneously recording contractile force and $[Ca^{2+}]_i$ transients from culture day 7 MDSC-3DGB in which we observed spontaneous tissue contraction. A rise in intracellular $[Ca^{2+}]$ preceded force generation (Figure 4-11A) and each $[Ca^{2+}]_i$ transient was associated with a concurrent contraction. MDSC-3DGB displayed a negative force-frequency relationship between 1 to 6 Hz based on reduced $[Ca^{2+}]_i$ transients and active force at increasing pacing rates and was associated with increased diastolic ratio (suggesting increased diastolic $[Ca^{2+}]_i$ and passive force) (Figure 4-11B), similar to immature myocardium[200, 201]. MDSC-3DGB force as well as $[Ca^{2+}]_i$ transient developed calcium (Ratio = F_{340}/F_{380}) [0.48 ± 0.16 (n=3)] was similar to ENCT (engineered cardiac tissue from cardiac cells isolated from day 1 neonatal rats) [0.56 ± 0.11 (n=5)]. These data indicate that MDSC-3DGB display the intracellular calcium ion transient features of immature CM with incomplete maturation of excitation-contraction coupling.

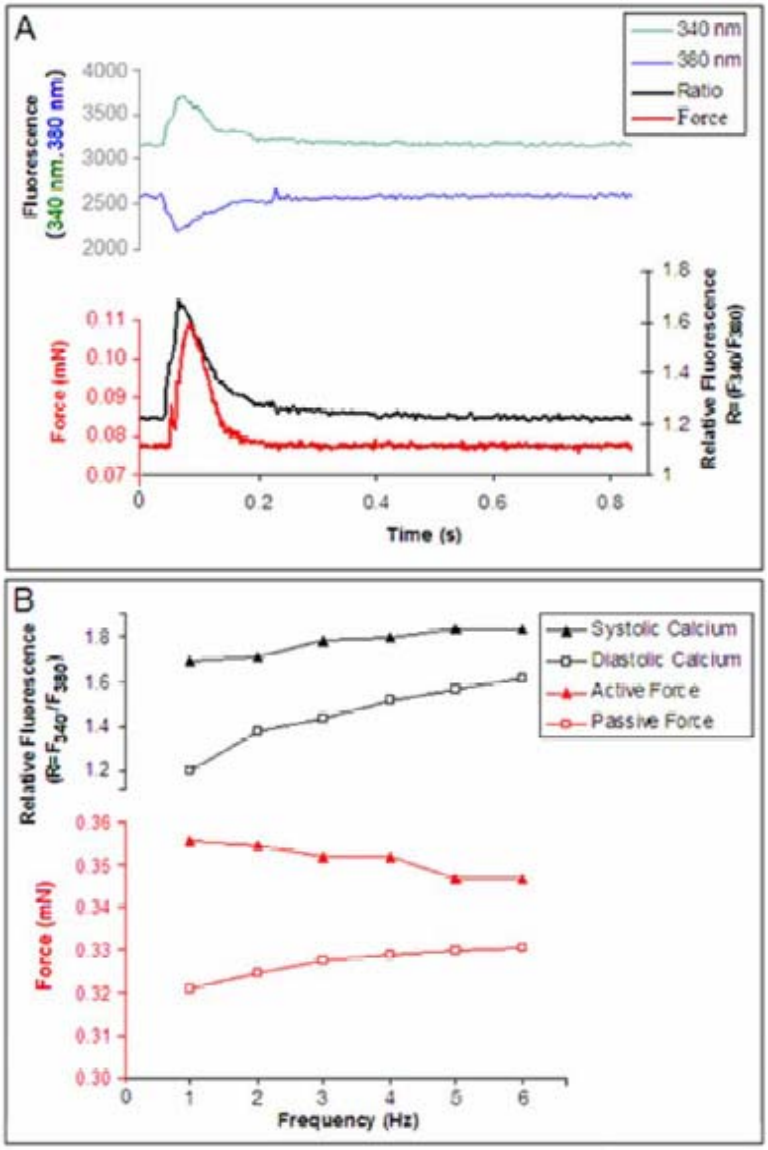

Figure 4-11. Simultaneous contractile force and intracellular [Ca^{2+}] transient measurement of MDSC-3DGB. **(A)** Representative single beat force **(red)**, fluorescence at 340 nm **(green)** and at 380 nm **(blue)**, and the relative fluorescence [ratio ($R=F_{340}/F_{380}$)] **(black)** tracing of culture day 7 MDSC-3DGB electrically stimulated at 1 Hz at 50V and 4 msec duration. A rise in intracellular [Ca^{2+}] preceded force generation and each $[Ca^{2+}]_i$ transient was associated with a concurrent contraction. **(B)** Culture day 7 MDSC-3DGB electrically stimulated at rates of 1 to 6 Hz at 50V and 4 msec duration. MDSC-3DGB showed increased diastolic $[Ca^{2+}]_i$ and reduced systolic $[Ca^{2+}]_i$ transient ratios **(black)** associated with increased diastolic and decreased active force **(red)** at increasing pacing rates, similar to immature myocardium.

4.3.6 Effect of cyclical mechanical stretch on MDSC-3DGB CM and non-CM proliferation activity

In 2.0 we found that EEECT responds to mechanical stretch with increased active force and CM, not non-CM, proliferation, which is similar to the developing fetal myocardium[120]. Since the results of this study indicate the MDSC-derived CMs within MDSC-3DGB have an immature CM phenotype we investigated the impact of cyclic mechanical stretch on MDSC-derived CM contractile force and proliferation in MDSC-3DGB.

MDSC-3DGB were subjected to cyclic mechanical stretch (0.5Hz, 5% elongation) for 48 hours beginning at culture day 5. Histological assessment revealed that mechanical stretch significantly increased the phospho-histone H3 positive cell ratio only in the CM fraction not the non-CM fraction CM (Table 4-2).

Table 4-2. Effects of cyclic mechanical stretch on MDSC-3DGB CM and non-CM proliferation. Data are mean ± SE. n; number of samples. *; $P<0.05$ vs. Control MDSC-3DGB within group. Stretch MDSC-3DGB: MDSC-3DGB subjected to uniaxial cyclic mechanical stretch (0.5Hz, 5% elongation)

	H3 positive ratio	
	CM	non-CM
MDSC-3DGB	13.05 ± 0.40 (n=3)	4.24 ± 0.55 (n=3)
Stretch MDSC-3DGB	19.30 ± 0.56 (n=4)*	5.40 ± 0.69 (n=4)

Western blot analysis indicated that total cTn-T and cTn-I (normalized by β-actin) expression did not change in response to 48 hours cyclic mechanical stretch stimulation suggesting CM proliferation, not hypertrophy (Figure 4-12). Phospho-histone H3 and Cx-43 expression significantly increased following 48 hours cyclic mechanical stretch (Figure 4-12).

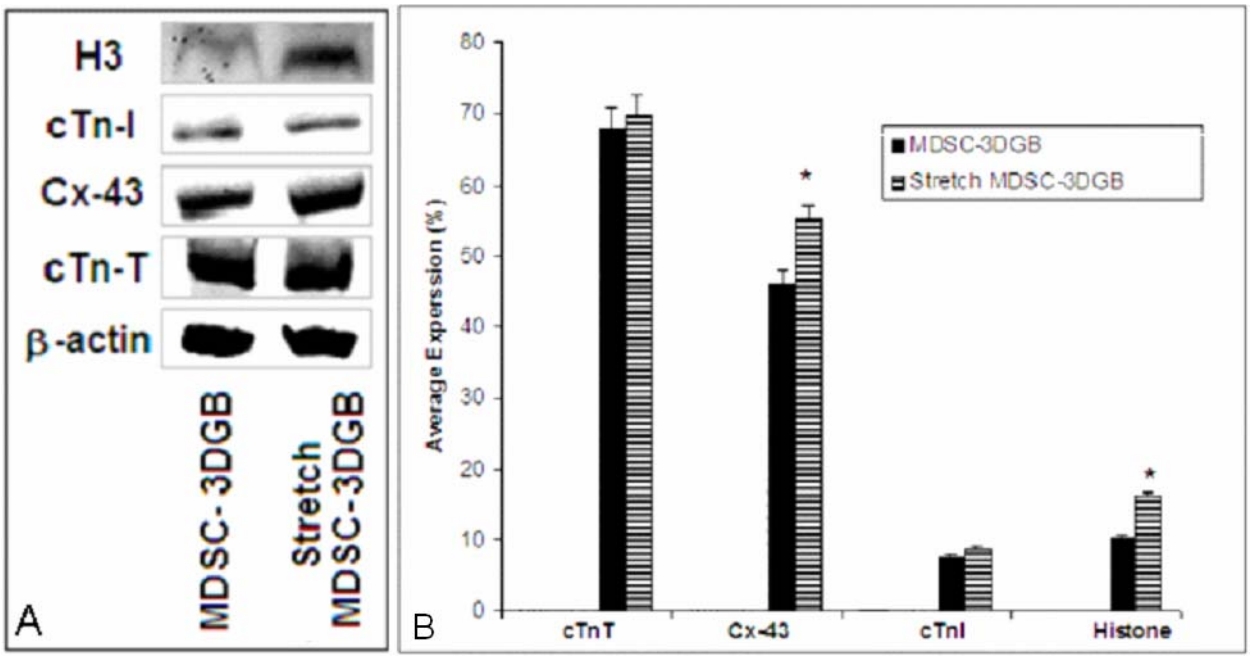

Figure 4-12. Representative western blot of MDSC-3DGB expression following mechanical stretch stimulation**.** Stretch stimulation increased MDSC-3DGB Cx-43 and H3 expression **P*<0.05 vs. normalized control MDSC-3DGB expression.

MDSC-3DGB generated contractile force similar to EEECT. Cyclic mechanical stretch increased active contractile force versus control MDSC-3DGB (Figure 4-13).

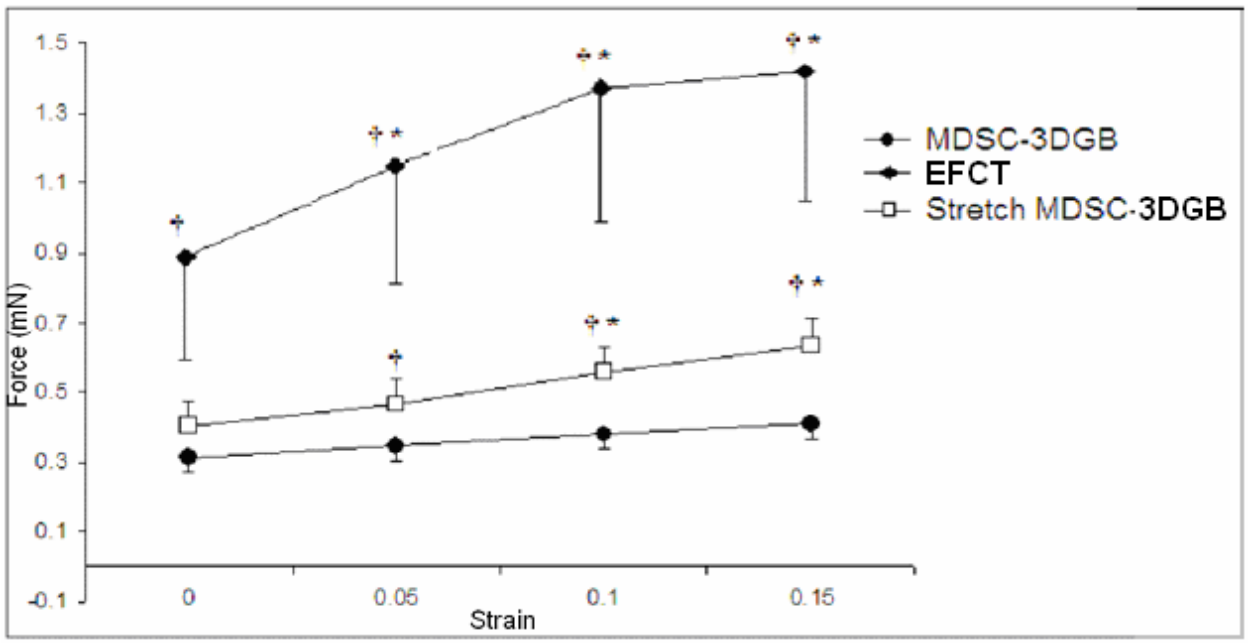

Figure 4-13. MDSC-3DGB contractile properties in response to mechanical stretch. Active force-strain relations of stretch (n=9) and non-stretched (n=8) MDSC-3DGB and engineered cardiac tissue from fetal cardiac cells (EEECT) (n=6) at 0 to 0.15 strains. The active stress increased in parallel with increases in strain (*, Frank-Starling law). Cyclic mechanical stretch stimulation significantly increased active force at given strain. (†; $P<0.05$ vs. non-stretch MDSC-3DGB). Data are mean ± SE.

Results suggest that CMs within MDSC-3DGB respond to cyclic mechanical stretch with increased active force and CM proliferation, similar to EEECT and the developing fetal myocardium.

4.3.7 MDSC-3DGB implantation on post-infarcted myocardium

In 3.0 we found that implanted EFCTs onto post-infarcted LV myocardium maintained active CM proliferation with minimal CM apoptosis, preserved myocardial tissue structure, and attenuated functional deterioration of post-infarcted LV, which suggested that active CM proliferation of donor cardiac tissue graft may play an important role for graft survival and

functional contribution to the recipient injured myocardium. Thus, we investigated whether MDSC-3DGB is implantable and improves injured recipient heart function, similar to EFCT.

Two weeks after a myocardial infarction via a left coronary artery ligation MDSC-3DGB was implanted on the injured myocardium (Figure 4-14).

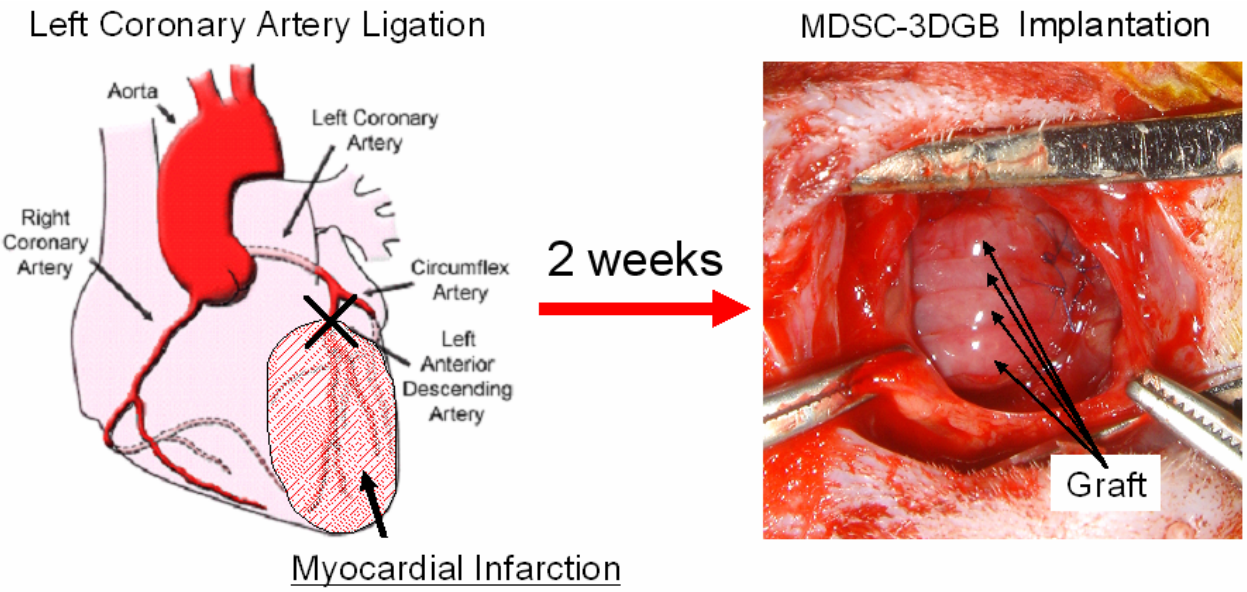

Figure 4-14. MDSC-3DGB implantation onto post-infarcted LV surface. **(Left panel)** Schematic of left coronary artery ligation generating myocardial infarction**.** Photograph of MDSC-3DGB graft implantation onto the post-infarcted myocardium. **(Right panel)** Four MDSC-3DGBs (indicated by arrows) were implanted to cover the infarct myocardium**.**

There were no early or late postoperative deaths related to graft implantation in any experimental group. Eight weeks after MDSC-3DGB implantation onto post-infarcted rat myocardial surface, cells within MDSC-3DGB did not migrate out from the implanted MDSC-3DGB and maintained MDSC-3DGB myocardial tissue integrity. The implanted grafts were still recognized without dislocation from the original implanted area and the grafts were merged with host LV surface by visual inspection. Hematoxylin-eosin (HE) staining of microtome sections revealed that implanted MDSC-3DGBs were recognized as an eosin positive muscle like tissue

at the implanted sites (epicardial surface) of infarcted myocardium in all hearts, which was not observed in the sham operated LVs (Figure 4-15). We note that typical tumor-like tissue formations assessed by HE staining were not found in all graft implanted LVs.

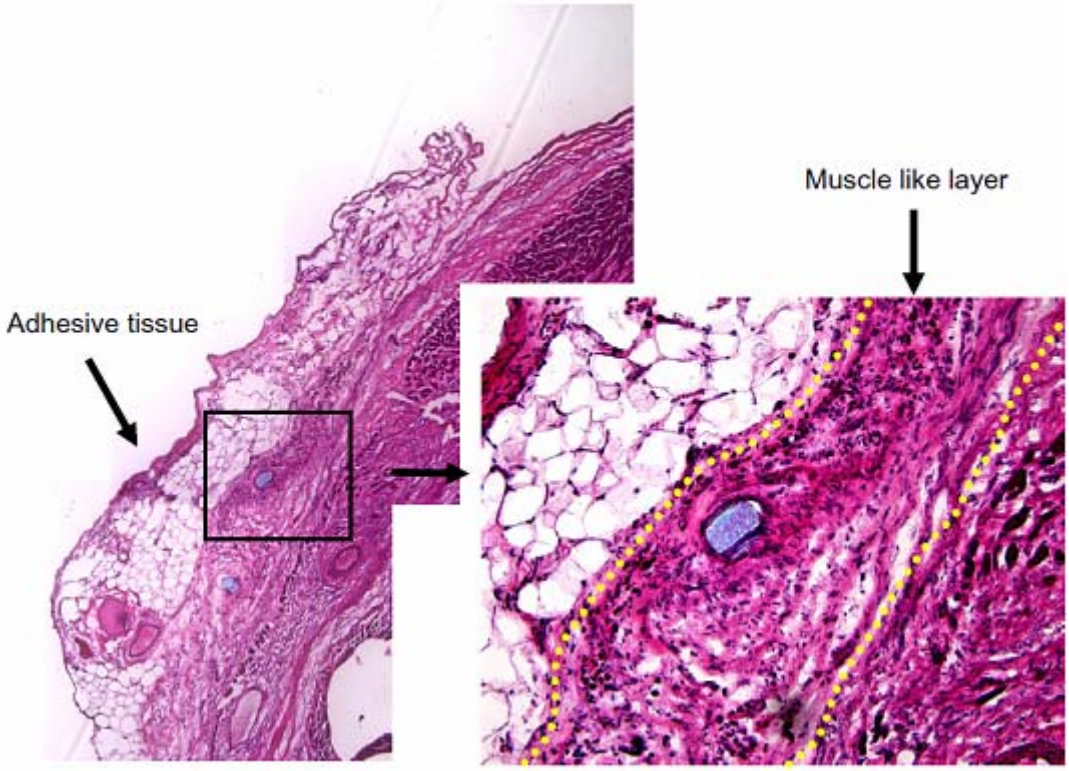

Figure 4-15. Histological assessment of implanted MDSC-3DGB fate within post-infarcted LV myocardium. Cells within MDSC-3DGB stayed within the implanted site and preserved the graft myocardial tissue structure *in vivo*. Implanted MDSC-3DGBs were well merged onto host infarcted myocardial surface and maintained a muscle-like tissue layer **(insert*)***. Yellow dot curves indicate implanted MDSC-3DGB.

At 2 weeks after permanent coronary artery ligation (pre-implantation state, 0 week) LV EDA was increased approximately twice larger than pre-coronary artery ligation state and LV FAC was decreased compared to the pre-coronary artery ligation state indicating that the permanent coronary artery ligation induced post-myocardial infarcted heart failure (LV dilatation and impaired LV contraction). Longitudinal echocardiography after graft implantation showed that

the sham operated LVs further increased EDA at 8 weeks. MDSC-3DGB tended to not increase EDA similar to EFCT implanted LVs indicating that implantation of MDSC-3DGB prevented further LV dilatation (Figure 4-16, left panel). LV FAC decreased in the sham operated LV by 8 weeks whereas MDSC-3DGB implanted LV significantly increased contractile function at 8 weeks, again similar to EFCT implanted LV (Figure 4-16, right panel).

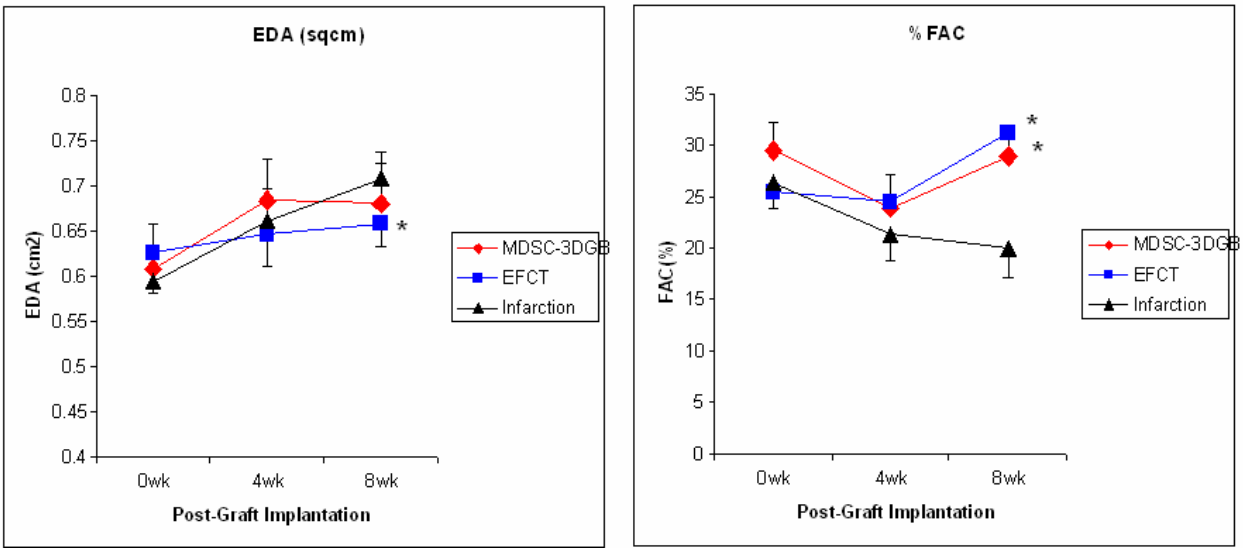

Figure 4-16. Echocardiographic assessment of MDSC-3DGB and EFCT implanted post-infarcted myocardium. Data are expressed as % change in both LV EDA and FAC ± SE. The value of 100% EDA indicates EDA at cardiac graft implantation. **(Left panel)** Sham operated LV cavity area increased and contractile function decreased by 8 weeks after graft implantation**,** (*, $P<0.05$, ANOVA) but MDSC-3DGB implanted LV tended to not increase LV cavity area. **(Right panel)** LV contraction of sham operated LV decreased by 8 weeks (*, $P<0.05$) whereas MDSC-3DGB and EFCT implanted LV increased LV contraction (*, $P<0.05$). MDSC-3DGB and implanted LVs at 8 weeks after graft implantation significantly increased LV FAC in comparison to sham operated LVs ($P=0.009$ vs. sham-operated LV). Data support that implanted MDSC-3DGBs attenuate LV remodeling of post-infarcted LV similar to EFCT implanted LVs. *; P<0.05 within group (ANOVA). 0wk; pre-implantation, 4wks and 8wks; 4 weeks and 8 weeks after implantation.

4.4 DISCUSSION

Previous studies have shown that stem cells isolated from skeletal muscle specimens have the ability to differentiate into CMs[76, 189, 191-194], however, the efficiency of CM differentiation remains unclear and with limited functional characterization. In the current study we found that; 1) Low serum growth medium treated rat MDSCs expressed cardiac specific genes similar to native adult myocardium, consistent with the findings from others in both human and mouse skeletal muscle derived cells; 2) the combination of MDSC-aggregate formation and 3DGB culture significantly increased cardiac specific protein expression, spontaneous beating cell activity, and contractile properties; 3) MDSC-3DGB subjected to cyclic mechanical stretch for 48hrs increases active force and CM proliferation, similar to EEECT and the developing fetal myocardium; and 4) MDSC-3DGB survives and improves heart function *in vivo.* Our results suggest that 3D microenvironmental cues provided by MDSC-aggregate and 3DGB culture play an important role in differentiation of cells with an immature functional CM phenotype from MDSCs and the 3DGB system provides the necessary environment to evaluate the contractile properties *in vitro,* which indicates increased CM proliferation and contractile force in response to mechanical stretch, and *in vivo*, which indicates survival and improvement of heart function similar to EFCT.

Various experiments have highlighted the importance of the microenvironment on stem cell-derived CM induction, differentiation, and survival[61, 62]. Tamaki et al. have recently shown that skeletal muscle-derived multipotent Sk-34 cells can give rise to CMs and that cell-to-cell relationships and cellular milieu were important for this differentiation[193]. However, these results were achieved with co-culture with embryonic CMs, and there was no functional characterization of the SK-34 derived-CMs *in vitro*. Thus it is unclear how these cells function in

comparison to native CMs in either a healthy or diseased heart. Rota et al. have shown that bone marrow stem cells can engraft into the injured myocardium and differentiate into functionally competent CMs and vascular structures by establishing a microenvironment necessary to adopt the cardiac phenotype[74]. However, despite these positive results there is still limited information on the use of physical stimuli and unique microenvironments to control CM induction from progenitor/stem cells, CM maturation, and contractile function.

Three dimensional growth of cells in aggregate spheres has been shown to direct and facilitate cell-cell interactions as well as to modify the differential expression of both morphogenic and angiogenic pathways in CMs[17] and hepatocytes[25]. Cell aggregate culture has been shown to enhance CM gene expression patterns[17], increase the synthesis and release of ECM components[26], and accelerate CM differentiation efficiency of embryonic stem cells[27] and liver stem cells[18]. Similarly, Albrecht et al. found that chondrocyte matrix biosynthesis was dependent on cell cluster size, rather than overall cell density[28]. Aggregate culture has also been used to enhance survival and differentiation of various stem cell types[27, 29, 30], versus static culture. These studies suggest that aggregation imparts many of the necessary structural cues required for maintaining differentiated phenotype, including proper dimensionality, shape, cell–ECM, and cell–cell interactions.

Cardiac cells within 3D cultured tissue display distinct features that are more representative of native myocardium than do cells within 2D culture[20, 47]. Bursac et al. investigated the effect of 3D vs. 2D culture on CM properties and found that the 3D microenvironment plays a critical role in maintenance of CM metabolism, sarcomere formation, cell-to-cell connections, and electrophysiological properties[31]. 3D growth of fibroblasts[14, 32], endothelial cells[33], and mammary gland cells[34] also exhibits cell morphology and function

similar to native tissue over 2D culture[35]. In the current study we showed that the 3D culture condition increased differentiation of cells with a functional CM phenotype at both the gene and protein levels. Furthermore the combination of MDSC-aggregate formation and 3DGB culture significantly increased expression of the cardiac specific proteins cTn-I and Cx-43 in comparison to the MDSC-aggregate group; indicating that MDSC-aggregate formation followed by 3DGB culture synergistically promoted differentiation and maturation of cells with a functional CM phenotype *in vitro*. Chronotropic effects of ISP and cadmium chloride treatment clearly showed that MDSC-3DGB contractile properties are mimicking cardiac tissue, not twitching mature skeletal muscle or tissue derived from myoblasts. MDSC-3DGB exhibited synchronous contraction and cardiac $[Ca^{2+}]_i$ transients in response to electric field stimulation similar to engineered cardiac tissue from native CMs, suggesting that cells within MDSC-3DGB are a functional syncytium. MDSC-3DGB exhibited a positive force-length (Frank-Starling) and a negative force-frequency relationship consistent with incomplete maturation of CM calcium cycling[20, 202] which was similar to engineered cardiac tissue from native fetal CMs. These results suggested that the combination of MDSC-aggregate formation and 3DGB tissue culture was required for differentiation of cells with a functioning CM phenotype from MDSCs.

Studies in cellular cardiomyoplasty showed that the microenvironment of the injured myocardium includes the release of matrix factors and cytokines that are clearly not conducive to supporting CM induction and/or survival from implanted stem cells[203, 204]. This may inhibit proper CM regeneration and/or lead to the potential for inappropriate differentiation in the absence of the proper cell-specific milieu. Therefore, our MDSC-3DGB provides a novel method for studying and optimizing *in vitro* conditioning of the micromechanical environment with direct assessment of contractile properties, and its role in stem cell commitment to

functioning CMs from MDSCs *in vitro*. Although the results of our current study clearly indicate that combined MDSC-aggregate formation and 3DGB culture drives induction of cells with a functioning cardiac phenotype from MDSCs and that the contractile properties mimic those of engineered tissue from native fetal cells, the underlying mechanisms as to how the 3D microenvironment regulates this induction from MDSCs remains unclear and necessitates further studies.

4.4.1 Limitations

There are several limitations that need to be mentioned. A major limitation to the current study is that we can not definitively determine the state of the cardiomyocyte-like cells within MDSC-3DGB. This is most likely due to the co-existence of many cardiac and skeletal muscle specific proteins (MHCs, troponins, etc.) as well as excitation-contraction coupling mechanisms which occur not only in cultured cells, especially those that are considered to be immature, but also within the developing tissue. Cognard et al. have shown that "cardiac" and "skeletal" excitation-contraction coupling mechanisms co-exist in the developing skeletal muscle with the "cardiac" type dominant in the early phases of myogenesis and the "skeletal" dominating in more mature muscle[91]. Rose et al. have reported bone marrow-derived mesenchymal stromal cells that acquire expression of CM genes in *in vitro* co-culture with native CMs but that did not generate action potentials or display ionic currents typical of CMs, and thus remain functionally non-CM[205]. Therefore, further studies are necessary to determine whether CM phenotypic cells within MDSC-3DGB develop further and mature similarly to the native developing immature myocardium, and whether the 3DGB culture in its present form is able to do this. In the present study, we showed that cTn-T positive cells consist of approximately 20% of the entire number of

MDSCs within the MDSC-3DGB, a population which may contain both undifferentiated MDSCs and MDSCs differentiated into other types of cells. Thus, it is necessary to develop a method to enrich CM phenotype cells from the MDSC-3DGB. It is likely that more contractile apparatuses within each differentiated CM as well as more CMs within MDSC-3DGB (~20% compared to ~60-70% within EFCT) and a better organization and communication within the tissue would serve to increase the contractile properties to be similar to the EFCT or native tissue, however further studies are necessary. Similarly, it is also necessary to observe the CM phenotypic cells within MDSC-3DGB over longer culture periods. It is possible that the CM phenotypic cells will 1) acquire a more mature CM phenotype, 2) remain an immature CM population, or 3) return to an undifferentiated state. It remains unknown whether CM differentiation and maturation from MDSCs require other types of cells *in vitro*. Previous studies have shown that preconditioned MDSCs transplanted into injured myocardium survive and differentiate into a more matured CM phenotype based on histological assessment[191-193], while in the current study, differentiated cells exhibited a more immature CM phenotype. The factors which drive differentiated CM phenotypic cells toward a more mature CM phenotype remain unknown. The studies investigating MDSC-3DGB response to mechanical stretch and survival on post-infarcted myocardium are preliminary and an increased sample size is necessary to come to a valid conclusion. Similarly, investigation into the underlying mechanisms that play a role in the noted response of increased CM proliferation and contractile properties similar to EEECT are necessary, p38MAPK and Akt could play a role similar to EEECT or other MAP-kinases, such as JNK, or ERK that have also been closely associated with the regulation of CM growth, survival, and proliferation may directly or indirectly participate in the regulation of both CM and non-CM responses to cyclic mechanical stretch.

4.4.2 Conclusion

In summary, our results suggest that 3D environmental cues provided by MDSC-aggregate formation and 3DGB culture are complementary and sufficient to trigger differentiation of cells with an immature functioning CM phenotype from rat skeletal MDSCs *in vitro* and that this 3DGB culture responds to mechanical stretch with increased CM proliferation and contractile properties similar to EEECT and the native immature myocardium. MDSC-3DGB can be implanted on the injured myocardium and improve contractile function post injury. MDSC-3DGB can be used as a method to directly assess the contractile properties of differentiated CMs from MDSCs *in vitro*. This novel induction approach may be useful in generating scalable, functioning, donor CMs for cardiac repair and regeneration.

5.0 EFFECT OF MECHANICAL STRAIN ON CARDIOMYOCYTE DIFFERENTIATION WITHIN MDSC-3DGB

5.1 INTRODUCTION

The regulation of stem cell differentiation has been a challenge in regenerative medicine. The decision made by a stem cell to commit to a particular program is highly context dependent and requires multiple targets in different pathways to be simultaneously perturbed to switch the response between growth, differentiation, and apoptosis. Time-varying changes in stresses and strains significantly influence the fundamental cellular response in terms of cell morphology, phenotype, and function of growing cardiac tissue[92-95]. Various methods have been used to manipulate endogenous and exogenous progenitor cells to differentiate into CMs[127] with the focus being on chemical or growth factors and co-culture. However, previous studies have shown that soluble induction factors tend to be less selective than mechanical factors in driving cell specification[128].

The role of the mechanical environment on cardiomyocyte (CM) growth, proliferation, maturation, and death have been well documented[4, 92-105]. Mechanical strain has been shown to reprogram gene expressions, increase protein synthesis, and trigger adaptive responses in muscle phenotype via the expression of contractile proteins within engineered cardiac tissue. We have shown previously in 2.0 and 4.0 that when subjected to cyclic mechanical stretch EEECT and

MDSC-3DGB responds by increasing cellular proliferation, not hypertrophy, and contractile function; specifically, that mechanical stretch positively regulates CM proliferation, but not non-CM proliferation[20, 120]. However, few studies have been devoted to understanding the role of the mechanical environment on CM induction from progenitor/stem cells[121-123]. Understanding the role of mechanical forces on CM induction is essential because there is clear evidence that cardiac cells within 3-dimensional (3D) cultured tissues display distinct features that are more representative of native tissues[20-22] that do not occur in 2D culture[23, 24], including increased contractility and mechanical properties[36-38, 74, 178, 206].

We have shown in 4.0 that skeletal muscle-derived stem cells differentiate into cells with an immature functioning CM phenotype within a three-dimensional engineered tissue construct (MDSC-3DGB)[209]. MDSC-3DGB expressed cardiac specific genes and proteins, and contractile force and intracellular calcium ion transients similar to engineered cardiac tissue from native cardiac cells. However, only approximately 20% of these cells differentiate into CMs and they are not evenly distributed without the construct. MDSC-3DGB generated force that was approximately 10% of the force generated by EFCT. Most tissue engineered cardiac constructs generate less than 15% of the developed stress of natural isolated myocardial trabeculae[13, 20, 120, 207-209]. Thus a way to improve the number of CMs within MDSC-3DGB as well as the force is necessary. We will use MDSC-3DGB as a model to analyze mechanically driven stem cell derived CM differentiation with the hypothesis being that as MDSC-3DGB development proceeds, MDSC-derived CM induction, maturation, and contractile function will increase with the rates dependent upon the location within MDSC-3DGB via MDSC morphology changes: evidenced by cell size, shape, and orientation changes due to the construct strain variations.

5.2 METHODS

5.2.1 MDSC-3DGB construction

MDSCs were isolated according to 4.2.1. GFP positive (+) and negative (-) MDSCs were expanded on 2D flasks and were trypsinized using a 0.05% trypsin/EDTA solution (Invitrogen). The cell suspension of GFP(-) to GFP(+) cells at a 5:1 ratio, respectively, was cultured on a 100mm-dimeter suspension culture dish (Corning, Lowell, MA) for 24 hours at 37°C using a gyrating shaker (50 rotations/min) to form 50 to 70μm diameter MDSC aggregates (MDSC-aggregate, 330-350 cells/aggregate) under standard MDSC growth medium. Acid-soluble rat tail collagen type-I solution (pH 3, Sigma, St. Louis, MO, USA) was neutralized with alkali buffer (0.2 M NaHCO3, 0.2 M HEPES, 0.1 M NaOH) on ice. Matrigel (13% of total volume, BD biosciences) was then added and the cell suspension and matrix solution mixed to reach a final collagen type-I concentration of 0.67 mg/mL. Approximately 200μL of the cell/matrix mixture was poured into the 20mm long x 2mm wide cylindrical cast of a Flexcell Tissue Train collagen type-I coated silicone membrane culture plate (FX4000TT, Flexcell International, Hillsborough, NC) and incubated for 120 minutes (37°C, 5% CO_2)[20] to form a cylindrical MDSC-3DGB. Each MDSC-3DGB was cultured in a 5% FBS containing growth medium.

5.2.2 3D Mechanical strain mapping

15 μm diameter red fluorescent polymer microspheres (Thermo Scientific, Fremont, CA) were mixed with the cell suspension and incorporated within MDSC-3DGBs. Triangular arrays of microspheres were tracked throughout the construct and over development. The microsphere

3D (x, y, z) orientation was determined by capturing digital images of the x-y plane at various positions on the x-z plane of a construct (Figure 5-1) using a standard laser confocal microscopy system (Leica SP5, Leica Microsystems, Mannheim, Germany) and post-processing using custom made MatLAB code (Appendix A). 3D image correlation was performed step-wise, i.e. between the n^{th} and $(n+1)^{th}$ developmental day end-point image stacks, and the resulting displacement vectors of each microsphere triplicate were determined and differentiated directly to give the strain map. MDSC-3DGB strain variations were quantified temporally, over development at culture days 1 (the day after tissue construction), 3, 5, 7, and 9, and spatially, the construct constrained ends (END) and the unconstrained middle (MID)) for n=8 constructs. MDSC-3DGB-END is defined as the 4 mm from the edge of the Tissue Train culture plate anchors. The MDSC-3DGB-MID is defined beginning from 5.5 mm from the edge of the Tissue Train culture plate anchor and extending 4 mm.

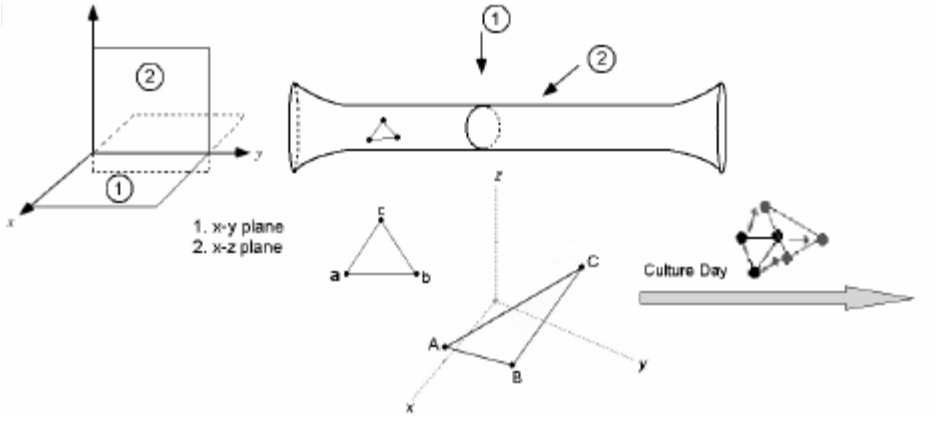

Figure 5-1. 3D mechanical strain mapping schematic.

5.2.3 Analysis of cell shape, size, and orientation

5.2.3.1 Cell shape

To determine cell shape, the cell geometry will be approximated from the images by segmentation of the GFP (+) cells within the chimeric construct (using custom made MatLAB software, Appendix A). Briefly, the extracted green color channel from the RGB images was thresholded and binarised. A MatLAB algorithm was employed to generate a 3D (x, y, z) orientation for each cell by adding the images together and the GFP (+) cell shape was characterized by its eccentricity using the following equation $E = \sqrt{1 - (ER)^2}$ where the eccentric ratio (ER) is defined as the cell minor axis over the major axis. Values of eccentricity range from 0 to 1 with 0 being a perfect circle and 1 an extremely stretched ellipse.

5.2.3.2 Cell size

To analyze cell size, in addition to the above calculation, 3D volume rendering from the segmented cell shape was calculated to determine cell size. Briefly, the individual (x, y, z) pixel coordinates for each cell was converted into a volume (μm^3) based on the image scale using a custom made MatLAB program (Appendix A).

5.2.3.3 Cell orientation

To determine cell orientation, principle component analysis (PCA) was employed using the cell shape data. The orientation was quantified by determining each segment vector length and the angle from the three principle cell directions to the sample coordinate axes using a custom made MatLAB program (Appendix A).

5.2.4 Determination of MDSC-derived CM differentiation within MDSC-3DGB

MDSC-3DGB CM differentiation was quantified over development at time points between culture day 1 (the day after tissue construction) and culture day 9 at 48 hour intervals to determine the phenotypic state of the MDSC-CM within each construct region (END or MID). To determine MDSC-derived CMs combined histology and western blot analysis was assessed.

5.2.4.1 Histological Assessment

MDSC-3DGB-END and MDSC-3DGB-MID samples were fixed with 4% paraformaldehyde/PBS for 15 minutes and embedded in the 13% polyacrylamide gel. 150μm thick sections were made using a vibratory microtome (Vibratome-1000, Vibrotome.com)[20]. Sections were permeabilized with 0.1% Triton X-100 for 30 and stained for mouse monoclonal anti-cTn-T (Abcam), cTn-I (Abcam), Cx-43 (Abcam), anti-phospho-S10 Histone H3 (Upstate cell signaling solutions, Temecula, CA), or monoclonal skeletal fast myosin heavy chain (sk-fMHC) (Sigma, St. Louis, MO) primary antibodies and Alexa Fluor 647 or Alexa Fluor 594 secondary antibodies (Invitrogen). We reconstructed 3D projection images from stacks of z-axis optical scans using a standard laser confocal microscopy system (FV1000, Olympus, Tokyo, Japan) and Scion Image software (Scion Corp, MD)[20]. The composite 3D projection images were further processed using Adobe Photoshop software (Adobe, San Jose, CA). Total cell number per region (END vs. MID) was calculated as [DAPI (+) nuclei]. CM cell ratio (%) per region was calculated by [Cardiac troponin-T expression area] / [DAPI (+) expression area] (%).

5.2.4.2 Western Blot analysis

Whole cell lysates were prepared from MDSC-3DGB tissue (n=9) at each developmental day (1, 3, 5, 7, and 9) pooled populations, and separated by SDS-PAGE (10% separating gel, Bio-Rad Laboratories). Immunoblotting was carried out using routine protocols. Each lane contained 20μg of total protein. Mouse monoclonal β-actin antibody (Abcam, Cambridge, MA), mouse monoclonal cardiac troponin-T (cTn-T, Abcam), mouse monoclonal anti-connexin-43 (Cx-43, Abcam), mouse monoclonal cardiac troponin-I (cTn-I, Abcam), anti-phospho-S10 Histone H3 (Upstate cell signaling solutions, Temecula, CA), and monoclonal skeletal fast myosin heavy chain (sk-fMHC) (Sigma, St. Louis, MO) were visualized with IR-Dye 800 or IR-680 donkey anti-mouse secondary antibody (Rockland Immunochemicals, Gilbertsville, PA, USA). All proteins were visualized using an infrared western blot imaging system (Odyssey, LI-COR Biosciences Lincoln, NE, USA). Immunoblots were performed in triplicate and quantified using densitometry and an expression ratio was calculated (Odyssey, LI-COR Biosciences Lincoln, NE, USA).

5.2.5 Mechanical testing

The passive force of MDSC-3DGB END and MDSC-3DGB MID (n=6) was measured as previously described[20]. In brief, each construct was cut into its respective regions (END and MID) and each region was then transferred from the Flexcell culture dish to the perfusion chamber of the muscle testing station containing a cold (25^{o}C) high potassium calcium free Ringer solution composed of (in mM): 82 NaCl, 60 KCl, 10 Trizma-HCl, 10 Trizma-base, 11.0 glucose and gassed with 95% O_2 /5% CO_2 (pH 7.4). One end of the construct was attached to a force transducer (model 403A, Aurora Scientific, Ontario, Canada) and the other end to a length

controller mounted on a micromanipulator using 10-0 mono-filament nylon sutures. The buffer within the perfusion chamber (1.5mL total chamber volume) was then replaced with a warmed Ringer solution buffer (37^{o}C, containing 2mM Ca^{2+}) and perfused at a rate of 1 mL/min. The longitudinal length of the construct was increased in 5% increments up to a 15% elongation from original length ($L_{0.15}$). The external diameters of the construct were recorded at each stretch increment using a digital video microscopy system (Model KPD-50, Hitachi, Japan, and Scion Image Software with a CG-7 frame-grabber board, Scion Corp.).

5.2.6 Statistical analysis

Data are expressed as mean ± SE. One-factor analysis of variance (ANOVA) was used to compare the protein analysis among experimental groups. Two-factor ANOVA was performed to compare the spatial and temporal strain relations among experimental groups. Two-factor repeated ANOVA was performed to compare the passive stress-strain relations among experimental groups. We performed a Tukey post-hoc test to determine individual differences between experimental groups. Statistical significance was defined by a value of $P<0.05$. All calculations were performed using SigmaStat (Systat Software Inc, Point Richmond, CA, USA).

5.3 RESULTS

5.3.1 Cell morphology

MatLAB assisted post-processing of time-lapse confocal imaging allowed us to follow the behaviors of many GFP (+) cells within MDSC-3DGB. Morphogenetic deformations result from variation in the speed or direction of cell trajectories that change the relative positions of cells[210]. To quantify deformations of a single cell over time, we followed a cell within a microsphere domain. The domain was defined by a central microsphere triplicate and a small number of microspheres neighboring all sides of the cell that were found in every image at every time point. The intrinsic cell morphology changes were determined by: 1) cell shape change; defined as eccentricity; 2) cell size: defined as volume changes; and 3) cell orientation changes. We estimated cell shape and size changes from traced cell outlines based on their best-fit ellipses. The best fit ellipses' principle axes relative to the construct coordinate axes were then used to determine cell orientation changes.

The cells within MDSC-3DGB were randomly oriented at culture day 1 at both the construct end (END) and middle (MID). The cells expanded and were oriented along the construct longitudinal axis by culture day 3 at both the END and MID and this orientation persisted throughout culture (Figure 5-2, Table 5-1).

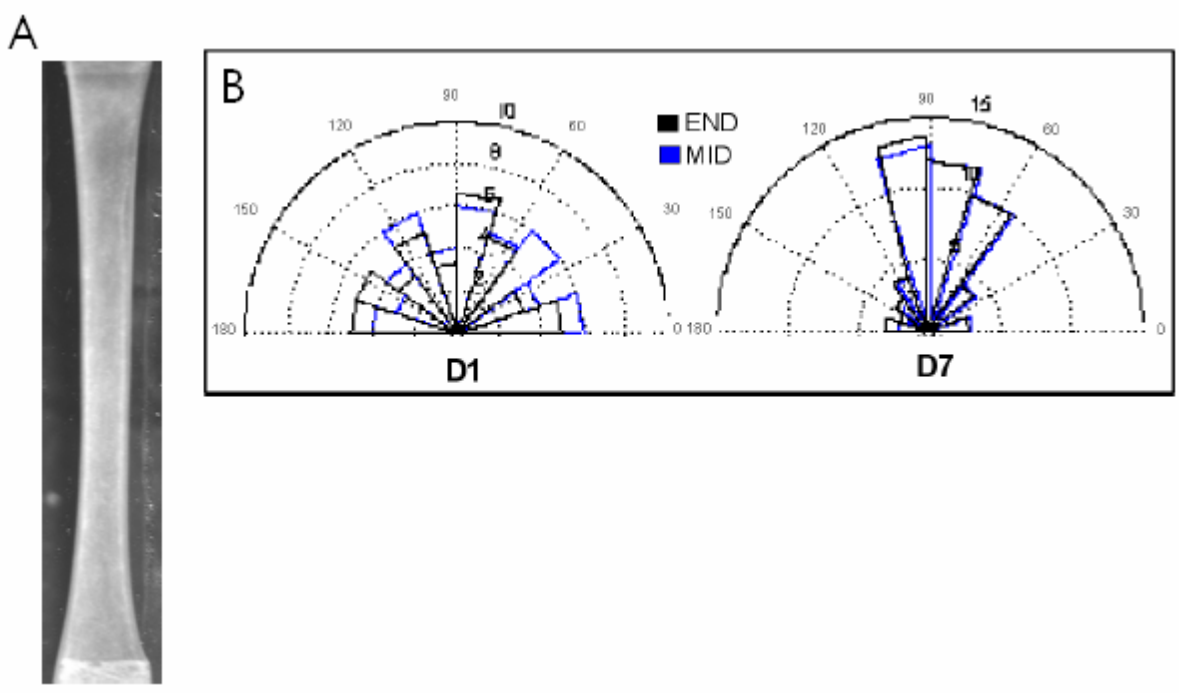

Figure 5-2. MDSC-3DGB cell orientation over culture. **(A)** Image of culture day 7 MDSC-3DGB to indicate direction of orientation scale with the longitudinal direction of the tissue equal to 90°. **(B)** Rose plot of average MDSC-3DGB cell orientation at culture day 1 (D1) and culture day 7 (D7). Cells were oriented randomly at culture day 1 (D1) at both the construct END (black) and MID (blue) and in the longitudinal direction (indicated at 90°) of the construct at culture day 7.

Table 5-1. MDSC-3DGB cell orientation over culture. Data are mean ± SE. Culture day 1 (D1) MDSC-3DGB cell orientation was significantly different from every other culture day. *; $P<0.05$ vs. D1 orientation. There was no statistical differences between END and MID at any culture day.

Orientation (°)			
END		MID	
D1	43.2 ±12.6	D1	49.4 ±20.4
D3	82.1 ±9.9*	D3	74.3 ±7.8*
D5	85.5 ±4.3*	D5	86.0 ±6.3*
D7	89.9 ±6.2*	D7	90.8 ±4.8*

The cells within MDSC-3DGB started out round at culture day 1, eccentricity E = 0.60 ± 0.03 at the END and E = 0.62 ± 0.03 at the MID with no significant differences between the regions. Cells at both the END and MID become more elliptical over time, however, cells at the END become more elliptical by culture day 3, E = 0.88 ± 0.05 vs. E = 0.77 ± 0.04 at the MID. By culture day 5 cells at the END and MID are both similarly elliptical and this similarity continues throughout culture (Table 5-2).

Table 5-2. MDSC-3DGB cell eccentricity change over culture. Data are mean ± SE. MDSC-3DGB END and MID cell eccentricity was similar at D1 but significantly different at D3. MDSC-3DGB MID cell eccentricity was again similar to END eccentricity by D5 and continued to be similar throughout the rest of culture. *; $P<0.05$ vs. MID eccentricity for each respective culture day.

END	Eccentricity
D1	0.60 ±0.03
D3	0.88 ±0.05*
D5	0.99 ±0.01
D7	0.99 ±0.01

MID	Eccentricity
D1	0.62 ±0.03
D3	0.77 ±0.04
D5	0.90 ±0.02
D7	0.98 ±0.01

When assessing cell size changes we noted that the cells became larger and more elongated over time, regardless of the spatial placement (END or MID). The cells became even larger and more elongated at the END compared to the MID (Figure 5-3, Table 5-3).

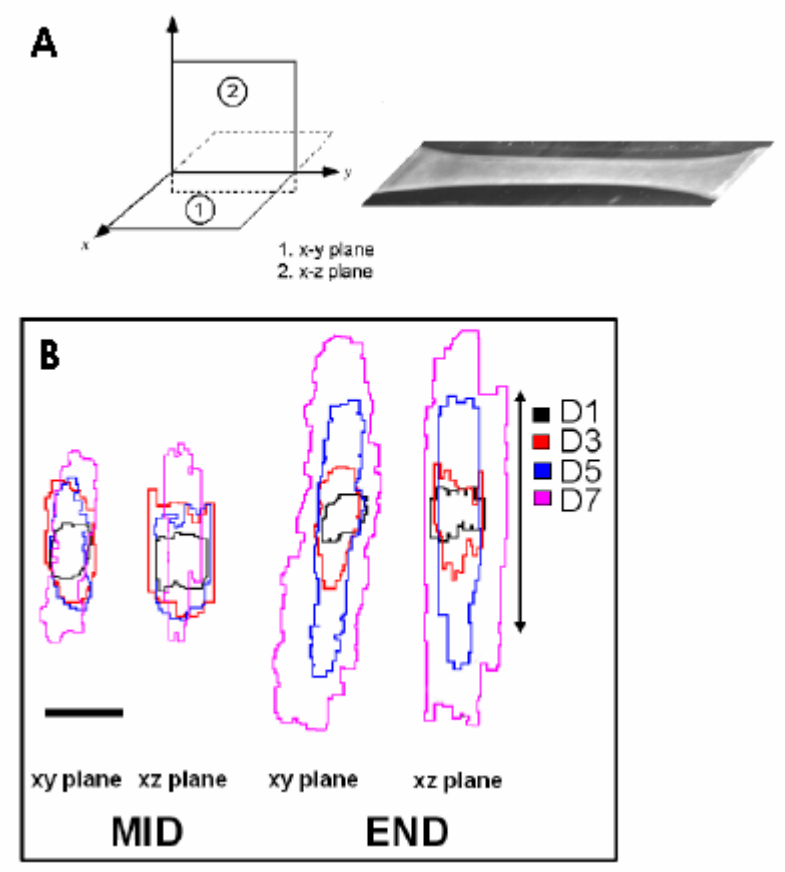

Figure 5-3. MDSC-3DGB cell shape change over culture days 1-7. **(A)** A schematic illustrating the orientation of the MDSC-3DGB for the cell shape analysis with the x-y plane and the x-z plane represented. **(B)** A representative cell from the construct end (**END**) and middle (**MID**) visualized at 2 different planes, the x-y plane and the x-z plane, at culture days 1, 3, 5, and 7 (**D1-D7**). Scale bar indicates 10 μm. Arrow indicates the longitudinal direction of the construct.

Table 5-3. MDSC-3DGB cell shape change over culture. Data are mean ± SE. MDSC-3DGB END cell shape was significantly different at every culture day whereas MID D1 and D3 shape was not significantly different. MDSC-3DGB END cell shape was significantly different from MDSC-3DGB MID at every culture day except D1. *; $P<0.05$ vs. previous culture day volume for each respective region (END or MID). †; $P<0.05$ vs. MID respective culture day.

END	Volume (μm^3)
D1	643.9 ±90.4
D3	1338.5 ±212.3*†
D5	3928.4 ±178.9*†
D7	10248.8 ±331.7*†

MID	Volume (μm^3)
D1	776.2 ±101.2
D3	844.4 ±139.1
D5	2323.3 ±343.6 *
D7	4718.1 ±366.8 *

Cells at the END expanded over 15 fold of their original size over the culture period whereas cells at the MID expanded only 6 fold. The cells at the END expanded at a steady approximately 2 fold increase in volume every 48hrs whereas the cells at the MID were not significantly larger at D3 but then increase in size at a similar rate of 2 fold increase every 48hrs to the cells at the END by culture day 5 (Table 5-3). Thus cell morphology in terms of cell shape and size changes; cell volume and eccentricity changes, is significantly different between the MDSC-3DGB END and MID whereas cell orientation changes are not significantly different between the END and MID.

5.3.2 3D Mechanical Strain

MatLAB assisted post-processing of time-lapse confocal imaging allowed us to follow the behaviors of many red fluorescent microsphere triplicates within MDSC-3DGB. To quantify 3D mechanical strain we followed a microsphere triplicate that was found in every image at every time point. The centroid of each microsphere within the triplicate was determined and the segment length and angle with respect to the MDSC-3DGB coordinate axes was determined and a strain map generated (Figure 5-4).

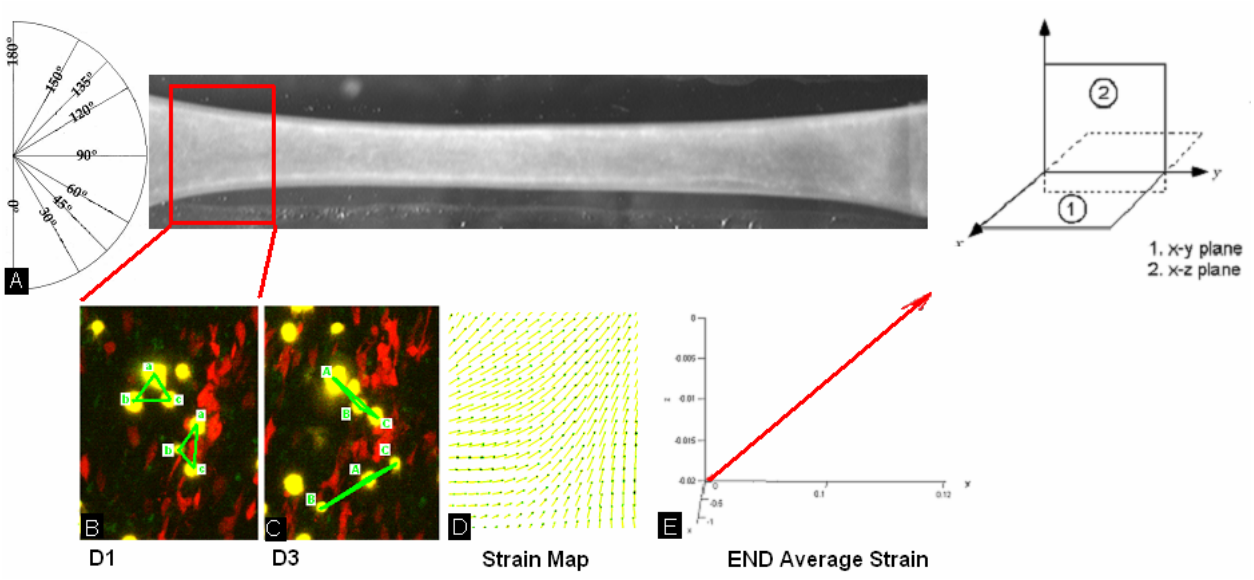

Figure 5-4. Schematic of MDSC-3DGB mechanical strain calculation. **(A)** Image of culture day 7 MDSC-3DGB to indicate direction of orientation scale with the longitudinal direction of the tissue equal to 90° and the orientation of the MDSC-3DGB x-y plane and the x-z plane represented Selected box indicates area where image was taken. Representative microsphere triplicates **(yellow)** followed from **(B)** culture day 1 to **(C)** culture day 3. Lowercase letters represent the microsphere at D1 whereas Uppercase letters represent the microsphere at D3. Green lines indicate the segments that were analyzed **(B-C).** **(D)** The segment displacements were differentiated directly to generate a strain map of the corresponding region**. (E)** The average strain magnitude and direction for the region, in this case D1-3 END, was determined.

It was observed at every time point that cells grow and populate the collagen scaffold regardless of whether or not microspheres were embedded. Based on this observation, the degree to which the microspheres are interfering with or inhibiting cell growth is minimal. Also, the stiffness of the construct with or without embedded microspheres is unchanged at multiple time points. Thus it can be inferred that the microspheres are not a major contributor toward changes in the stiffness of the engineered tissue. There was little to no strain in the x-z plane; END average strain magnitude 0.02 ± 0.03 and MID average strain magnitude 0.01 ± 0.01 over culture, thus, we determined the average strain direction with respect to the x-y plane only. MDSC-3DGB END strain magnitude was similar over every time point. MDSC-3DGB END principal strain direction became parallel to the longitudinal direction of the MDSC-3DGB at culture day 7. MDSC-3DGB MID strain magnitude was significantly higher at D1-3 and D3-5 vs. END but was similar at D5-7. MDSC-3DGB MID principal strain direction became parallel to the longitudinal direction of the MDSC-3DGB by D5 which was significantly faster than the END (Table 5-4).

Table 5-4. MDSC-3DGB mechanical strain change over culture. Data are mean ± SE. Regional mechanical strain was maintained at a lower value in the ENDs whereas strain at the MID started higher and decreased to similar levels as the ENDs by D7. Strain angle was parallel to the longitudinal direction of the MDSC-3DGB by D7 *; $P<0.05$ vs. previous culture day value for each respective region (END or MID). t; $P<0.05$ vs. END respective culture day value.

	D1-3		D3-5		D5-7	
	END	MID	END	MID	END	MID
Strain Magnitude	0.72 ± 0.29	3.11 ± 0.13†	0.64 ± 0.32	2.04 ± 0.14*†	0.57 ± 0.18	0.48 ± 0.20*†
Strain angle (°)	130 ± 25	145 ± 10	160 ± 13	72 ± 10*†	81 ± 14*	-88 ± 5

The END strain angle directions range was larger at D1-3 and D3-5 compared to MID strain angle directions range, but was similar by D5-7. The mechanical strain magnitude within

MDSC-3DGB is lower at the END vs. MID till day 7 and this is correlated with the larger more elongated cells at the END vs. MID.

5.3.3 Cardiomyocyte Differentiation

As stated in 4.0 MDSC-3DGB expressed cardiac specific genes and proteins, and contractile force and intracellular calcium ion transients similar to engineered cardiac tissue from native cardiac cells. Okada et al., have shown that donor cells differentiate into both skeletal muscle and cardiac muscle phenotypes *in vivo*, sustaining recipient injured myocardial function. These donor cells also express skeletal muscle specific fast myosin heavy chain (sk-fMHC) within infarcted myocardium[76]. We have shown that some cells within MDSC-3DGB express skeletal muscle specific and cardiac specific genes and proteins both *in vitro* and *in vivo*. Within MDSC-3DGB only approximately 20% of cells differentiate into CMs and they are not evenly distributed without the construct. It has been widely accepted that terminally differentiated mature cardiac muscle does not express proteins that are specific to skeletal muscle. However, studies have shown that several skeletal muscle specific proteins, such as skeletal muscle specific troponins or ion channels, are transiently present in the developing heart[89, 90]. Similarly, "cardiac" and "skeletal" excitation-contraction coupling mechanisms co-exist in the developing skeletal muscle with the "cardiac" type dominant in the early phases of myogenesis and the "skeletal" dominating in more mature muscle[91]. These studies suggest the co-existence of many cardiac and skeletal muscle specific proteins (MHCs, troponins, etc.) as well as excitation-contraction coupling mechanisms within the developing tissue, but also within cultured cells, especially those that are considered to be immature. Therefore, it remains to be elucidated whether MDSC derived sk-fMHC positive cells are terminally differentiating skeletal muscle

cells or potentially differentiating cardiomyocytes. Thus, we investigated the presence of sk-fMHC within the developing myocardium as well as MDSC-3DGB.

5.3.3.1 Sk-fMHC presence within the developing myocardium

The presence of sk-fMHC within the myocardium from gestational day (GD) 13 and 20, neonatal day (ND) 4, post-natal day (PND) 10 or 17 (juvenile), and adult Lewis rat myocardium and skeletal muscle was assessed using immunohistochemical staining, western blot, and PCR (Detailed methods found in Appendix B). sk-fMHC was expressed as a typical striated cardiac muscle pattern throughout the entire gestational day 13 (GD13) ventricular myocardium (Figure 5-5A and 5-5B). At this gestational day, cardiac troponin-I (cTn-I) was negative.

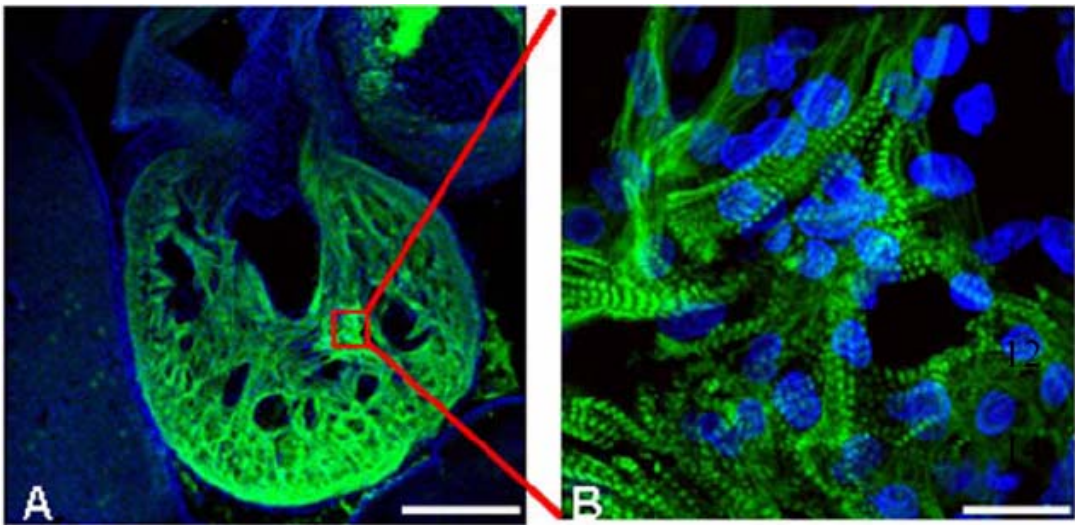

Figure 5-5. Sk-fMHC presence within GD13 myocardium. **(A)** sk-fMHC expression. **(B)** sk-fMHC expression of red boxed area in panel A shown at a higher magnification. cTn-I expression was negative. Scale bars indicate 500 μm in A and 20μm in B.

By gestational day 20 (GD20) striated sk-fMHC expression was restricted to the LV papillary muscle (Figure 5-6A), whereas LV myocardial wall expressed sk-fMHC without striation (Figure 5-6B). Cardiac troponin-I was very weakly expressed without striation. At neonatal day

4 (ND4) sk-fMHC was expressed in both the LV papillary muscle (Figure 5-6C) and LV myocardium (Figure 5-6D), however, typical striation was completely lost in both. Cardiac troponin-I expression was weakly expressed without striation pattern similar to GD20.

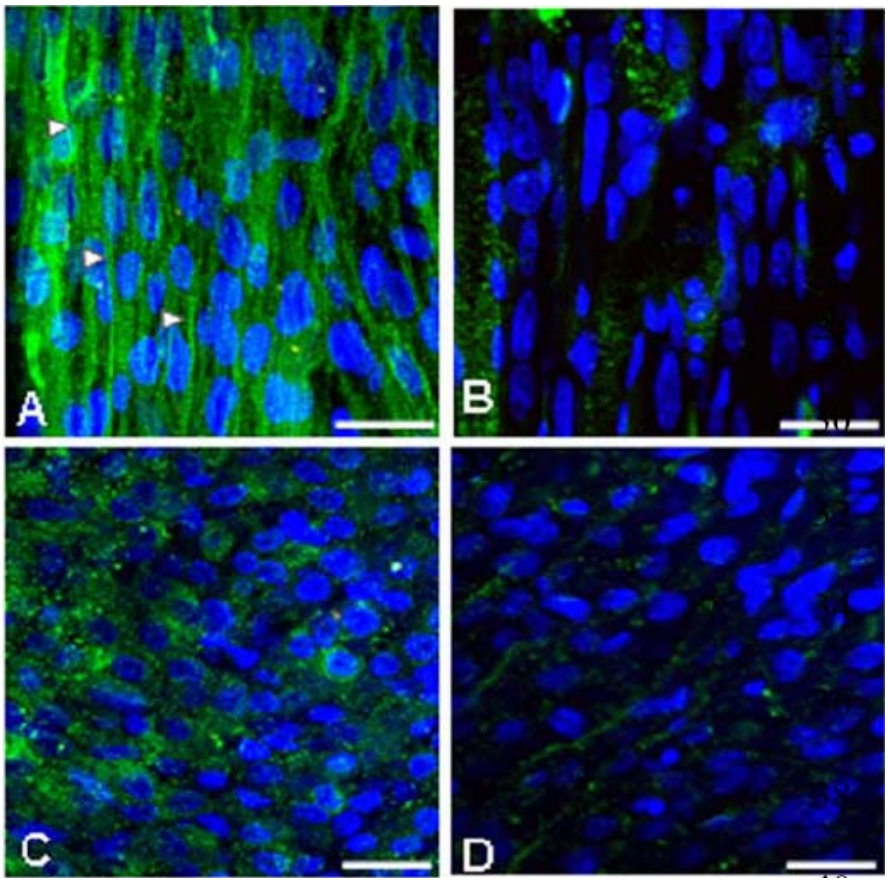

Figure 5-6. Sk-fMHC and cTn-I presence within GD20 and ND4 papillary muscle and LV myocardial wall. **(A)** sk-fMHC expression within GD20 papillary muscle **(B)** and LV myocardial wall. **(C)** sk-fMHC expression within ND4 papillary muscle **(D)** and LV myocardial wall. cTn-I expression was weakly expressed without striation in both GD20 and ND4 myocardium. Scale bars indicate 20 µm.

By post natal day 17 (PND17), equivalent to a juvenile, the LV myocardium did not express sk-fMHC whereas cTn-I was expressed with a typical striated pattern (Figure 5-7A). Conversely, PND17 skeletal muscle expressed sk-fMHC as a typical striated muscle pattern and did not express cTn-I (Figure 5-7B).

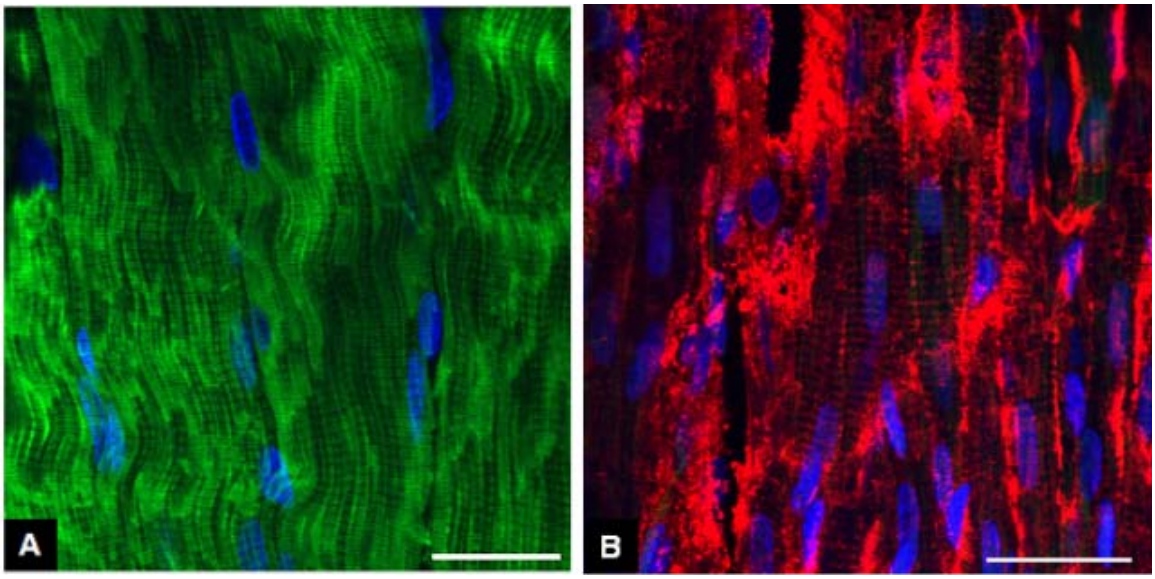

Figure 5-7. Sk-fMHC and cTn-I presence within PND17 myocardium and skeletal muscle. **(A)** sk-fMHC expression in PND17 skeletal muscle; cTn-I expression was negative. **(B)** cTn-I expression within PND17 myocardium; sk-fMHC was negative. Scale bars indicate 20 μm.

Western blot analysis indicated that in the myocardium, sk-fMHC is expressed in decreasing amounts until PND10 (juvenile) and is not expressed in the adult myocardium, whereas cTn-I is expressed in increasing amounts at all developmental stages. In skeletal muscle, sk-fMHC is expressed at high levels at all developmental stages while cTn-I is expressed in a low amount only in GD20 (Figure 5-8).

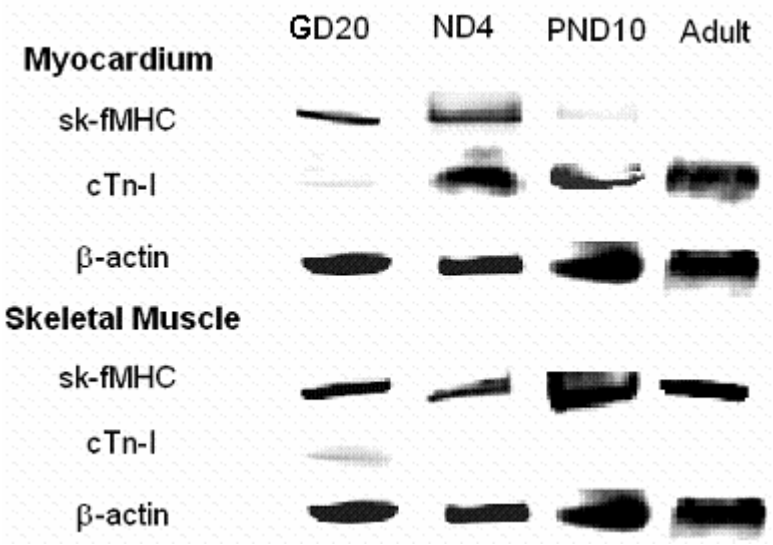

Figure 5-8. Western blot analysis of developing myocardium. **Lane 1:** GD20; **Lane 2**: ND4; **Lane 3**: PND10; **Lane 4**: Adult. **Top panel:** myocardium; **Bottom panel:** skeletal muscle.

PCR analysis indicated that sk-fMHC is expressed in the developing myocardium up to PND10, but is not present in the adult myocardium and cardiac α-MHC is present at all stages of development. Conversely, in skeletal muscle, sk-fMHC is expressed at all developmental stages except for the adult myocardium and cardiac α-MHC is not present in the adult skeletal muscle (Figure 5-9).

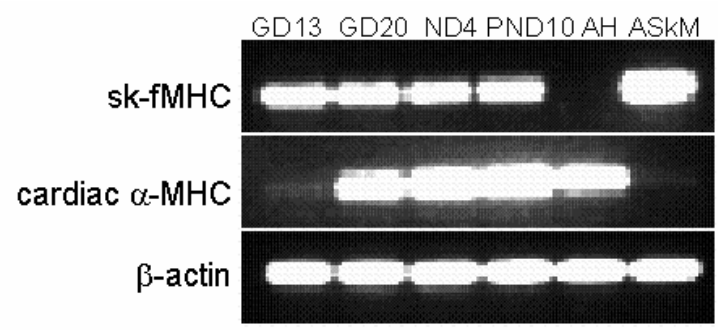

Figure 5-9. Gene expression of developing myocardium. **Lane 1**: GD13 heart; **Lane 2**: GD20 heart; **Lane 3**: ND4 heart; **Lane 4**: PND10 heart; **Lane 5**: Adult heart (AH); **Lane 6**: Adult skeletal muscle (ASkM).

In summary, this shows evidence for the first time that skeletal muscle specific fast myosin heavy chain is transiently expressed in the developing immature myocardium. This indicates that the expression of skeletal muscle specific proteins does not necessitate differentiation into skeletal muscle, specifically that MDSC-derived sk-fMHC expressing cells can be potentially differentiating cardiomyocytes.

5.3.3.2 Cardiomyocyte differentiation within MDSC-3DGB

Histological analysis indicated that cardiac specific protein expression as well as skeletal fast myosin heavy chain (sk-fMHC) expression increased over culture. Cell density was similar at both the END and MID at all time points. The CM ratio (% Area based on cTn-T/DAPI expression) was increased at D3 and D5 at the END vs. the MID and was similar at D7 and D9 (Table 5-5).

Table 5.5. CM ratio of MDSC-3DGB. CM ratio was defined as the [(area of cTn-T (+) expression / area of DAPI (+) expression)*100] within a confocal image. Data are mean ± SE. CM ratio was increased at the END vs. MID at D3 and D5 and was similar at D7,and D9. *; $P<0.05$ vs. END respective culture day value.

	D3		D5		D7		D9	
	END	MID	END	MID	END	MID	END	MID
CM ratio (%)	51.1 ± 3.2	28.6 ± 2.1*	82.6 ± 7.8	53.7 ± 5.5*	52.2 ± 3.4	49.2 ± 6.6	58.0 ± 3.1	62.8 ± 2.9

We looked at the passive force of the MDSC-3DGB END and MID at culture days 3, 5, 7, and 9. At lengths greater than their resting length, muscle tissue develops tension or force. This force is passive since it exists whether or not the muscle is active. Passive force was used here as a measure of tissue stiffness. A stiffer tissue will develop more force during a given amount of elongation. The stiffer the tissue the steeper the slope of its stress-strain curve. Over culture MDSC-3DGB becomes stiffer regardless of END or MID. When we compare the MDSC-3DGB

END vs. MID at their respective culture days we find that the % increase in stress relative to the baseline stress (stress generated at resting length) is similar at D3, but significantly increased at the MID at D5, and again is similar at D7 and D9 (Figure 5-10).

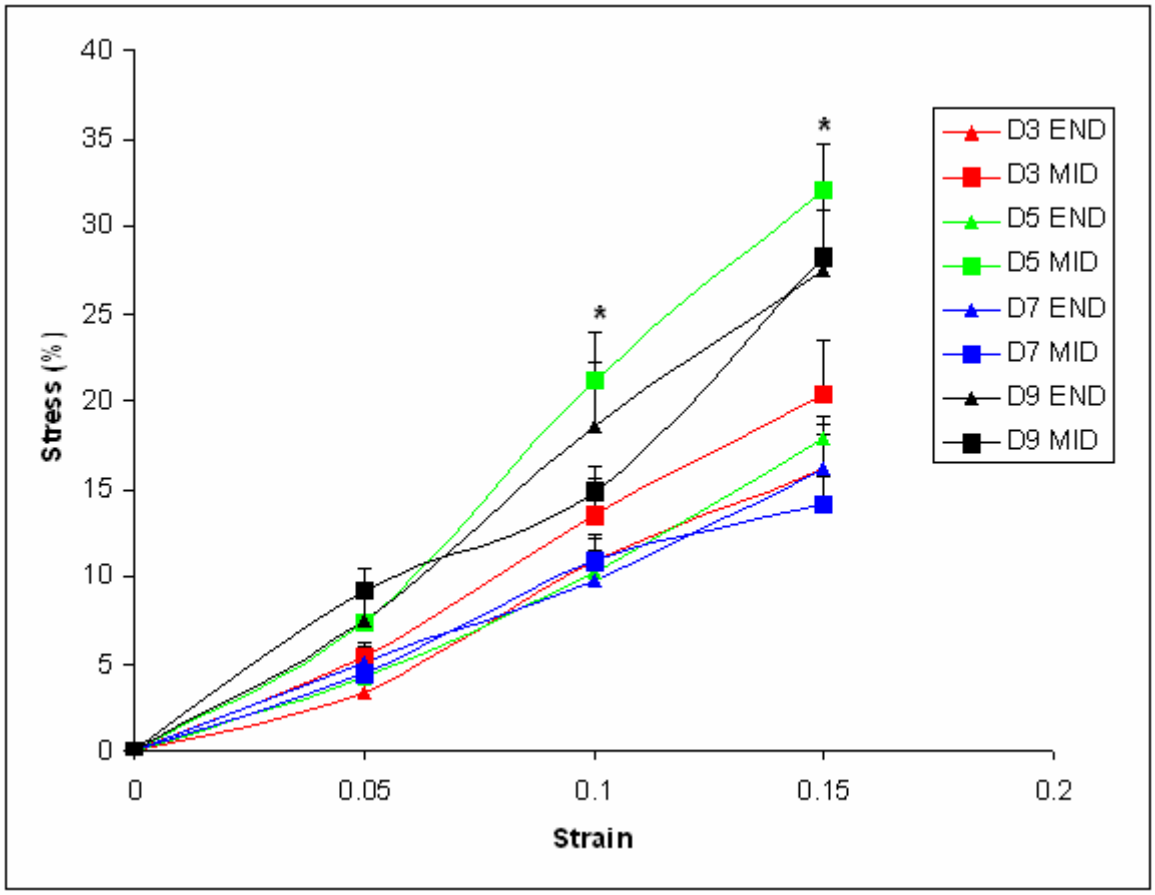

Figure 5-10. Passive stress-strain relation of MDSC-3DGB END and MDSC-3DGB MID. Passive stress-strain relations of MDSC-3DGB END (n=12) and MID (n=12) at 0 to 0.15 strains. The passive stress increased in parallel with increases in strain (*, Frank-Starling law). The passive stress of D5 MID at 0.1 and 0.15 strains was significantly increased compared to the END. (*; $P<0.05$ vs. MDSC-3DGB END). Data are mean ± SE.

We looked at expression of cTn-T, cTn-I, Cx-43, and sk-fMHC expression at culture days 1-9 at 48hr intervals at the END and MID. CM proteins or sk-fMHC were not expressed at D1. Cx-43 was expressed at the END but not the MID at D3, but by D5 and throughout culture

the expression was maintained at both the END and MID. cTn-T was expressed at the END with a weaker expression at the MID at D3 and was seen as a typical striated pattern at both the END and MID at D5 and throughout the rest of culture. cTn-I was not expressed in either the END and MID until D5 and typical striations were not seen until D7 for either the END or MID. sk-fMHC was expressed similarly at both the END and MID at D3 and D5. A similar characteristic striation pattern was seen at D7 at the END and MID. The typical striation pattern was lost at D9 at the END but was maintained at the MID. This CM protein expression over culture is summarized in Figure 5-11.

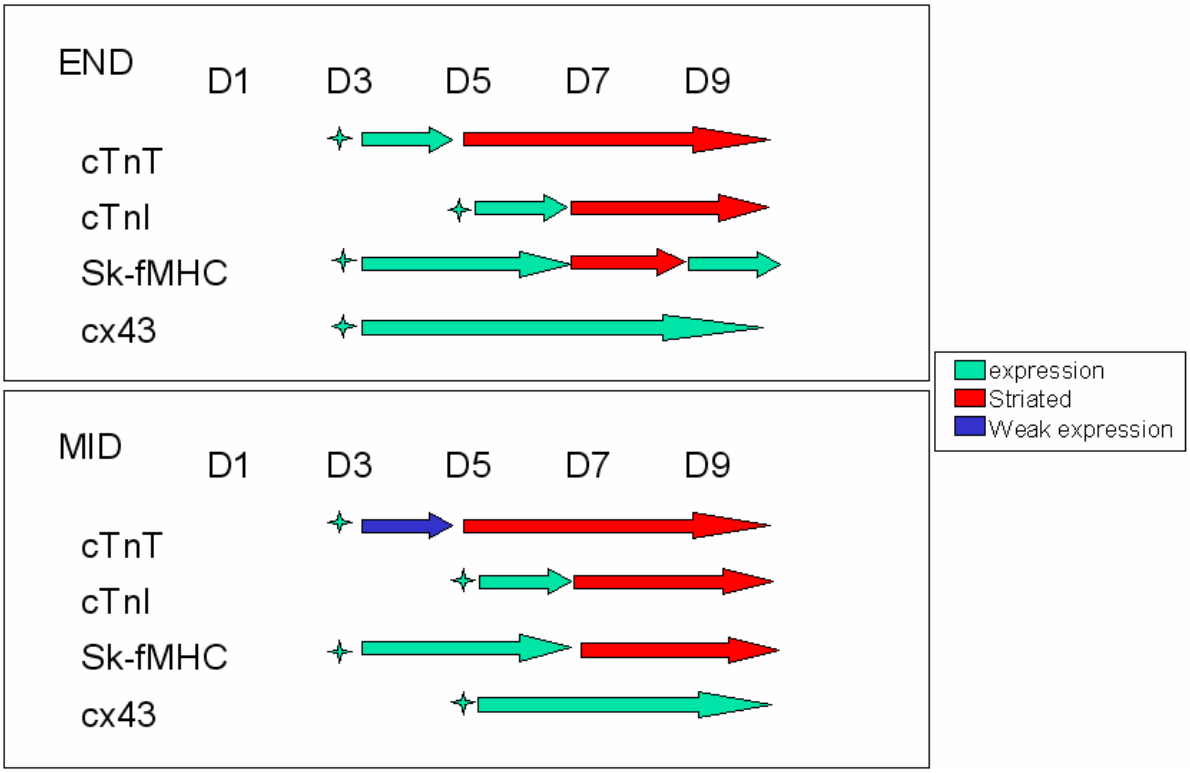

Figure 5-11. Summary of CM protein and sk-fMHC expression in MDSC-3DGB END vs. MID. ; indicates start of expression. Colored arrows indicate continued expression.

Along with the presence of expression and striation with cTn-I and sk-fMHC we also investigated the co-expression of these proteins based on the results of the expression of sk-

fMHC in the developing myocardium. At D5 we saw expression of cTn-I and sk-fMHC within MDSC-3DGB, however, these areas of expression rarely overlapped and striations were not seen in either (Figure 5-12).

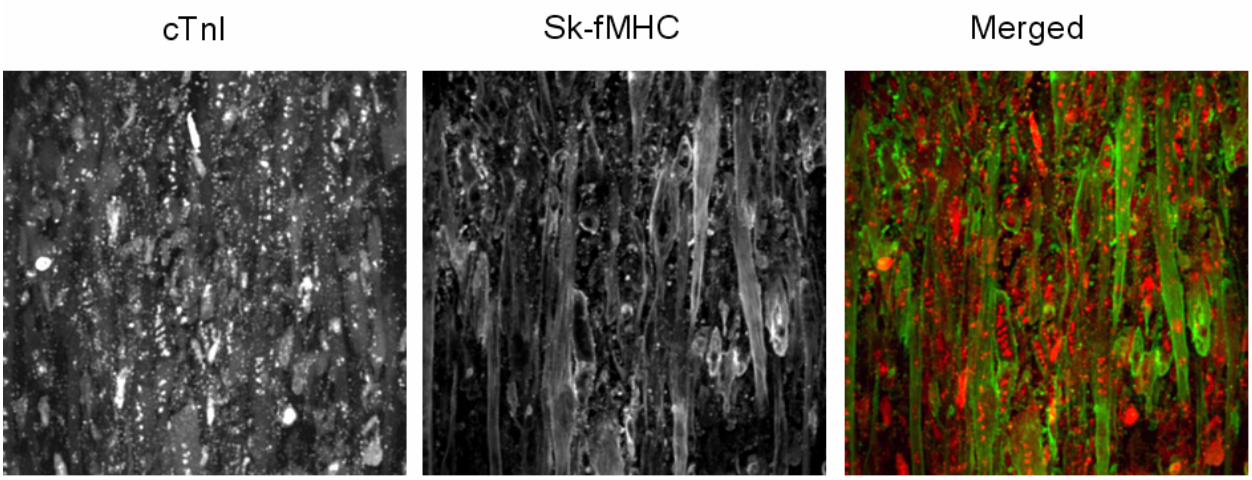

Figure 5-12. MDSC-3DGB D5 cTn-I and sk-fMHC expression. There was no co-expression of cTn-I and sk-fMHC expression at D5.

At D7 we saw typical striation patterns of expression of both cTn-I and sk-fMHC within MDSC-3DGB. There were areas of co-expression of cTn-I and sk-fMHC, with the areas of co-expression only ever having one protein with striations. The areas of co-expression of both striated cTn-I and sk-fMHC was not seen (Figure 5-13).

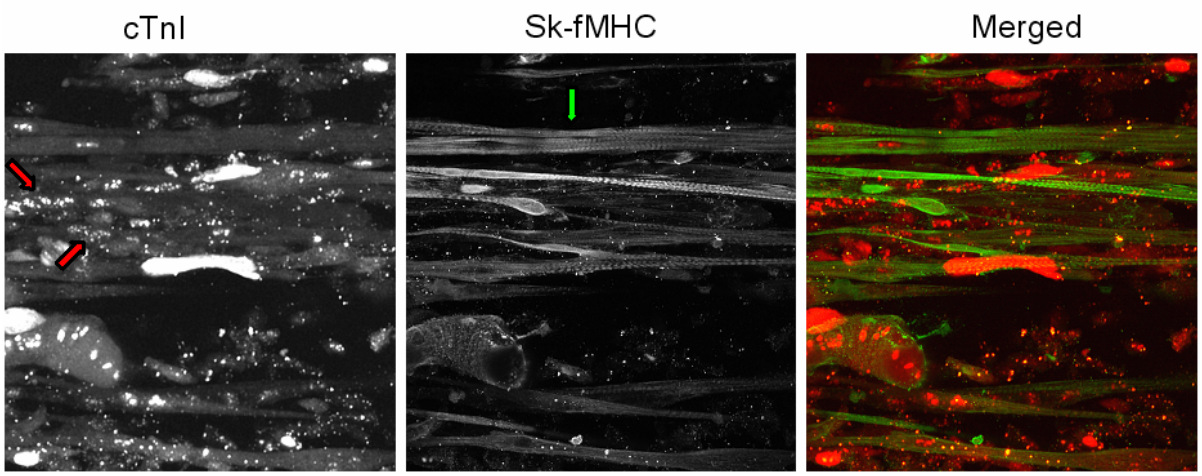

Figure 5-13. MDSC-3DGB D7 cTn-I and sk-fMHC expression. Typical striation patterns were seen in both cTn-I (red arrows) and sk-fMHC (green arrows). There areas of co-expressed had only cTn-I or sk-fMHC striated expression.

At D9 we still saw typical striation patterns of expression of both cTn-I and sk-fMHC within MDSC-3DGB. There were areas of co-expression of cTn-I and sk-fMHC, with the areas of co-expression having one or both proteins with striations (Figure 5-14).

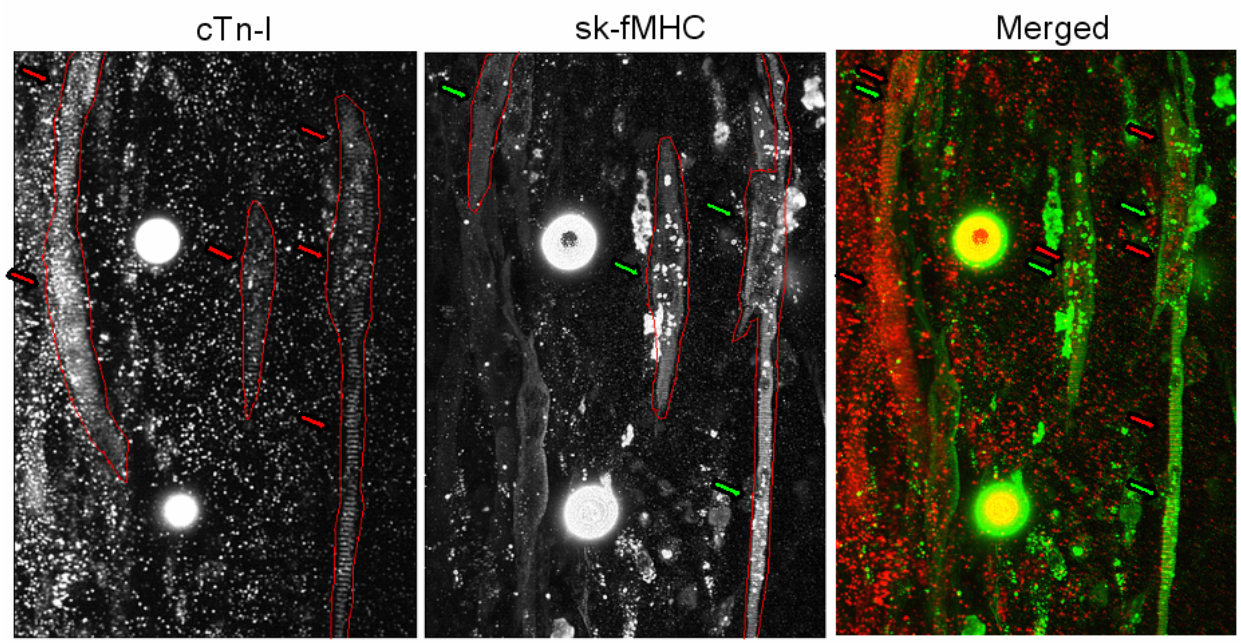

Figure 5-14. MDSC-3DGB D9 cTn-I and sk-fMHC expression. Typical striation patterns were seen in both cTn-I (red outlined areas with red arrows) and sk-fMHC (green arrows with red outlined areas). There areas of co-expressed had either cTn-I or sk-fMHC striated expression or both cTn-I and sk-fMHC striated expression.

Western blot analysis of MDSC-3DGB at culture days 1-9 at 48hr intervals at the END and MID analyzed expression of cTn-T, cTn-I, Cx-43, sk-fMHC, and phospho-Histone H3 (a marker of proliferation) (Figure 5-15A). Densitometry analysis of each protein normalized to β-actin expression demonstrated that CM specific protein expression increased with culture similar to the histological analysis (Figure 5-15B). Specifically H3 expression was significantly decreased at the END vs. MID at D1 and D3 and significantly increased at D7 ($P<0.05$). H3 expression was similar at D5 and D9. cTn-I was not expressed at D1 or D3 in either the END or MID, however expression was significantly increased at the END vs. MID at D5. D7 and D9 had similar expression of cTn-I. Cx-43 was not expressed at D1. Expression was similar at D3, but was significantly increased at D5 END vs. MID and was similar at D7 and D9. sk-fMHC expression remained low compared to the CM specific protein expression at all culture days with

expression being significantly decreased at D5 END vs. MID. cTn-T expression was significantly increased at D3 and D9 END vs. MID.

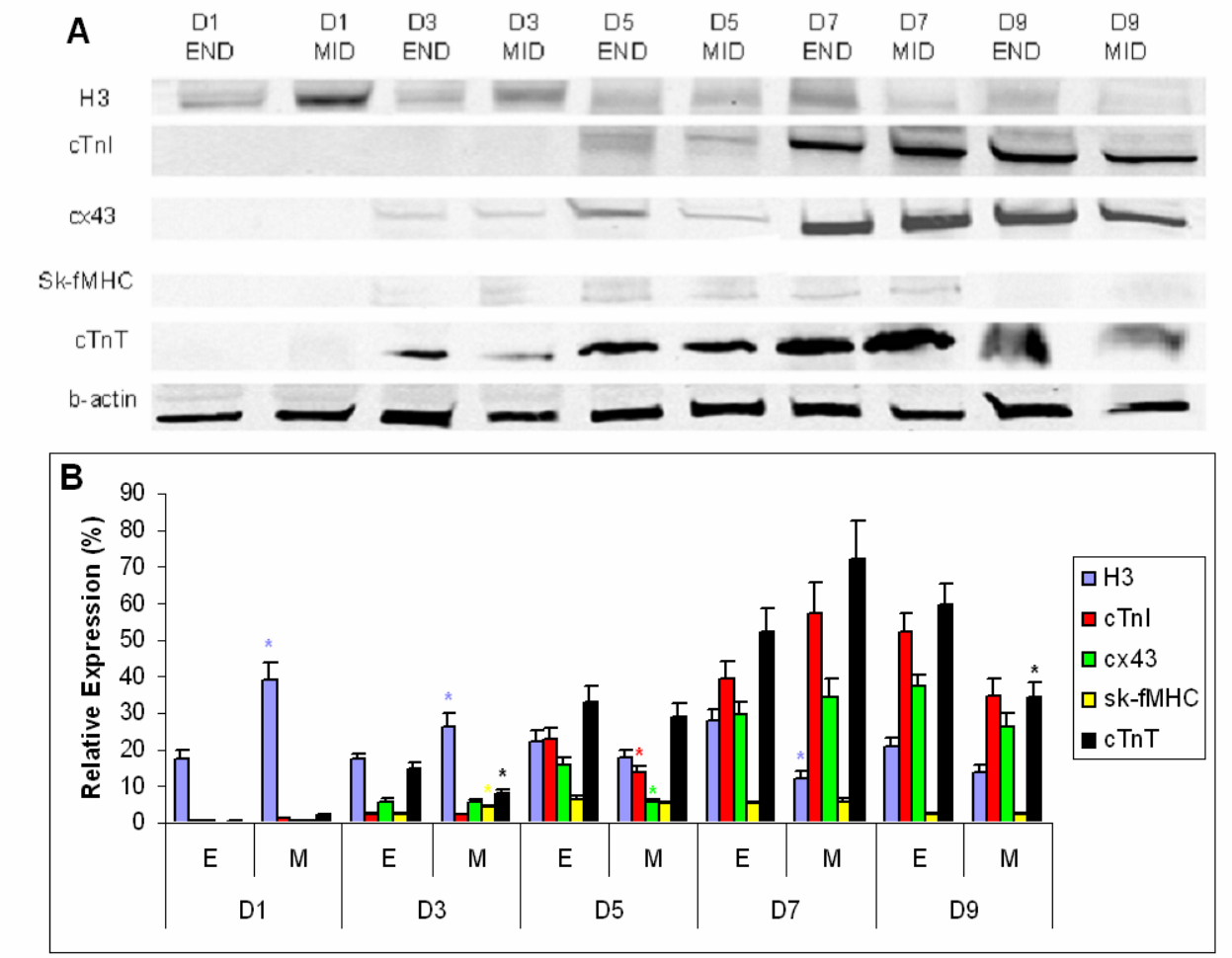

Figure 5-15. Western blot analysis of MDSC-3DGB. **(A)** Representative western blot analysis of **Lane 1**: culture day 1 MDSC-3DGB END; **Lane 2:** culture day 1 MDSC-3DGB MID; **Lane 3:** culture day 3 MDSC-3DGB END; **Lane 4**: culture day 3 MDSC-3DGB MID; **Lane 5**: culture day 5 MDSC-3DGB END; **Lane 6:** culture day 5 MDSC-3DGB MID; **Lane 7:** culture day 7 MDSC-3DGB END; **Lane 8**: culture day 7 MDSC-3DGB MID; **Lane 9:** culture day 9 MDSC-3DGB END; **Lane 10**: culture day 7 MDSC-3DGB MID. **(B)** Densitometric data normalized to β-actin expression (Average Expression vs. β-actin, %). *; $P<0.05$ vs. END respective culture day normalized expression, colors correspond to each respective protein. Each lane contains 20 µg of protein per sample and experiments were repeated in triplicate.

The combination of histological and western blot analysis show that over culture MDSCs within MDSC-3DGB differentiate into CMs throughout the construct. However, this CM differentiation is differential with the END having faster differentiation, an increased number of CMs, decreased proliferation, and decreased sk-fMHC expression. On the other hand, the MID has increased proliferation, slower differentiation, less CMs, maintenance of sk-fMHC expression, and a decrease in CM specific proteins.

MDSC-3DGB cell morphology changes, driven by mechanical strain cues, are correlated with CM differentiation and are dependent upon the time of MDSC-3DGB development (Figure 5-16).

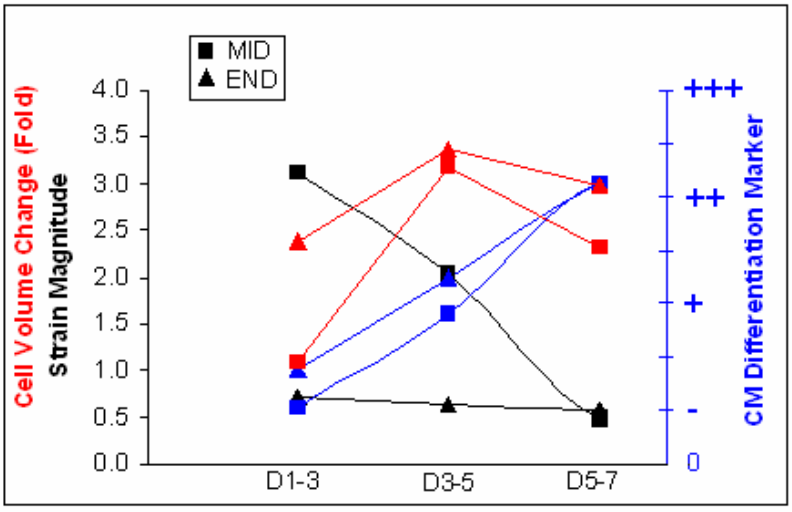

Figure 5-16. MDSC-3DGB mechanical strain correlated with cell morphology and CM differentiation. MDSC-3DGB END represented by triangles. MDSC-3DGB MID represented by squares. The colors represent different markers: strain magnitude **(Black)**, CM differentiation **(Blue)**, and Cell growth (Fold increase over previous culture day) **(Red).**

The mechanical strain at the END starts low and remains low throughout culture which is correlated with larger more elongated cells that have an increased CM differentiation. In contrast, the mechanical strain at the MID starts high and decreases to a similar level as the END

by D7. The initial high strain early in development is correlated with significantly increased proliferation, smaller cells, and less CM differentiation. The decrease in MID strain to levels similar to END strain later in development is correlated to a decrease in proliferation, an increase in cell growth, and an increase in CM differentiation that is similar to the END. By D7, the strain as well as CM differentiation and cell morphology is similar between the END and MID.

5.4 DISCUSSION

Mechanical strain has been shown to reprogram gene expressions, increase protein synthesis, and trigger adaptive responses in muscle phenotype via the expression of contractile proteins within engineered cardiac tissue. Our previous study showed that MDSC-3DGB expressed cardiac specific genes and proteins, and contractile force and intracellular calcium ion transients similar to engineered cardiac tissue from native cardiac cells[209]. However, the efficiency and directed location of this CM differentiation remain limited. The current study has demonstrated that spatially and temporally distributed mechanical displacements and strains can be mapped with micron-scale resolution in MDSC-3DGB as groups of cells begin to grow, proliferate, and differentiate measurably within a 3D collagen gel bioreactor. We found that the MDSC-3DGB mechanical strain is correlated with cell morphology: evidenced by cell shape, cell size, and cell orientation, and CM differentiation which is time-dependent. The END had low strain and increased cell size and CM differentiation, whereas when the MID had high strain compared with the END, it had increased proliferation, decreased cell size, and decreased CM differentiation. Later in development, when the MID had a similar strain to the END, the cell morphological changes, CM differentiation, and cell proliferation were similar.

The commitment of a particular stem cell to a particular lineage is dependent upon several factors, of which we focus on cell morphology: cell shape, size, and orientation, and the mechanical environment in this study. The mechanical strain seen from D1-D5 within the MDSC-3DGB END was significantly decreased compared to the MID but by D7 the mechanical strain seen at the END and MID was similar. While we only measure one facet of mechanical force, regional mechanical strain, other mechanical factors as well as chemical, growth factor, matrix, and morphogenic factors also have been shown to affect cell differentiation. Recent studies have shown that the surface microenvironment in which certain stem cells grow plays a key role in initiating and controlling differentiation. For example, by changing the elasticity of the substrate, the polymer material to which the cells adhere or the number of cells on the surface all influence the differentiation process[236, 237]. Studies have shown that cells on the periphery of a pattern are able to sense the edge or corners of the pattern and are able to influence the total differentiation rate of the cells within the pattern. This pattern edge phenomenon is well known to influence cell division, cell cytoskeleton dynamics, and migration from patterns[238-241] and has recently been observed for stem cell differentiation[242]. While much is know about how soluble factors and adhesion receptors regulate differential gene expression, the molecular basis for how mechanical signaling controls gene transcription and differentiation programs is only now coming into focus[214]. The means by which cells integrate multiple mechanical (and soluble) cues to generate an appropriate response can be seen in cell shape changes.

Tensegrity, a theory proposing that biological structures stabilize and regulate themselves through a balance of tensional and compressive forces, is an effective way of explaining cellular responses to mechanical stimuli[133, 246]. For instance, a shape change from a round to flattened morphology can profoundly alter the organization of the actin cytoskeleton and the assembly of

focal adhesions[243, 244]. Similarly, when human or rabbit corneal fibroblasts were placed on collagen and the ECM local tension was reduced, the cells responded by first rapidly contracting, and then re-spreading[245]. The changing substrate tension upset the tensional homeostasis of the cell and caused the initial contraction which began a signaling pathway conducted by the cytoskeleton that resulted in a reduction of internally-generated forces and a gradual re-spreading of the cells[246]. The cytoskeleton converts a given set of cues into a varity of outputs. Generalized cell deformation, via mechanical cues, has been shown to produce discrete changes in cellular phenotype[132, 134, 135, 137]. In this study, cells within MDSC-3DGB at D1 are round at both the END and MID which is accompanied by high proliferation, significantly higher at the MID than the END, as well as a lack of CM differentiation. By D3 the cells at the END double in volume and elongate adopting a spread shape. At this time the large elongated cells also start to express CM specific proteins. In contrast, cells at the MID do not significantly increase in size and maintain significantly increased proliferation and have less CM specific protein expression compared to the END. A review by Cohen et al. explores how mechanical forces are integrated through cell shape and the actin cytoskeleton and transduced into biochemical signals that target the activity and expression of transcription factors and chromatin remodeling enzymes directly involved in gene expression[214]. Thus a change in cell shape as directed by the temporal and spatial differences in mechanical strain can be sufficient to cause lineage specification, specifically to differentially increase CM differentiation within MDSC-3DGB.

At D5 and D7 the cells at the MID and END have similar eccentricity and increase in cell size, however at D5 there are still significant differences observed in CM differentiation, observations that were not seen at D7. Of the markers of interest noted above, only cell orientation had no significant differences between the END or MID at any time point. Within

MDSC-3DGB the cells quickly orient, by D3, parallel to the longitudinal direction of the construct regardless of the cell placement within the END or MID. A study by Costa et al.[211] suggests cells align parallel to a local free boundary rather than to local lines of tension. The geometrical constraints of the MDSC-3DGB could be the determining factor in the cell orientation within MDSC-3DGB, regardless of the mechanical strain differences within the END and MID. However, mechanical strain plays a role in stem cells differentiation and proliferation, and a study has shown that the effects of the strain were dependent on the orientation with respect to the strain axis[212]. Within MDSC-3DGB, the principle strain direction becomes parallel to the longitudinal axis of the construct by D3-5 at the MID and by D5-7 at the END. At these times, the CM differentiation is significantly increasing in both expression and maturity, as evidenced by cTn-I expression and increased striations. Thus while the construct cylindrical geometry might dictate the cell orientation, the orientation parallel to the principle strain direction might be necessary for the CM specific lineage specification.

In 4.0 we found that the MDSC-derived CMs within MDSC-3DGB are similar to immature native CMs[209]. However, it is also known that several skeletal muscle specific proteins, such as skeletal muscle specific troponins or ion channels, are transiently present in the developing heart[89-91]. This is important to note because of the cell source used here and the presence of skeletal muscle specific and cardiac specific genes and proteins within MDSC-3DGB both *in vitro* and *in vivo*. When we looked at the presence of a specific skeletal muscle specific protein, fast skeletal myosin heavy chain (sk-fMHC), in the developing immature myocardium we found transient expression. As development progresses, sk-fMHC became negative and the myocardium then expressed cardiac specific troponin-I. Fast skeletal muscle is more prone to fatigue, utilizes ATP quickly, and uses less oxygen, whereas cardiac muscle is

made to resist fatigue and generally needs more oxygen. Thus, from a physiological standpoint, the benefit of sk-fMHC in the immature developing fetal heart may be that the shorter, quicker contraction allows blood ejection throughout the system necessary for adapting rapid fetal growth prior to the establishment of coronary artery circulation and conduction system. As the myocardium matures, the contraction pattern shifts towards less rapid but continuous contraction under an aerobic condition, when the coronary circulation and conduction system are developed and sk-fMHC expression decreases. Continued expression of sk-fMHC would be detrimental because if fast muscle tissue were to exist in the post-natal and adult heart, it would fatigue much faster, leading to higher levels of cardiac failure. Thus, the presence of sk-fMHC and co-expression with cTn-I within MDSC-3DGB is consistent with an immature CM phenotype.

CM specific protein cTn-I and sk-fMHC expression increases, albeit variably, with development of MDSC-3DGB. Of interest the patterns of expression, determined by striation, also differ with respect to developmental stage. In striated muscle, like cardiac or skeletal muscle, contractile properties result from a strictly defined organization of functional proteins within the sarcomere. The presence of striated patterns of expression of the cardiac and skeletal muscle specific proteins: cTn-T, cTn-I, and sk-fMHC, evaluated here are evidence of functional maturation of the contractile structures. We first see diffuse cTn-T expression at D3 and striated structure at D5 which is maintained throughout culture. sk-fMHC is diffusely expressed at D3 and cTn-I at D5. Both acquire a striated pattern by D7. This is consistent with previous studies of muscle development. However, we see noted differences in the co-expression patterns of sk-fMHC and cTn-I from D5: beginning with diffuse non-overlapping patterns of expression at D5, to co-expression of one diffuse and one striated pattern of expression at D7, to co-expression of both striated patterns of expression at D9. The results that sk-fMHC is transiently expressed in

the developing immature myocardium is the first to provide evidence of non-cardiac specific MHCs in the developing heart, and to date there have been no studies on the developmental changes in expression patterns of these proteins. Thus, further studies are necessary.

Although the current study clearly shows that the mechanical strain directed cell morphology changes are correlated with CM differentiation within MDSC-3DGB, the mechanisms by which mechanical strain affects MDSC-derived CM differentiation within MDSC-3DGB are not yet clear. Some key issues remain to be settled, including: the mechanism by which MDSCs sense mechanical strain, the signal transduction pathways active in MDSCs, the interaction of different signaling pathways in modulating expression of mechano-responsive genes, the crosstalk between mechanical and chemical signaling pathways in MDSCs, and investigation of the molecular mechanisms by which signaling pathways activated or repressed by mechanical strain lead to the CM differentiation of the MDSC-3DGB.

5.4.1 Limitations

The limitations noted in 4.4.1 apply here.

There are also several more limitations to the current study that need to be discussed. First, the method used to determine 3D MDSC-3DGB regional mechanical strain was developed independently for this study. We used several methods to verify and validate the robustness of calculations and confidence of results, including use of commercially available elastic registration analysis from ImageJ (Appendix A.1) as well as analysis by hand. Even though all method results were not statistically different and we are confident of the quantitative values generated in this study, the qualitative comparisons of MDSC-3DGB END and MID provide results significant enough for similar conclusions to be drawn. Additionally the imaging method

was limited by the spatial resolution of the camera and the Flexcell plate geometry necessary for construction of the MDSC-3DGB. Additionally while image stacks were taken and the 3D orientation of the microspheres analyzed, the sample itself was not guaranteed to be perfectly planar to the camera, indeed the planar position of the MDSC-3DGB changed from image time-point to image time-point. Preliminary data and previous studies have indicated that the movement in the x-z plane was minimal, which was consistent with the results of this study.

Second, we only report average MDSC-3DGB regional mechanical strain. These values may or may not be the mechanical strain all or any cells within the region see. Our methods implicitly use the assumption that the region studied can be treated as homogeneous, which, of course, does not necessarily hold.

Third, we show significant correlation between mechanical strain guided cell morphology changes and CM differentiation. However, the mechanical environment is only one of the many factors shown to affect cell fate changes. The chemical environment as well as cell density and cell-cell and cell-ECM contacts also play a role[213] and one or the other or complementary signals along with the mechanical cues measured here might be necessary. The chemical environment as well as cell density and cell-cell and cell-ECM contacts also play a role[213] and one or the other or complementary signals along with the mechanical cues measured here might be necessary. Cell-cell contacts, both hetero- and homotypic, have been shown to play a crucial role in cardiomyocyte induction from stem cells[61, 62]. Similarly, the importance of the ECM on stem cell fate has been shown with particular emphasis on the interactions of ECM ligands with cell surface receptors, ECM geometry, or ECM elasticity. The nutrient and oxygen distribution within MDSC-3DGB may also play a role in the cell distribution, proliferation, and differentiation of the construct. MDSC-3DGB gets its oxygen and nutrient supply through

simple diffusion. Oxygen tension has been shown to influence cell proliferation and differentiation in a number of tissues, as well as in mouse embryonic stem cells[251]. The distribution of oxygen and nutrients within MDSC-3DGB also influences the cell distribution (localized to the outer circumference of the construct) and may affect the differentiation independent of the mechanical strain. Previous studies have shown that cells on the periphery of a pattern are able to influence the total differentiation rate of the cells (through influencing cytoskeletal dynamics) or proliferation rate (through influencing cell division) within a pattern[238-242]. Independent of the physical properties mentioned here, the stimulus-response decisions made by a stem cell can be further complicated temporally by systems biology[247]: tissue-specific patterns of ligand and receptor expression[248], as well as by sequential autocrine and paracrine inductive loops[249] that arise as cell populations develop and adapt[250]. While we note no significant changes in cell density within MDSC-3DGB at all time points, we did see a difference in tissue stiffness at D5. This difference in tissue stiffness may play a role in the disparate CM differentiation seen here. Despite the studies indicating cell shape as a read-out for integration of multiple applied and cell-generated mechanical forces, an interesting study by McBeath[137] found that cell shape alone is not sufficient to dictate lineage commitment. Thus, more in-depth methods of assessing the multiple factors and pathways involved in directed cell differentiation would be necessary.

In this study we note that by D9, a loss of cardiac specific protein expression at the MID. It remains unknown whether sustained CM differentiation or maturation from MDSCs require additional factors not present in the quiescent developing MDSC-3DGB. Further studies investigating these factors over a longer time period are necessary.

5.4.2 Conclusion

In summary, our results suggest that MDSC-3DGB mechanical strain guided cell morphology changes: evidenced by cell shape, size, and orientation are correlated with CM differentiation and this is time-dependent. This information is the first step in investigating the role of mechanical strain in CM lineage directed cell differentiation within a stem cell engineered tissue. This may be useful in providing the information necessary to generate an engineered tissue with a mechanical environment that can control and direct stem cell fate changes.

6.0 CONCLUSION

The overall goal of this doctoral thesis was to determine the role of mechanical strain on CM differentiation within a 3D engineered tissue to use as a system for evaluation of strategies for enhancing directed CM differentiation and tissue contractile properties. Substantial progress towards this goal was made by a combination of testing new strategies for monitoring differential CM differentiation and contractile function, such as using MDSCs in a 3D collagen gel bioreactor to induce CM differentiation and applying mechanical strain to determine the responsive cell type, and by developing new tools and methods for characterizing CM differentiation and cell morphology changes. The following section summarizes the main results of the four research-focused chapters of the thesis. A final section provides suggestions for future research building on this work.

6.1 THESIS SUMMARY

The first half of the thesis, chapters 2 and 3, explored in depth engineered cardiac tissue from native ventricular cells. In chapter 2, we investigated which cell type, CM or non-CMs, was the responsive cell population in an accepted response of increased proliferation and contractile properties to mechanical stretch and investigated one possible signaling pathway that could be involved in the stretch mediated responses observed. By isolating CMs from non-CMs

histologically in a control and mechanically stretched EEECT, we reported that while both CMs and non-CMs proliferate within EEECT, CMs, but not non-CMs, increase proliferation in response to cyclic mechanical stretch stimulation. Analysis of p38MAPK activation in response to mechanical stretch demonstrated significant increases in phosphorylation, which preceded increases in EEECT contractile force and CM proliferation. In contrast, the inhibition of p38MAPK significantly decreased CM proliferation activity and the negative effects of p38MAPK inhibition overrode the positive cyclic mechanical stretch stimulation effects on EEECT contractile function and CM proliferation. The significant increase in cellular proliferation in the CM population only within EEECT is an important finding because it provides a method of targeting a single cell population with a global non-specific perturbation within a fully connected tissue, without affecting the non-CM population or the tissue architecture.

In chapter 3, we investigated the implantation of EFCT and ENCT on a post-infarcted myocardium. We found that the proliferating fetal CMs within EFCT graft maintain CM proliferative activity *in vivo*, survive as a donor myocardial tissue, and contribute to the cardiac functional recovery of injured recipient myocardium whereas ENCT maintains a significantly lower proliferation activity and functional recovery of the injured myocardium. These results suggest that the maintenance of high proliferation activity is a factor that contributes to increased functional recovery of the injured myocardium.

In the second half of this thesis we investigated the use of a stem cell population, specifically skeletal muscle derived stem cells (MDSCs), within the 3D collagen gel bioreactor used to generate EEECT or EFCT. In chapter 4, we showed that the 3D environmental cues provided by MDSC-aggregate formation and 3D collagen gel bioreactor (3DGB) culture are

complementary and sufficient to trigger differentiation of cells with an immature functioning CM phenotype *in vitro.* We also investigated the MDSC-3DGB response to mechanical stretch and implantation on an injured myocardium to see if the MDSC-3DGB immature CM phenotype would respond similarly to chapter 2's EEECT and 3's EFCT. MDSC-3DGB culture responded to mechanical stretch with increased CM, not non-CM, proliferation and increased contractile properties similar to EEECT. MDSC-3DGB could be implanted on the injured myocardium, survive, and improve contractile function post injury, similar to EFCT. The magnitude of contractile force, increased CM proliferation, and improvement of recipient injured myocardial function is significantly less in MDSC-3DGB than EEECT and EFCT respectively, however the CM fraction, ~20% in MDSC-3DGB as opposed to the 60-70% CM fraction within EEECT and EFCT, could be responsible. These results are important because although the MDSC-3DGB has incomplete CM differentiation compared with engineered cardiac tissue from native ventricular cells, it still behaves similarly.

The distribution of the CM fraction was not uniform within MDSC-3DGB, suggesting that the CM differentiation in response to the 3DGB environment is a spatial- and temporal-dependent process, which may be characterized more fully with a system that encompasses longitudinal and regional study of the tissue formation.

Such a measurement system was developed in chapter 5 of this thesis. Custom generated MatLAB code for post-processing of live time-lapse confocal imaging was generated for the longitudinal and regional study of MDSC-3DGB. Mechanical strain directed cell morphology changes: evidenced by cell shape, size, and orientation changes were significant factors in directing CM differentiation from MDSCs within MDSC-3DGB.

In summary we have investigated the role of mechanical forces in CM proliferation within an engineered cardiac tissue from native ventricular cells. Additionally we have used a 3D engineered tissue culture system to induce CM differentiation from skeletal muscle derived stem cells. Lastly, we have developed a system to quantify the longitudinal and regional differences to determine the role of mechanical forces in directed CM differentiation within a 3D engineered tissue.

6.2 FUTURE DIRECTIONS

While cell shape appears to play a major role in governing the response of stem cells to mechanical forces, it is not yet clear whether this, along with other factors, converge on a single mechano-sensitive cellular compartment or molecule, and a mechano-transduction pathway connecting tension to mechano-responsive transcriptional machinery remains elusive[214]. Focal adhesions, which are areas that attach the actin cytoskeleton to the matrix bound integrins, likely factor into tension-dependent mechano-transduction. Cell generated traction forces are transmitted to the extracellular matrix at focal adhesions[215-217], which implies the development of stress within these structures, and these stresses regulate the assembly/disassembly of focal adhesions[215, 218-221]. Focal adhesions are also molecular signaling hubs implicated in the recruitment and activation of key mechano-sensitive kinases such as FAK, Src, and ERK[222-225]. Thus, investigation into the role of focal adhesions in the differentially directed CM differentiation via mechanically directed cell morphological changes seen in MDSC-3DGB would be of particular interest.

In addition to focal adhesions, MAPK signaling and primary cilia can also play a role in mechano-transduction. MAPK signaling is distinctive in that it can be activated in response to numerous types of applied forces[226], sits at a cross-roads between soluble factor and adhesion signaling (like RhoA[227, 228]), and regulates differentiation of stem cells[229, 230]. p38MAPK signaling has already been shown to play a role in CM specific proliferation in EEECT. Since MDSC-3DGB responds similarly to mechanical stretch, it will be interesting to investigate whether the signaling pathways activated by mechanical stretch in EEECT are also similar.

Primary cilia develop from and are anchored to the centriole, the cell's microtubule organizing center. They have been shown to act as mechano-sensors in a number of cell types including: osteocytes, chondrocytes, and kidney cells. Primary cilia have also been shown to play a key role in development in a number of cellular biological processes including the regulation of proliferation, differentiation, and cell cycle progression. They have also been shown to play key roles in controlling the Hedgehog signaling pathway[231, 232], one of the major determinants of embryonic patterning[233, 234]. Given the presence of primary cilia in cultured stem cells including MDSCs and MDSCs within MDSC-3DGB (unpublished data) and embryonic stem cells[235], exploring the role of primary cilia in mechanical regulation of differentiation, perhaps by altered Hedgehog signaling, represents an exciting future direction for stem cell research.

As of yet, no stem-cell specific mechano-sensory mechanisms have been proposed, and any number of aforementioned mechanisms may contribute to mechanical control of stem cell differentiation. Thus, MDSC-3DGB as well as the quantitative methods used to measure the temporal and spatial variations in MDSC-3DGB directed CM differentiation is an ideal *in vitro* platform to investigate these questions in depth. .

APPENDIX A

ALGORITHM FOR MORPHOLOGICAL ASSESSMENT AND 3D STRAIN MAPPING

See section 5.2 for explanation of use of this code. The code is implemented by typing CellAnalysis at the MatLAB command prompt. The functions: makefilelist.m, process2d.m, and CellBrowser.m are called and a GUI to generate a 3D plot of images in which each component is a different color and where one can export component orientation, major axis, minor axis, volume, and centroid parameters, etc. to an excel spreadsheet for statistical analysis is created.

CellAnalysis.m

```
function [  ] = CellAnalysis( input_args )
%--------------------------------------------------
% Cell shape, size, orientation, alignment analaysis
% Kelly clause with help from Peter Backeris
% last modified: 01/09
% Master File for executing cell morphology or microsphere analysis
%--------------------------------------------------


%------------------------------------------------------------
```

```
% Code to generate list of 2D images to be analyzed as a stack
%-------------------------------------------------------------


A = makefilelist();


% ---------------------------------------------------------------
% Code to generate the watershed segmentation
% and to make a new file list of the generated segmented images
% ---------------------------------------------------------------


B = process2d(A);


%-------------------------------------------------------------------------------
% code to call GUI to generate 3D plot of images in which each component is a
% different color and where one can export component properties to an excel spreadsheet
%for statistical analysis
%-------------------------------------------------------------------------------


CellBrowser(B);


end
```

makefilelist.m

```
function [ filenamelist ] = makefilelist(  )
%-----------------------------------------------------
% Code to generate list of 2D images to be analyzed as a stack
% Image files should be 8 bit greyscale Tiff (*.tif) images and should be named with a
%increasing number at the end.
% the filename should be something like ‘IMG0’ or  ‘IMG1’ plus the number at the end
%scaling from ‘0001’ to  ‘9999’.
% The full name would be for the first file ‘IMG10001.tif’.
%-------------------------------------------------------------------------
prompt = {'Enter number of first image (i.e. "3" for IMG10003):','Enter number of last
image (i.e. "100" for IMG10100):'};
dlg_title = 'Input images to be used for the analysis';
num_lines= 1;
def     = {'1','100'};
answer = inputdlg(prompt,dlg_title,num_lines,def);
F2 = str2num(cell2mat(answer(1,1)));
F = str2num(cell2mat(answer(2,1)));

% Choose first name of images
G = 'PIC1';
prompt = {'Enter Image Name (first 4 letters):'};
dlg_title = 'Input images to be used for the analysis';
```

```
num_lines= 1;
def     = {'IMG1'};
answer = inputdlg(prompt,dlg_title,num_lines,def);
G = cell2mat(answer(1,1));

E='.tif';

namelist(1:F-F2+1,1)=G(1,1);
namelist(1:F-F2+1,2)=G(1,2);
namelist(1:F-F2+1,3)=G(1,3);
namelist(1:F-F2+1,4)=G(1,4);

% create the numberlist
num=((10000+F2):(10000+F))';

% Creation of final results
filenamelist=namelist;
str=num2str(num);
filenamelist(:,5:8)=str(:,2:5);

filenamelist(1:F-F2+1,9)=E(1,1);
filenamelist(1:F-F2+1,10)=E(1,2);
filenamelist(1:F-F2+1,11)=E(1,3);
```

```
filenamelist(1:F-F2+1,12)=E(1,4);


% Save results
[FileNameBase,PathNameBase] = uiputfile('filenamelist.mat','Save as "filenamelist" in
image directory (recommended)');
cd(PathNameBase)
save(FileNameBase,'filenamelist');


end
```

process2d.m

```
function [lstack] = process2d( filenamelist )


% ------------------------------------------------------------
% Code to generate the watershed segmentation
% and to make a new file list of the generated segmented images
% ------------------------------------------------------------


[r,c]=size(filenamelist);


for i = 1:r          % run through all images
  I1 =  imresize(imread(filenamelist(i,:)),.5);
```

```
    I2 = im2bw(I1, graythresh(I1));
    I2 = bwareaopen(I2, 20);
    I2 = imfill(I2,'holes');
     filename = filenamelist(i,:);
    newname = strrep(filename,'.tif', 'a.tif');
     imwrite(I2, newname);
    segfilenamelist(i, :) = newname;
    stack(:,:,i) = I2;

end

lstack = bwlabeln(stack);
maxi = max(max(max(lstack)));
   volumes = regionprops(lstack, 'Area');
   [x1,y1] = size(I2);
   for x = 1:maxi
      a1 = volumes(x).Area;
      if (a1>20000)
      lstack(find(lstack==x))=0;
      end
      if (a1<100)
       lstack(find(lstack==x))=0;
```

```
        end

    end

    lstack = bwlabeln(lstack);


    %{

    [FileNameSeg,PathNameSeg] = uiputfile('SegFilenameList.mat','Save as
"SegFilenameList" in image directory (recommended)');

    cd(PathNameSeg)

    save(FileNameSeg,'segfilenamelist')

    %}
```

CellBrowser.m

```
    function varargout = CellBrowser(varargin)
    % CELLBROWSER M-file for CellBrowser.fig
    %      CELLBROWSER, by itself, creates a new CELLBROWSER or raises the
    %      existing singleton*.
    %
    %      H = CELLBROWSER returns the handle to a new CELLBROWSER or the
    %      handle to the existing singleton*.
    %
    %      CELLBROWSER('CALLBACK',hObject,eventData,handles,...) calls the
            %local function named CALLBACK in CELLBROWSER.M with the given
            %input arguments.
    %
    %      CELLBROWSER('Property','Value',...) creates a new CELLBROWSER or
    %      raises the existing singleton*.  Starting from the left,
            %property value pairs are applied to the GUI before %CellBrowser_OpeningFcn
            gets called.  An unrecognized property %name or invalid value makes property
            application stop.  All %inputs are passed to CellBrowser_OpeningFcn via
            varargin.
    %
    %      *See GUI Options on GUIDE's Tools menu.  Choose "GUI allows only
```

```
        %one instance to run (singleton)".
%
% See also: GUIDE, GUIDATA, GUIHANDLES

% Edit the above text to modify the response to help CellBrowser

% Last Modified by GUIDE v2.5 08-Feb-2009 00:47:41

% Begin initialization code - DO NOT EDIT
gui_Singleton = 1;
gui_State = struct('gui_Name',       mfilename, ...
                   'gui_Singleton',  gui_Singleton, ...
                   'gui_OpeningFcn', @CellBrowser_OpeningFcn, ...
                   'gui_OutputFcn',  @CellBrowser_OutputFcn, ...
                   'gui_LayoutFcn',  [] , ...
                   'gui_Callback',   []);
if nargin && ischar(varargin{1})
   gui_State.gui_Callback = str2func(varargin{1});
end

if nargout
   [varargout{1:nargout}] = gui_mainfcn(gui_State, varargin{:});
else
   gui_mainfcn(gui_State, varargin{:});
end
% End initialization code - DO NOT EDIT


% --- Executes just before CellBrowser is made visible.
function CellBrowser_OpeningFcn(hObject, eventdata, handles, varargin)
% This function has no output args, see OutputFcn.
% hObject    handle to figure
% eventdata  reserved - to be defined in a future version of MATLAB
% handles    structure with handles and user data (see GUIDATA)
% varargin   command line arguments to CellBrowser (see VARARGIN)
stack = varargin{1};
handles.multselect=0;

%retrieve centroid information
cellinfo = regionprops(stack,'Centroid');

%store cell volume information
handles.Volume = regionprops(stack, 'Area');

%find number of cells
maxi = max(max(max(stack)));
```

```
%store centroid z parameter for each cell to nearest integer
for k = 1:maxi
zstack(k) = round(cellinfo(k).Centroid(3));
end

%create array to store height of each cell
handles.zheight = zeros(1,maxi);


%find and store height of each cell
z = 1:maxi;
for i = 1:size(stack,3)
   h = ismember(z,stack(:,:,i));
   handles.zheight = handles.zheight + h;



end

%get bounds of planes containing cell centroids (may not be some of the end
%planes)

maxm =max(zstack);
minm = min(zstack);




%find 2d cell information based on the cell's centroid z parameter
for m = minm:maxm
   temp = stack(:,:,m);
   x = find(zstack==m);
   temp1 = ismember(temp,x);
   temp(temp1==0) = 0;

   R = regionprops(temp, 'MinorAxisLength', 'MajorAxisLength','Orientation',
'Eccentricity');
    for n = 1:size(x,2)

      handles.celldata(x(n),1) = R(x(n),1);
    end
```

```
        end

        %zheight will now hold ellipsoid volume
        for p = 1:maxi

           handles.zheight(p) = (1/3)*3.14*(handles.celldata(p).MajorAxisLength)
*(handles.celldata(p).MinorAxisLength)*handles.zheight(p);
        end


        %color each cell randomly
        rgb = rand(maxi,3);
        handles.prev_cell = 0;


        %plot cell patch objects
        for i = 1:maxi

        p = patch(isosurface(stack==i, .8));
        reducepatch(p, .3);
        set(p,'facecolor',rgb(i,:),'edgecolor','none','buttondownfcn', {@selectcell,i},  'tag',
num2str(i));

        end

        %set plot properties
        set(handles.axes1,'projection','perspective');
        box on;

        light('position',[1,1,1])
        light('position',[-1,-1,-1])

        set(handles.axes1,'xlim',[0 512], 'ylim',[0 512])
        zscale= .5;
        set(handles.axes1,'DataAspectRatio',[1,1,zscale])




        % Choose default command line output for CellBrowser
        handles.output = hObject;

        % Update handles structure
        guidata(hObject, handles);
```

```
% UIWAIT makes CellBrowser wait for user response (see UIRESUME)
% uiwait(handles.figure1);

%executes when a cell patch object is clicked with mouse
function selectcell(hObject, eventdata, j)

   if (strcmp(get(hObject,'Selected'), 'on'))
      set(hObject,'Selected', 'off');
   else

   handles = guidata(gcf);

   %fill in table fields with cell information
   temp(1,1)= j;
   temp(2,1)= handles.celldata(j).MajorAxisLength;
   temp(3,1)= handles.celldata(j).MinorAxisLength;
   temp(4,1)= -(handles.celldata(j).Orientation);
   temp(5,1)= handles.celldata(j).Eccentricity;
   temp(6,1)= handles.Volume(j).Area;
   temp(7,1)=handles.zheight(j);
   set(handles.uitable1, 'data', temp);
   if (get(handles.checkbox1,'Value') == 0)
     set(handles.prev_cell, 'Selected', 'off');
   end
   set(hObject, 'Selected', 'on');

   handles.prev_cell = hObject;
   guidata(gcf,handles);
   end


% --- Outputs from this function are returned to the command line.
function varargout = CellBrowser_OutputFcn(hObject, eventdata, handles)
% varargout  cell array for returning output args (see VARARGOUT);
% hObject    handle to figure
% eventdata  reserved - to be defined in a future version of MATLAB
% handles    structure with handles and user data (see GUIDATA)

% Get default command line output from handles structure
varargout{1} = handles.output;



% --- Executes on button press in checkbox1.
function checkbox1_Callback(hObject, eventdata, handles)
```

```
% hObject    handle to checkbox1 (see GCBO)
% eventdata  reserved - to be defined in a future version of MATLAB
% handles    structure with handles and user data (see GUIDATA)

% Hint: get(hObject,'Value') returns toggle state of checkbox1


% --- Executes on button press in pushbutton2.
function pushbutton2_Callback(hObject, eventdata, handles)
% hObject    handle to pushbutton2 (see GCBO)
% eventdata  reserved - to be defined in a future version of MATLAB
% handles    structure with handles and user data (see GUIDATA)
h = findobj('Selected', 'on');
sizeh = size(h);

%construct table containing selected cell information

if (sizeh>0)
       t = {'Cell Number', 'Major Axis Length', 'Minor Axis Length',
       'Orientation','Eccentricity', 'Pixel Volume', 'Ellips. Volume (cubic um)'};
   for i = 2:sizeh+1
       t{i,1} = str2num(get(h(i-1),'tag'));
            t{i,2} = handles.celldata(str2double(get(h(i-1),'tag'))).MajorAxisLength;
              t{i,3} = handles.celldata(str2double(get(h(i-1),'tag'))).MinorAxisLength;
              t{i,4} = handles.celldata(str2double(get(h(i-1),'tag'))).Orientation;
              t{i,5} = handles.celldata(str2double(get(h(i-1),'tag'))).Eccentricity;
       t{i,6} = handles.Volume(str2double(get(h(i-1),'tag'))).Area;
       t{i,7} = handles.zheight(str2double(get(h(i-1),'tag')));

   end
   [filename,pathname] = uiputfile('cell_data','Save your cell data');

   if pathname == 0 %if the user pressed cancelled, then we exit this callback
      return
   end
%construct the path name of the save location
    saveDataName = fullfile(pathname,filename);


   xlswrite(saveDataName, t);

end


% --- Executes on button press in pushbutton4.
function pushbutton4_Callback(hObject, eventdata, handles)
```

```
% hObject    handle to pushbutton4 (see GCBO)
% eventdata  reserved - to be defined in a future version of MATLAB
% handles    structure with handles and user data (see GUIDATA)
h = findobj('Selected', 'on');
set(h, 'Selected', 'off');
```

A.1 IMAGEJ ALGORITHM

We also used ImageJ to verify and validate the robustness of calculations and confidence of results from the MatLAB code found above. This code used a commercially available ImageJ elastic registration plugin, bUnwarpJ, along with a macro file provided by Dr. Lance Davidson to make the absolute and x- and y- displacement files between two images.

Macro: "MakeAbsDisp1 from Raw[1]"

```
{
  file = File.openDialog("Select the Raw File");
  path = File.directory();

  bigstring = File.openAsString(file);

  absdisWindow = raw2abs(bigstring, path);
}



function raw2abs(bigstring, path)
{
  lines = split(bigstring, "\n");

  widstr = split(lines[0], "=");
  heistr =  split(lines[1], "=");

  width = parseInt(widstr[1]);
  height = parseInt(heistr[1]);
```

```
// real data starts at lines[4].

newImage("rawX", "32-bit", width, height, 1);
selectWindow("rawX");

for (i=4; i<4+height; i++)
{

        pixels = split(lines[i],"");
        for (j=1; j<width; j++)
        {
                x = j-1;
                y = i-4;
                setPixel(x, y, x - parseFloat(pixels[j-1]));
        }

}

// *** this is the line I want to start the Y data.

newImage("rawY", "32-bit", width, height, 1);
selectWindow("rawY");

for (i=6+height; i<6+(2*height); i++)
{

        pixels = split(lines[i],"");
        for (j=1; j<width; j++)
        {
                x = j-1;
                y = i-(6+height);
                setPixel(x, y, y - parseFloat(pixels[j-1]));
        }
}

imageCalculator("Multiply create 32-bit", "rawX","rawX");
imageCalculator("Multiply create 32-bit", "rawY","rawY");
imageCalculator("Add create 32-bit", "Result of rawX","Result of rawY");
run("Square Root");
rename("AbsDisp");save(path+"AbsDisp.tif");

//
// close all other windows
//

selectWindow("rawX"); save(path+"deltaX.tif"); close();
```

```
  selectWindow("rawY"); save(path+"deltaY.tif"); close();
  selectWindow("Result of rawX"); close();
  selectWindow("Result of rawY"); close();

  return "AbsDisp";
}
```

APPENDIX B

SK-FMHC PRESENCE WITHIN THE DEVELOPING MYOCARDIUM: METHODS

The presence of sk-fMHC within the myocardium from gestational day (GD) 13 and 20, neonatal day (ND) 4, post-natal day (PND) 10 or 17 (juvenile), and adult Lewis rat myocardium and skeletal muscle was assessed using immunohistochemical staining, western blot, and PCR.

B.1 IMMUNOHISTOCHEMICAL STAINING

Heart samples were fixed with 4% paraformaldehyde/PBS for 15 minutes and embedded in the 13% polyacrylamide gel. 150μm thick sections were made using a vibratory microtome (Vibratome-1000, Vibrotome.com)[120] and stained for mouse monoclonal sk-fMHC (Sigma, St. Louis, MO, USA) and cardiac specific Troponin-I (cTn-I, Abcam, Cambridge, MA, USA) primary antibodies and Alexa Fluor 488 or Alexa Fluor 594 secondary antibodies (Invitrogen, Carlsbad, CA, USA).

B.2 SDS-PAGE AND IMMUNOBLOTTING

Fresh frozen heart samples were used. Protein was extracted from pooled samples and immunoblotting was carried out using routine protocols. Each lane contained 20µg of total protein. Mouse monoclonal β-actin antibody (Abcam), mouse monoclonal cardiac troponin-I (cTn-I, Abcam), and mouse monoclonal sk-fMHC (Sigma) were visualized with IR-Dye 800 donkey anti-mouse secondary antibody (Rockland Immunochemicals, Gilbertsville, PA, USA). All proteins were visualized using an infrared western blot imaging system (Odyssey, LI-COR Biosciences Lincoln, NE, USA). Immunoblots were performed in triplicate (n=3 in each developmental stage).

B.3 RT-PCR

Fresh frozen pooled heart samples were used. Total RNA was prepared using Trizol solution (Invitrogen) and treated with TURBO DNA-free kit (Ambion, Austin, TX, USA). Primers, whose target genes were *α-cardiac MHC,* and *sk-fMHC* were obtained from Qiagen Quanti-Tect Primer Assay with the target fragment sizes approximately 100 base pairs. One step RT was performed with a total volume of 1µg RNA in a total volume of 25µL that used MuLy (Roches, Pleasanton, CA, USA) with the program: 42^{o}C 15 min, 99^{o}C 5min, 5^{o}C 5min, 1 cycle. cDNA (1µL) was used for PCR which used the program: 94^{o}C 2min, 95^{o}C 50second, 58^{o}C 30 second, 72^{o}C 1 min, 35 cycles 72°C 7 min extension. For normalization of RT-PCR results, *β-actin* was used as an internal control. All PCR products were confirmed by University of

Pittsburgh DNA Sequence Core Facilities, performed by Eppendorf Mastercycles. All RT-PCR assays were completed in triplicate (n=3 in each developmental stage).

BIBLIOGRAPHY

1. Lloyd-Jones, et al., *Heart Disease and Stroke Statistics--2009 Update: A Report From the American Heart Association Statistics Committee and Stroke Statistics Subcommittee.* Circulation, 2009. **119**(3): p. e21-181.

2. Lloyd-Jones DM, et al., *Lifetime risk of developing coronary heart disease* The Lancet, 1999. **353**(9147): p. 89-92.

3. Li, F., et al., *Hyperplasia and hypertrophy of chicken cardiac myocytes during posthatching development.* Am J Physiol, 1997. **273**(2 Pt 2): p. R518-26.

4. Sedmera, D., et al., *Cellular changes in experimental left heart hypoplasia.* Anat Rec, 2002. **267**(2): p. 137-45.

5. *Prevalence and incidence of cardiac malformation*, in *Surgery of Congenital Heart Disease: Pediatric Cardiac Care Consortium, 1984-1995*, M. JH, Editor. 1998, Futura Publishing Co: Armonk, NY.

6. Centers for Disease Control and Prevention. *Compressed mortality file: underlying cause of death, 1979 to 2005*. Atlanta, GA: Centers for Disease Control and Prevention. Available at: http://wonder.cdc.gov/mortSQL.html. Accessed August 11, 2008.

7. Laflamme, M.A., et al., *Cell-based therapy for myocardial ischemia and infarction: pathophysiological mechanisms.* Annu Rev Pathol, 2007. **2**: p. 307-39.

8. Payne, T.R., et al., *A relationship between vascular endothelial growth factor, angiogenesis, and cardiac repair after muscle stem cell transplantation into ischemic hearts.* J Am Coll Cardiol, 2007. **50**(17): p. 1677-84.

9. Laflamme, M.A. and C.E. Murry, *Regenerating the heart.* Nat Biotechnol, 2005. **23**(7): p. 845-56.

10. Pasumarthi, K.B. and L.J. Field, *Cardiomyocyte cell cycle regulation.* Circ Res, 2002. **90**(10): p. 1044-54.

11. Roell, W., et al., *Engraftment of connexin 43-expressing cells prevents post-infarct arrhythmia.* Nature, 2007. **450**(7171): p. 819-24.

12. Zimmermann, W.H., et al., *Heart muscle engineering: an update on cardiac muscle replacement therapy.* Cardiovasc Res, 2006. **71**(3): p. 419-29.

13. Zimmermann, W.H., et al., *Engineered heart tissue grafts improve systolic and diastolic function in infarcted rat hearts.* Nat Med, 2006. **12**(4): p. 452-8.

14. Christoforou, N. and J.D. Gearhart, *Stem cells and their potential in cell-based cardiac therapies.* Prog Cardiovasc Dis, 2007. **49**(6): p. 396-413.

15. Zammaretti, P. and M. Jaconi, *Cardiac tissue engineering: regeneration of the wounded heart.* Curr Opin Biotechnol, 2004. **15**(5): p. 430-4.

16. Chien, K.R., *Stem cells: lost in translation.* Nature, 2004. **428**(6983): p. 607-8.

17. Akins, R.E., et al., *Gene expression profile of bioreactor-cultured cardiac cells: activation of morphogenetic pathways for tissue engineering.* DNA Cell Biol, 2007. **26**(6): p. 425-34.

18. Anderson, P.A., et al., *Calcium signals induce liver stem cells to acquire a cardiac phenotype.* Cell Cycle, 2007. **6**(13): p. 1565-9.

19. Steinberg, M.S., *Reconstruction of tissues by dissociated cells. Some morphogenetic tissue movements and the sorting out of embryonic cells may have a common explanation.* Science, 1963. **141**: p. 401-8.

20. Tobita, K., et al., *Engineered early embryonic cardiac tissue retains proliferative and contractile properties of developing embryonic myocardium.* Am J Physiol Heart Circ Physiol, 2006. **291**(4): p. H1829-37.

21. Vacanti, J.P. and R. Langer, *Tissue engineering: the design and fabrication of living replacement devices for surgical reconstruction and transplantation.* Lancet, 1999. **354 Suppl 1**: p. SI32-4.

22. Zimmermann, W., et al., *Three-dimensional engineered heart tissue from neonatal rat cardiac myocytes.* Biotechnol Bioeng, 2000. **68**: p. 106-114.

23. Claycomb, W.C., *Cardiac muscle cell proliferation and cell differentiation in vivo and in vitro.* Adv Exp Med Biol, 1983. **161**: p. 249-265.

24. Claycomb, W.C., *Proliferative potential of the mammalian ventricular cardiac muscle cells*, in *The Development and Regenerative Potential of Cardiac Muscle*, Oberpriller J and M. A, Editors. 1991, Harwood Academic: Amsterdam p. 236-351.

25. Hansen LK, et al., *Enhanced Morphology and Function in Hepatocyte Spheroids: A Model of Tissue Self-Assembly.* Tissue Engineering, 1998. **4**(1): p. 65-74.

26. Watzka, S.B., et al., *Selection of viable cardiomyocytes for cell transplantation using three-dimensional tissue culture.* Transplantation, 2000. **70**(9): p. 1310-7.

27. Carpenedo, R.L., C.Y. Sargent, and T.C. McDevitt, *Rotary suspension culture enhances the efficiency, yield, and homogeneity of embryoid body differentiation.* Stem Cells, 2007. **25**(9): p. 2224-34.

28. Albrecht, D.R., et al., *Probing the role of multicellular organization in three-dimensional microenvironments.* Nat Methods, 2006. **3**(5): p. 369-75.

29. Suenaga H, et al., *Aggregate formation of bone marrow stromal cells by rotation culture.* Mat Sci Eng, 2004. **C24**: p. 421-424.

30. Kehat, I., et al., *Human embryonic stem cells can differentiate into myocytes with structural and functional properties of cardiomyocytes.* J Clin Invest, 2001. **108**(3): p. 407-14.

31. Bursac, N., et al., *Cultivation in rotating bioreactors promotes maintenance of cardiac myocyte electrophysiology and molecular properties.* Tissue Eng, 2003. **9**(6): p. 1243-53.

32. Dimmeler, S., A.M. Zeiher, and M.D. Schneider, *Unchain my heart: the scientific foundations of cardiac repair.* J Clin Invest, 2005. **115**(3): p. 572-83.

33. Ott, H.C., B.H. Davis, and D.A. Taylor, *Cell therapy for heart failure--muscle, bone marrow, blood, and cardiac-derived stem cells.* Semin Thorac Cardiovasc Surg, 2005. **17**(4): p. 348-60.

34. Tossios, P., et al., *No evidence of myocardial restoration following transplantation of mononuclear bone marrow cells in coronary bypass grafting surgery patients based upon cardiac SPECT and 18F-PET.* BMC Med Imaging, 2006. **6**: p. 7.

35. Panorchan, P., et al., *Microrheology and ROCK signaling of human endothelial cells embedded in a 3D matrix.* Biophys J, 2006. **91**(9): p. 3499-507.

36. Eschenhagen, T., et al., *Cardiac tissue engineering.* Transpl Immunol, 2002. **9**(2-4): p. 315-21.

37. Eschenhagen, T., et al., *Three-dimensional reconstitution of embryonic cardiomyocytes in a collagen matrix: a new heart muscle model system.* FASEB J, 1997. **11**(8): p. 683-94.

38. Eschenhagen, T. and W. Zimmermann, *Engineering Myocardial Tissue.* Circ Res, 2005. **97**: p. 1120-1123.

39. Zimmermann, W.H., et al., *Engineered heart tissue for regeneration of diseased hearts.* Biomaterials, 2004. **25**: p. 1639-1647.

40. Radisic, M., et al., *Functional assembly of engineered myocardium by electrical stimulation of cardiac myocytes cultured on scaffolds.* Proc Natl Acad Sci U S A, 2004. **101**(52): p. 18129-34.

41. Shimizu, T., et al., *Fabrication of pulsatile cardiac tissue grafts using a novel 3-dimensional cell sheet manipulation technique and temperature-responsive cell culture surfaces.* Circ Res, 2002. **90**(3): p. e40.

42. Lee, E.J., et al., *Engineered cardiac organoid chambers: toward a functional biological model ventricle.* Tissue Eng Part A, 2008. **14**(2): p. 215-25.

43. Schwarzkopf, R., et al., *Autospecies and post-myocardial infarction sera enhance the viability , proliferation, and maturation of 3D cardiac cell culture.* Tissue Eng, 2006. **12**(12): p. 3467-3475.

44. Huang, Y.C., et al., *Contractile three-dimensional bioengineered heart muscle for myocardial regeneration.* J Biomed Mater Res A, 2007. **80**(3): p. 719-731.

45. Naito, H., et al., *Optimizing engineered heart tissue for therapeutic applications as surrogate heart muscle.* Circulation, 2006. **114**(1 Suppl): p. I72-8.

46. Kofidis, T., et al., *In vitro engineering of heart muscle: artificial myocardial tissue.* J Thorac Cardiovasc Surg, 2002. **124**(1): p. 63-69.

47. Zimmermann, W.H., et al., *Tissue engineering of a differentiated cardiac muscle construct.* Circ Res, 2002. **90**(2): p. 223-30.

48. McDevitt, T.C., et al., *Spatially organized layers of cardiomyocytes on biodegradable polyurethane films for myocardial repair.* J Biomed Mater Res A, 2003. **66**(3): p. 586-595.

49. Feng, Z., et al., *Measurements of the mechanical properties of contracted collagen gels populated with rat fibroblasts or cardiomyocytes.* J Artif Organs, 2003. **6**(3): p. 192-196.

50. Ishii, O., et al., *In vitro tissue engineering of a cardiac graft using a degradable scaffold with an extracellular matrix-like topography.* J Thorac Cardiovasc Surg, 2005. **130**(5): p. 1358-1363.

51. Lee, E., et al., *Engineered Cardiac Tissue Chambers Demonstrate Functional Frank-Starling Mechanism and Positive Stroke Work.* Circ Res, 2005. **97**(11): p. II-1200.

52. Yildirim, Y., et al., *Development of a Biological Ventricular Assist Device: Preliminary Data From a Small Animal Model.* Circulation, 2007. **116**(11_suppl): p. I-16-23.

53. Li, R.K., et al., *Survival and function of bioengineered cardiac grafts.* Circulation, 1999. **100**(19 Suppl): p. II63-9.

54. Leor, J. and S. Cohen, *Myocardial tissue engineering: creating a muscle patch for a wounded heart.* Ann N Y Acad Sci, 2004. **1015**: p. 312-319.

55. Dar, A., et al., *Optimization of cardiac cell seeding and distribution in 3D porous alginate scaffolds.* Biotechnol Bioeng, 2002. **80**(3): p. 305-312.

56. Christman, K., et al., *Fibrin glue alone and skeletal myoblasts in a fibrin scaffold preserve cardiac function after myocardial infarction.* Tissue Eng, 2004. **10**(3-4): p. 403-409.

57. Carrier, R., et al., *Cardiac tissue engineering: cell seeding, cultivation parameters, and tissue construct characterization.* Biotechnol Bioeng, 1999. **64**(5): p. 580-589.

58. Layland, J., I. Young, and J. Altringham, *The effect of cycle frequency on the power output of rat papillary muscles in vitro.* J Exp Biol, 1995. **198**(4): p. 1035-1043.

59. Arai, A., K. Yamamoto, and J. Toyama, *Murine cardiac progenitor cells require visceral embryonic endoderm and primitive streak for terminal differentiation.* Dev Dyn, 1997. **210**(3): p. 344-353.

60. Lough, J. and Y. Sugi, *Endoderm and heart development.* Dev Dyn, 2000. **217**: p. 327-342.

61. Iijima, Y., et al., *Beating is necessary for transdifferentiation of skeletal muscle-derived cells into cardiomyocytes.* FASEB J, 2003. **17**(10): p. 1361-3.

62. Rudy-Reil, D. and J. Lough, *Avian precardiac endoderm/mesoderm induces cardiac myocyte differentiation in murine embryonic stem cells.* Circ Res, 2004. **94**(12): p. e107-16.

63. Armstrong, M.T., D.Y. Lee, and P.B. Armstrong, *Regulation of proliferation of the fetal myocardium.* Dev Dyn, 2000. **219**(2): p. 226-36.

64. Eisenberg, L. and C. Eisenberg, *Embryonic myocardium shows increased longevity as a functional tissue when cultured in the presence of a noncardiac tissue layer.* Tissue Eng, 2006. **12**: p. 853-865.

65. Narmoneva, D., et al., *Endothelial cells promote cardiac myocyte survival and spatial reorganization: implications for cardiac regeneration.* Circulation, 2004. **110**(8): p. 962-968.

66. Bick, R., et al., *Physical, contractile and calcium handling properties of neonatal cardiac myocytes cultured on different matrices.* Cell Adhes Commun, 1998. **6**(4): p. 301-310.

67. Zandstra, P., et al., *Scalable production of embryonic stem cell-derived cardiomyocytes.* Tissue Eng, 2003. **9**(4): p. 767-778.

68. Kehat, I. and L. Gepstein, *Human embryonic stem cells for myocardial regeneration.* Heart Fail Rev, 2003. **8**(3): p. 229-236.

69. Dvorin, E., et al., *Quantitative evaluation of endothelial progenitors and cardiac valve endothelial cells: proliferation and differentiation on poly-glycolic acid/poly-4-hydroxybutyrate scaffold in response to vascular endothelial growth factor and transforming growth factor beta 1* Tissue Eng, 2003. **9**(3): p. 487-493.

70. Krupnick, A., et al., *A novel small animal model of left ventricular tissue engineering.* J Heart Lung Tansplant, 2002. **21**(2): p. 233-243.

71. Fukuhara, S., et al., *Bone marrow cell-seeded biodegradable polymeric scaffold enhances angiogenesis and improves function of the infarcted heart.* Circ J, 2005. **69**(7): p. 850-857.

72. Fujita, M., et al., *Proliferation and differentiation of rat bone marrow stromal cells on poly(glycolic acid)-collagen sponge.* Tissue Eng, 2005. **11**(9-10): p. 1346-1355.

73. Giraud, M., et al., *Current State of the Art in Myocardial Tissue Engineering.* Tissue Eng, 2007.

74. Rota, M., et al., *Bone marrow cells adopt the cardiomyogenic fate in vivo.* Proc Natl Acad Sci U S A, 2007. **104**(45): p. 17783-8.

75. Dowell, J.D., et al., *Myocyte and myogenic stem cell transplantation in the heart.* Cardiovasc Res, 2003. **58**(2): p. 336-50.

76. Okada, M., et al., *Myogenic Endothelial Cells Purified From Human Skeletal Muscle Improve Cardiac Function After Transplantation Into Infarcted Myocardium.* JACC, 2008. **52**(23): p. 1869-1865.

77. Kolossov, E., et al., *Engraftment of engineered ES cell-derived cardiomyocytes but not BM cells restores contractile function to the infarcted myocardium.* J Exp Med, 2006. **203**(10): p. 2315-27.

78. Nag, A., *Study of non-muscle cells of the adult mammalian heart: a fine structural analysis and distribution.* Cytobios, 1980. **28**(109): p. 41-61.

79. Beltrami, C., et al., *Structural basis of end-stage failure in ischemic cardiomyopathy in humans.* Circulation, 1994. **89**(1): p. 151-163.

80. Brown, L., *Cardiac extracellular matrix: a dynamic entity.* Am J Physiol Heart Circ Physiol, 2005. **289**(3): p. H973-974.

81. Bouzeghrane, F., et al., *Enhanced expression of fibrillin-1, a constituent of the myocardial extracellular matrix in fibrosis.* Am J Physiol Heart Circ Physiol, 2005. **289**(3): p. H982-991.

82. Koshy, S., H. Reddy, and H. Shukla, *Collagen cross-linking: new dimension to cardiac remodeling.* Cardiovascular Research, 2003. **57**(3): p. 594-598.

83. Schaffer, W. and R.S. Williams, *Age-dependent changes in expression of alpha 1-adrenergic receptors in rat myocardium.* Biochem Biophys Res Commun, 1986. **138**(1): p. 387-91.

84. Rybin, V.O. and S.F. Steinberg, *Protein kinase C isoform expression and regulation in the developing rat heart.* Circ Res, 1994. **74**(2): p. 299-309.

85. Pandya, N., D. Santani, and S. Jain, *Role of mitogen-activated protein (MAP) kinases in cardiovascular diseases.* Cardiovasc Drug Rev, 2005. **23**(3): p. 247-54.

86. Hagege, A.A. and P. Menasche, *Cellular cardiomyoplasty: a new hope in heart failure?* Heart, 2000. **84**(5): p. 465-6.

87. Tenhunen, O., et al., *Identification of cell cycle regulatory and inflammatory genes as predominant targets of p38 mitogen-activated protein kinase in the heart.* Circ Res, 2006. **99**(5): p. 485-93.

88. Assmus, B., et al., *Transplantation of progenitor cells and regeneration enhancement in acute myocardial infarction (TOPCARE-AMI).* Circulation, 2002. **106**: p. 3009-3017.

89. Haufe, V., et al., *Expression pattern of neuronal and skeletal muscle voltage-gated Na+ channels in the developing mouse heart.* J Physiol, 2005. **564**(Pt 3): p. 683-96.

90. Saggin, L., et al., *Troponin I switching in the developing heart.* J Biol Chem, 1989. **264**(27): p. 16292-19298.

91. Cognard, C., et al., *Progressive predominance of 'skeletal' versus 'cardiac' types of excitation-contraction coupling during in vitro skeletal myogenesis.* Pflugers Arch, 1992. **422**(2): p. 207-9.

92. Galbraith, C. and M. Sheetz, *Forces on adhesive contacts affect cell function.* Curr Opin Cell Biol, 1998. **10**: p. 566-571.

93. Cowin, S., *How is a tissue built?* J Biomech Eng, 2000. **122**: p. 553-569.

94. Chiquet, M., *Regulation of extracellular matrix gene expression by mechanical stress.* Matrix Biol, 1999. **18**: p. 417-426.

95. Ingber, D., *In search of cellular control: Signal transduction in context.* J Cell Biochem Suppl, 1998. **30-31**: p. 232-237.

96. Clark, E.B., et al., *Effect of increased pressure on ventricular growth in stage 21 chick embryos.* Am J Physiol, 1989. **257**(1 Pt 2): p. H55-61.

97. Hall, C., R. Hurtado, and K. Hewett, *Hemodynamic-dependent patterning of endothelin converting enzyme 1 expression and differentiation of impulse conducting Purkinje fibers in the embryonic heart.* Development, 2004. **131**: p. 581-592.

98. Miller, C.E., C.L. Wong, and D. Sedmera, *Pressure overload alters stress-strain properties of the developing chick heart.* Am J Physiol Heart Circ Physiol, 2003. **285**: p. H1849-1856.

99. Reckova, M., et al., *Hemodynamics is a key epigenetic factor in development of the cardiac conduction system.* Circ Res, 2003. **93**: p. 77-85.

100. Schroder, E.A., et al., *Microtubule involvement in the adaptation to altered mechanical load in developing chick myocardium.* Circ Res, 2002. **91**(4): p. 353-9.

101. Sedmera, D., et al., *Remodeling of chick embryonic ventricular myoarchitecture under experimentally changed loading conditions.* Anat Rec, 1999. **254**(2): p. 238-52.

102. Tobita, K., et al., *Three-dimensional myofiber architecture of the embryonic left ventricle during normal development and altered mechanical loads.* Anat Rec A Discov Mol Cell Evol Biol, 2005. **283**(1): p. 193-201.

103. Tobita, K. and B.B. Keller, *Right and left ventricular wall deformation patterns in normal and left heart hypoplasia chick embryos.* Am J Physiol Heart Circ Physiol, 2000. **279**(3): p. H959-69.

104. Tobita, K., et al., *Regional passive ventricular stress-strain relations during development of altered loads in chick embryo.* Am J Physiol Heart Circ Physiol, 2002. **282**(6): p. H2386-96.

105. Yang, M., L. Taber, and E. Clark, *A nonlinear poroelastic model for the trabecular embryonic heart.* J Biomech Eng, 1994. **116**: p. 213-223.

106. Komuro, I., et al., *Mechanical loading stimulates cell hypertrophy and specific gene expression in cultured rat cardiac myocytes. Possible role of protein kinase C activation.* J Biol Chem, 1991. **266**(2): p. 1265-8.

107. Sadoshima, J. and S. Izumo, *Mechanical stretch rapidly activates multiple signal transduction pathways in cardiac myocytes: potential involvement of an autocrine/paracrine mechanism.* EMBO J, 1993. **12**(4): p. 1681-92.

108. Rauch, C. and P.T. Loughna, *Static stretch promotes MEF2A nuclear translocation and expression of neonatal myosin heavy chain in C2C12 myocytes in a calcineurin- and p38-dependent manner.* Am J Physiol Cell Physiol, 2005. **288**(3): p. C593-605.

109. Komuro, I., et al., *Mechanical stretch activates the stress-activated protein kinases in cardiac myocytes.* FASEB J, 1996. **10**(5): p. 631-6.

110. Farge, E., *Mechanical induction of Twist in the Drosophila foregut/stomodeal primordium.* Curr Biol, 2003. **13**(16): p. 1365-77.

111. Heng, B., et al., *Strategies for directing the differentiation of stem cells into the cardiomyogenic lineage in vitro.* Cardiovascular Research, 2004. **62**: p. 34-42.

112. Kada, K., K. Yasui, and K. Naruse, *Orientation change of cardiocytes induced by cyclic stretch stimulation: time dependency and involvement of protein kinases.* J Mol Cell Cardiol, 1999. **31**(1): p. 247-259.

113. Vandenburgh, H., R. Solerssi, and J. Shansky, *Response of neonatal rat cardiomyocytes to repetitive mechanical stimulation in vitro.* Ann N Y Acad Sci, 1995. **27**(752): p. 19-29.

114. Decker, M., D. Janes, and M. Barclay, *Regulation of adult cardiomyocyte growth: effects of active and passive mechanical loading.* Am J Physiol, 1997. **272**(6 Pt. 2): p. H2902-2918.

115. Ruwhof, C., A. vanWamel, and J. Egas, *Cyclic stretch induces the release of growth promoting factors from cultured neonatal cardiomyocytes and cardiac fibroblasts.* Mol Cell Biochem, 2000. **208**(1-2): p. 89-98.

116. Shyu, K., C. Chen, and B. Wang, *Angiotensin II receptor antagonist blocks the expression of connexin43 induced by cyclic mechanic stretch in cultured neonatal rat cardiac myocytes.* J Mol Cell Cardiol, 2003. **33**(4): p. 691-698.

117. Luther, H., S. Hille, and H. Haase, *Influence of mechanical activity, adrenergic stimulation, and calcium on the expression of myosin heavy chains in cultivated neonatal cardiomyocytes.* J Cell Biochem, 1997. **64**(3): p. 459-465.

118. Fink, C., et al., *Chronic stretch of engineered heart tissue induces hypertrophy and functional improvement.* FASEB J, 2000. **14**(5): p. 669-79.

119. Akhyari, P., et al., *Mechanical Stretch Regimen Enhances the Formation of Bioengineered Autologous Cardiac Muscle Grafts.* Circulation, 2002. **106**: p. I137-142.

120. Clause, K., et al., *Engineered early embryonic cardiac tissue increases cardiomyocyte proliferation by cyclic mechanical stretch via p38-MAP kinase phosphorylation.* Tissue Eng, 2009. **15**(6): p. 1373-1380.

121. Ko, H.J., et al., *Optical coherence elastography of engineered and developing tissue.* Tissue Eng, 2006. **12**(1): p. 63-73.

122. Mason, C., et al., *The potential of optical coherence tomography in the engineering of living tissue.* Phys Med Biol, 2004. **49**: p. 1097.

123. Xu, X., R. Wang, and E. Haj, *Investigation of changes in optical attenuation of bone and neuronal cells in organ culture or three-dimensional constructs in vitro with optical coherence tomography: relevance to cytochrome oxidase monitoring.* Eur Biophys J, 2003. **32**: p. 355.

124. Levenberg, S., et al., *Differentiation of human embryonic stem cells on three-dimensional polymer scaffolds.* Proc Natl Acad Sci U S A, 2003. **100**: p. 12741.

125. Sauer, H., et al., *Redox control of angiogenic factors and CD31-positive vessel-like structures in mouse embryonic stem cells after direct current electrical field stimulation.* Exp Cell Res, 2005. **304**: p. 380.

126. Park, J., et al., *Differential effects of equiaxial and uniaxial strain on mesenchymal stem cells* Biotechnol Bioeng, 2004. **88**: p. 359.

127. Passier, R. and C. Mummery, *Cardiomyocyte differentiation from embryonic and adult stem cells.* Curr Opin Biotechnol, 2005. **16**(5): p. 498-502.

128. Engler, A., et al., *Matrix Elasticity Directs Stem Cell Lineage Specification* Cell, 2006. **126**: p. 677-689.

129. Schuldiner, M., O. Yanuka, and J. Itskovitz-Eldor, *Effects of eight growth factors on the differentiation of cells derived from human embryonic stem cells.* Proc Natl Acad Sci U S A, 2000. **97**: p. 11307.

130. Boheler, K.R., et al., *Differentiation of pluripotent embryonic stem cells into cardiomyocytes.* Circ Res, 2002. **91**: p. 189.

131. Riha, G., P. Lin, and A. Lumsden, *Roles of hemodynamic forces in vascular cell differentiation.* Ann Biomed Eng, 2005. **33**: p. 772.

132. Sordella, R., W. Jiang, and G. Chen, *Modulation of Rho GTPase Signaling Regulates a Switch between Adipogenesis and Myogenesis.* Cell, 2003. **113**: p. 147-158.

133. Ingber, D., *Tensegrity II: How structural networks influence cellular information processing networks.* J Cell Sci, 2003. **116**: p. 1397-1408.

134. Dike, L., C. Chen, and M. Mrksich, *Geometric control of switching between growth, apoptosis, and differentiation during angiogenesis using micropatterned substrates.* IN Vitro Cell Dev Biol, 1999. **35**: p. 441-448.

135. Nelson, C.M., et al., *Emergent patterns of growth controlled by multicellular form and mechanics.* PNAS, 2005. **102**(33): p. 11594-11599.

136. Chicurel, M., C. Chen, and D. Ingber, *Cellular control lies in the balance of forces.* Curr Opin Cell Biol, 1998. **10**: p. 232-239.

137. McBeath, R., D. Pirone, and C.M. Nelson, *Cell Shape, Cytoskeletal Tension, and RhoA Regulate Stem Cell Lineage Commitment.* Dev Cell, 2004. **6**: p. 483-495.

138. Engler, A., M. Griffin, and S. Sen, *Myotubes differentiate optimally on substrates with tissue-like stiffness: pathological implications for soft or stiff microenvironments.* J Cell Biol, 2004. **166**: p. 877-887.

139. Yang, Y., et al., *Embryonic mesenchymal cells share the potential for smooth muscle differentiation: myogenesis is controlled by the cell's shape.* Development, 1999. **126**: p. 3027-3033.

140. Boublik, J., H. Park, and M. Radisic, *Mechanical properties and remodeling of hybrid cardiac constructs made from heart cells, fibrin, and biodegradable, elastomeric knitted fabric.* Tissue Eng, 2005. **11**(7-8): p. 1122-1132.

141. Ahuja, P., P. Sdek, and W.R. MacLellan, *Cardiac myocyte cell cycle control in development, disease, and regeneration.* Physiol Rev, 2007. **87**(2): p. 521-44.

142. Clerk, A. and P.H. Sugden, *Inflame my heart (by p38-MAPK).* Circ Res, 2006. **99**(5): p. 455-8.

143. Engel, F.B., et al., *p38 MAP kinase inhibition enables proliferation of adult mammalian cardiomyocytes.* Genes Dev, 2005. **19**(10): p. 1175-87.

144. Morissette, M.R., et al., *Myostatin regulates cardiomyocyte growth through modulation of Akt signaling.* Circ Res, 2006. **99**(1): p. 15-24.

145. Olson, A.K., et al., *Mitogen-activated protein kinase activation and regulation in the pressure-loaded fetal ovine heart.* Am J Physiol Heart Circ Physiol, 2006. **290**(4): p. H1587-95.

146. Tenhunen, O., et al., *p38 Kinase rescues failing myocardium after myocardial infarction: evidence for angiogenic and anti-apoptotic mechanisms.* FASEB J, 2006. **20**(11): p. 1907-9.

147. Hamburger, V. and H.L. Hamilton, *A series of normal stages in the development of the chick embryo. 1951.* Dev Dyn, 1992. **195**(4): p. 231-72.

148. van den Hoff, M.J., et al., *Increased cardiac workload by closure of the ductus arteriosus leads to hypertrophy and apoptosis rather than to hyperplasia in the late fetal period.* Naunyn Schmiedebergs Arch Pharmacol, 2004. **370**(3): p. 193-202.

149. Barbera, A., et al., *Right ventricular systolic pressure load alters myocyte maturation in fetal sheep.* Am J Physiol Regul Integr Comp Physiol, 2000. **279**(4): p. R1157-64.

150. Saiki, Y., et al., *Hemodynamic alteration by fetal surgery accelerates myocyte proliferation in fetal guinea pig hearts.* Surgery, 1997. **122**(2): p. 412-9.

151. Olson, A.K., et al., *The mitogen-activated protein kinases and Akt are developmentally regulated in the chronically anemic fetal sheep heart.* J Soc Gynecol Investig, 2006. **13**(3): p. 157-65.

152. Kandel, E. and N. Hay, *Multiple regulators and multiple downstream effectors of the serine/threonine kinase Akt/PKB.* Exp Cell Res, 1999. **253**: p. 210.

153. Khwaja, A., *Akt is more than just a Bad kinase.* Nature, 1999. **401**(6748): p. 33-4.

154. Cabane, C., et al., *The p38 pathway regulates Akt both at the protein and transcriptional activation levels during myogenesis.* Cell Signal, 2004. **16**(12): p. 1405-15.

155. Tamir, Y. and E. Bengal, *Phosphoinositide 3-kinase induces the transcriptional activity of MEF2 proteins during muscle differentiation.* J Biol Chem, 2000. **275**(44): p. 34424-32.

156. Zetser, A., E. Gredinger, and E. Bengal, *p38 mitogen-activated protein kinase pathway promotes skeletal muscle differentiation. Participation of the Mef2c transcription factor.* J Biol Chem, 1999. **274**(8): p. 5193-200.

157. Gude, N., et al., *Akt promotes increased cardiomyocyte cycling and expansion of the cardiac progenitor cell population.* Circ Res, 2006. **99**(4): p. 381-8.

158. Han, J. and J.D. Molkentin, *Regulation of MEF2 by p38 MAPK and its implication in cardiomyocyte biology.* Trends Cardiovasc Med, 2000. **10**(1): p. 19-22.

159. Sedmera, D., R.P. Thompson, and F. Kolar, *Effect of increased pressure loading on heart growth in neonatal rats.* J Mol Cell Cardiol, 2003. **35**(3): p. 301-9.

160. Tenhunen, O., et al., *Mitogen-activated protein kinases p38 and ERK 1/2 mediate the wall stress-induced activation of GATA-4 binding in adult heart.* J Biol Chem, 2004. **279**(23): p. 24852-60.

161. Aouadi, M., et al., *p38 mitogen-activated protein kinase activity commits embryonic stem cells to either neurogenesis or cardiomyogenesis.* Stem Cells, 2006. **24**(5): p. 1399-406.

162. Kyriakis, J.M. and J. Avruch, *Mammalian mitogen-activated protein kinase signal transduction pathways activated by stress and inflammation.* Physiol Rev, 2001. **81**(2): p. 807-69.

163. Xu, L., C.S. Kappler, and D.R. Menick, *The role of p38 in the regulation of Na+-Ca2+ exchanger expression in adult cardiomyocytes.* J Mol Cell Cardiol, 2005. **38**(5): p. 735-43.

164. Shepherd, N., et al., *Changes in regulation of sodium/calcium exchanger of avian ventricular heart cells during embryonic development.* Am J Physiol Cell Physiol, 2007. **292**(5): p. C1942-50.

165. Reppel, M., et al., *Regulation of the Na+/Ca2+ exchanger (NCX) in the murine embryonic heart.* Cardiovasc Res, 2007. **75**(1): p. 99-108.

166. Nagy, N., et al., *Ischemic preconditioning involves dual cardio-protective axes with p38MAPK as upstream target.* J Mol Cell Cardiol, 2007. **42**(5): p. 981-90.

167. Roell, W., et al., *Cellular cardiomyoplasty improves survival after myocardial injury.* Circulation, 2002. **105**(20): p. 2435-41.

168. Rubart, M., et al., *Physiological coupling of donor and host cardiomyocytes after cellular transplantation.* Circ Res, 2003. **92**(11): p. 1217-24.

169. Koh, G.Y., et al., *Stable fetal cardiomyocyte grafts in the hearts of dystrophic mice and dogs.* J Clin Invest, 1995. **96**(4): p. 2034-42.

170. Scorsin, M., et al., *Comparison of the effects of fetal cardiomyocyte and skeletal myoblast transplantation on postinfarction left ventricular function.* J Thorac Cardiovasc Surg, 2000. **119**(6): p. 1169-75.

171. Leor, J., S. Aboulafia-Etzion, and A. Dar, *Bioengineered cardiac grafts: A new approach to repair the infarcted myocardium?* Circulation, 2000. **102**(19 Suppl 3): p. III56-61.

172. Leor, J., M. Patterson, and M. Quinones, *Transplantation of fetal myocardial tissue into the infarcted myocardium of rat. A potential method for repair of infarcted myocardium?* Circulation, 1996. **94**(9 Suppl): p. II332-336.

173. Soonpaa, M.H. and L.J. Field, *Survey of studies examining mammalian cardiomyocyte DNA synthesis.* Circ Res, 1998. **83**(1): p. 15-26.

174. Maximilian Buja, L. and D. Vela, *Cardiomyocyte death and renewal in the normal and diseased heart.* Cardiovasc Pathol, 2008.

175. Toyokawa, H., et al., *3D-confocal structural analysis of bone marrow-derived renal tubular cells during renal ischemia/reperfusion injury.* Lab Invest, 2006. **86**(1): p. 72-82.

176. Fujimoto, K.L., et al., *An elastic, biodegradable cardiac patch induces contractile smooth muscle and improves cardiac remodeling and function in subacute myocardial infarction.* J Am Coll Cardiol, 2007. **49**(23): p. 2292-300.

177. Zimmermann, W., M. Didie, and G. Wasmeier, *Cardiac grafting of engineered heart tissue in syngeneic rats.* Circulation, 2002. **106**(12 Suppl 1): p. I151-157.

178. Evans, H., et al., *Novel 3D culture system for study of cardiac myocyte development.* Am J Physiol Heart Circ Physiol, 2003. **285**(2): p. H570-578.

179. Kleinman, H., et al., *Isolation and characterization of type IV procollagen, laminin, and heparan sulfate proteoglycan from the EHS sarcoma.* Biochemistry, 1982. **21**(24): p. 6188-6193.

180. Cheng, M., et al., *Insulin-like Growth Factor-I and Slow, Bi-directional Perfusion Enhance the Formation of Tissue-Engineered Cardiac Grafts.* Tissue Eng, 2009. **15**(3): p. 645-653.

181. Baharvand, H., et al., *The effect of extracellular matrix on embryonic stem cell-derived cardiomyocytes.* J Mol Cell Cardiol, 2005. **38**(3): p. 495-503.

182. Radisic, M., et al., *Cardiac tissue engineering using perfusion bioreactor systems.* Nat Protoc, 2008. **3**(4): p. 719-38.

183. Segers, V.F. and R.T. Lee, *Stem-cell therapy for cardiac disease.* Nature, 2008. **451**(7181): p. 937-942.

184. McDevitt, T.C., M.A. Laflamme, and C.E. Murry, *Proliferation of cardiomyocytes derived from human embryonic stem cells is mediated via the IGF/PI 3-kinase/Akt signaling pathway.* J Mol Cell Cardiol, 2005. **39**(6): p. 865-73.

185. Peng, H. and J. Huard, *Muscle-derived stem cells for musculoskeletal tissue regeneration and repair.* Transpl Immunol, 2004. **12**: p. 311.

186. Lee, J.Y., et al., *Clonal isolation of muscle-derived cells capable of enhancing muscle regeneration and bone healing.* J Cell Biol, 2000. **150**(5): p. 1085-100.

187. Jankowski, R.J., et al., *Flow cytometric characterization of myogenic cell populations obtained via the preplate technique: potential for rapid isolation of muscle-derived stem cells.* Hum Gene Ther, 2001. **12**(6): p. 619-28.

188. Zheng, B., et al., *Prospective identification of myogenic endothelial cells in human skeletal muscle.* Nat Biotechnol, 2007. **25**(9): p. 1025-34.

189. Oshima, H., et al., *Differential myocardial infarct repair with muscle stem cells compared to myoblasts.* Mol Ther, 2005. **12**(6): p. 1130-41.

190. Zuba-Surma, E.K., et al., *Sca-1 expression is associated with decreased cardiomyogenic differentiation potential of skeletal muscle-derived adult primitive cells.* J Mol Cell Cardiol, 2006. **41**(4): p. 650-60.

191. Winitsky, S.O., et al., *Adult murine skeletal muscle contains cells that can differentiate into beating cardiomyocytes in vitro.* PLoS Biol, 2005. **3**(4): p. e87.

192. Invernici, G., et al., *Human adult skeletal muscle stem cells differentiate into cardiomyocyte phenotype in vitro.* Exp Cell Res, 2008. **314**(2): p. 366-76.

193. Tamaki, T., et al., *Cardiomyocyte formation by skeletal muscle-derived multi-myogenic stem cells after transplantation into infarcted myocardium.* PLoS ONE, 2008. **3**(3): p. e1789.

194. Arsic, N., et al., *Muscle-derived stem cells isolated as non-adherent population give rise to cardiac, skeletal muscle and neural lineages.* Exp Cell Res, 2008. **314**(6): p. 1266-80.

195. Steinberg, M.S., *Reconstruction of tissues by dissociated cells.* Science, 1963. **141**: p. 401.

196. Dertinger, H. and D.F. Hulser, *Intercellular communication in spheroids.* Recent Results Cancer Res, 1984. **95**: p. 67-83.

197. Jankowski, R.J., B.M. Deasy, and J. Huard, *Muscle-derived stem cells.* Gene Ther, 2002. **9**(10): p. 642-7.

198. Deasy, B.M., et al., *Long-term self-renewal of postnatal muscle-derived stem cells.* Mol Biol Cell, 2005. **16**(7): p. 3323-33.

199. Gharaibeh, B., et al., *Isolation of a slowly adhering cell fraction containing stem cells from murine skeletal muscle by the preplate technique.* Nat Protoc, 2008. **3**(9): p. 1501-9.

200. Penefsky, Z., et al., *Mechanical responses of developing Fisher rat heart. Effects of steroid hormone.* J Dev Physiol, 1986. **8**: p. 333.

201. Liu, J., et al., *Functional sarcoplasmic reticulum for calcium handling of human embryonic stem cell-derived cardiomyocytes: insights for driven maturation.* Stem Cells, 2007. **25**: p. 3038.

202. Dolnikov, K., et al., *Functional properties of human embryonic stem cell-derived cardiomyocytes: intracellular Ca2+ handling and the role of sarcoplasmic reticulum in the contraction.* Stem Cells, 2006. **24**(2): p. 236-45.

203. Frangogiannis, N.G., *The mechanistic basis of infarct healing.* Antioxid Redox Signal, 2006. **8**(11-12): p. 1907-39.

204. Kastrup, J., et al., *Myocardial regeneration induced by granulocyte-colony-stimulating factor mobilization of stem cells in patients with acute or chronic ischaemic heart disease: a non-invasive alternative for clinical stem cell therapy?* Eur Heart J, 2006. **27**(23): p. 2748-54.

205. Rose, R.A., et al., *Bone Marrow-Derived Mesenchymal Stromal Cells Express Cardiac-Specific Markers, Retain the Stromal Phenotype and do not Become Functional Cardiomyocytes In Vitro.* Stem Cells, 2008. **26**: p. 2884.

206. Fijnvandraat, A., et al., *Cardiomyocytes derived from embryonic stem cells resemble cardiomyocytes of the embryonic heart tube.* Cardiovasc Res, 2003. **59**(2): p. 399-409.

207. Janssen, P., et al., *The travecula culture system: a novel technique to study contractile parameters over a multiday time period.* Am J Physiol, 1998. **275**(5 Pt 2): p. H1481-1488.

208. Asnes, C.F., et al., *Reconstitution of the Frank-Starling mechanism in engineered heart tissues.* Biophys J, 2006. **91**(5): p. 1800-10.

209. Clause, K., et al., *A three-dimensional gel bioreactor for assessment of cardiomyocyte induction in skeletal muscle-derived stem cells.* Tissue Eng, 2010. **15**: p. epub ahead of print.

210. England, S., et al., *A dynamic fate map of the forebrain shows how vertebrate eyes form and explains two causes of cyclopia.* Development, 2006. **133**: p. 4613-4617.

211. Costa, K.D., E.J. Lee, and J. Holmes, *Creating Alignment and Anisotropy in Engineered Heart Tissue: Role of Boundary Conditions in a Model Three-Dimensional Culture System.* Tissue Eng, 2003. **9**(4): p. 567-578.

212. Kurpinski, K., et al., *Anisotropic mechanosensing by mesenchymal stem cells.* Proc Natl Acad Sci U S A, 2006. **103**: p. 16095-16100.

213. Hwang, N., S. Varghese, and J. Elisseeff, *Controlled differentiation of stem cells.* Advanced Drug Delivery Reviews, 2008. **60**: p. 199-214.

214. Cohen, D. and C. Chen, *Mechanical control of stem cell differentiation*, in *StemBook*, The Stem Cell Research Community, Editor. 2008, StemBook. http://www.stembook.org.

215. Balaban, N., et al., *Force and focal adhesion assembly: a close relationship studied using elastic micropatterned substrates.* Nat Cell Biol, 2001. **3**: p. 466-472.

216. Beningo, K., et al., *Nascent focal adhesions are responsible for the generation of strong propulsive forces in migrating fibroblasts.* J Cell Biol, 2001. **153**: p. 881-888.

217. Tan, J., et al., *Cells lying on a bed of microneedles: an approach to isolate mechanical force.* Proc Natl Acad Sci U S A, 2003. **100**: p. 1484-1489.

218. Chrzanowska-Wodnicka, M. and K. Burridge, *Rho-stimulated contractility drives the formation of stress fibers and focal adhesions.* J Cell Biol, 1996. **133**: p. 1403-1415.

219. Helfman, D., et al., *Caldesmon inhibits nonmuscle cell contractility and interferes with the formation of focal adhesions.* Mol Biol Cell, 1999. **10**: p. 3097-4112.

220. Riveline, D., et al., *Focal contacts as mechanosensors: externally applied local mechanical force induces growth of focal contacts by an mDia1-dependent and ROCK-independent mechanism.* J Cell Biol, 2001. **153**: p. 1175-1186.

221. Sniadecki, N., et al., *Magnetic microposts as an approach to apply forces to living cells.* Proc Natl Acad Sci U S A, 2007. **104**: p. 14553-14558.

222. Miyamoto, S., et al., *Integrin function: molecular hierarchies of cytoskeletal and signaling molecules.* J Cell Biol, 1995. **131**: p. 791-805.

223. Fincham, V., et al., *Active ERK/MAP kinase is targeted to newly forming cell-matrix adhesions by integrin engagement and v-Src.* EMBO J, 2000. **19**: p. 2911-2923.

224. Wang, H., et al., *Shear stress induces endothelial differentiation from a murine embryonic mesenchymal progenitor cell line.* Arterioscler Thromb Vasc Biol, 2005. **25**: p. 1817-1823.

225. Cai, X., et al., *Spatial and temporal regulation of focal adhesion kinase activity in living cells.* Mol Cell Biol, 2008. **28**: p. 201-214.

226. Iqbal, J. and M. Zaidi, *Molecular regulation of mechanotransduction.* Biochem Biophys Res Commun, 2005. **328**: p. 751-755.

227. Estes, B., J. Gimble, and F. Builak, *Mechanical signals as regulators of stem cell fate.* Curr Top Dev Biol, 2004. **60**: p. 91-126.

228. Ross, R., *Molecular and mechanical synergy: cross-talk between integrins and growth factor receptors.* Cardiovasc Res, 2004. **63**: p. 381-390.

229. Jaiswal, R., et al., *Adult human mesenchymal stem cell differentiation to the osteogenic or adipogenic lineage is regulated by mitogen-activated protein kinase.* J Biol Chem, 2000. **275**: p. 9645-9662.

230. Binetruy, B., et al., *Concise review: regulation of embryonic stem cell lineage commitment by mitogen-activated protein kinases.* Stem Cells, 2007. **25**: p. 1090-1095.

231. Huangfu, D. and K. Anderson, *Cilia and Hedgehog responsiveness in the mouse.* Proc Natl Acad Sci U S A, 2005. **102**: p. 11325-11330.

232. Corbit, K., et al., *Vertebrate Smoothened functions at the primary cilium.* Nature, 2005. **437**(1018-1021).

233. Ingham, P. and A. McMahon, *Hedgehog signaling in animal development: paradigms and principles.* Genes Dev, 2001. **15**: p. 3059-3087.

234. Hirokawa, N., et al., *Nodal flow and the generation of left-right asymmetry.* Cell, 2006. **125**: p. 33-45.

235. Kiprilov, E., et al., *Human embryonic stem cells in culture possess primary cilia with hedgehog signaling machinery.* J Cell Biol, 2008. **180**: p. 897-904.

236. Spradling, A., D. Drummond-Barbosa, and T. Kai, *Stem cells find their niche.* Nature, 2001. **414**(6859): p. 98-104.

237. Streuli, C., *Extracellular matrix remodelling and cellular differentiation.* Curr Opin Cell Biol, 1999. **11**: p. 634-640.

238. Jiang, X., et al., *Directing cell migration with asymmetric micropatterns.* Proc Natl Acad Sci U S A, 2005. **102**: p. 975-978.

239. Thery, M., et al., *Anisotropy of cell adhesive microenvironment governs cell internal organization and orientation of polarity* Proc Natl Acad Sci U S A, 2006. **103**(52): p. 19771-19776.

240. Hoover, D., E. Chang, and M. Yousaf, *Asymmetric Peptide Nanoarray Surfaces for Studies of Single Cell Polarization.* J Am Chem Soc, 2008. **130**: p. 3280-3281.

241. Chan, E. and M. Yousaf, *A photo-electroactive surface strategy for immobilizing ligands in patterns and gradients for studies of cell polarization.* Mol BioSyst, 2008. **4**(7): p. 746-753.

242. Luo, W., S. Jones, and M. Yousaf, *Geometric Control of Stem Cell Differentiation Rate on Surfaces.* Langmuir, 2008. **24**: p. 12129-12133.

243. Chen, C., et al., *Micropatterned surfaces for control of cell shape, position, and function.* Biotechnol Prog, 1998. **14**: p. 356-363.

244. Chen, C., et al., *Cell shape provides global control of focal adhesion assembly.* Biochem Biophys Res Commun, 2003. **307**: p. 355-361.

245. Petroll, W., M. Vishwanath, and L. Ma, *Corneal fibroblasts respond rapidly to changes in local mechanical stress.* Investigative Ophthalmology and Visual Science, 2004. **45**(10): p. 3466-3474.

246. Ingber, D., *Tensegrity: The architectural basis of cellular mechanotransduction.* Ann Rev Physiol, 1997. **59**: p. 575-599.

247. Discher, D., D. Mooney, and P. Zandstra, *Growth Factors, Matrices, and Forces Combine and Control Stem Cells.* Science, 2009. **324**(5935): p. 1673-1677.

248. Kluger, Y., et al., *Lineage specificity of gene expression patterns.* Proc Natl Acad Sci U S A, 2004. **101**(17): p. 6508-6513.

249. Janes, K. and D. Lauffenburger, *A biological approach to computational models of proteomic networks.* Curr Opin Chem Biol, 2006. **10**(1): p. 73-80.

250. Kirouac, D. and P. Zandstra, *Understanding cellular networks to improve hematopoietic stem cell expansion cultures.* Curr Opin Biotechnol, 2006. **17**(5): p. 538-547.

251. Kimura, M., H. Kurosawa, and Y. Amano, *Effect of oxygen tension on the proliferation and the differentiation of mouse embryonic stem cells*, in *Animal Cell Technology: Basic and Applied Aspects*, S.I.a.K.-I. Nishijima, Editor. 2006, Springer: Nagoya Japan. p. 143-148.